

SKELETAL ANATOMY IN THE CHONDRICHTHYAN TREE OF LIFE

A thesis submitted in partial fulfillment of the requirements for the degree

MASTER OF SCIENCE

in

MARINE BIOLOGY

by

CALLIE CRAWFORD

DECEMBER, 2014

at

THE GRADUATE SCHOOL OF THE COLLEGE OF CHARLESTON

Approved by:

Dr. Gavin Naylor, Thesis Advisor

Dr. Shane Boylan

Dr. Andrew Clark

Dr. Cheryl Wilga

Dr. Amy McCandless, Dean of the Graduate School

UMI Number: 1585540

All rights reserved

INFORMATION TO ALL USERS

The quality of this reproduction is dependent upon the quality of the copy submitted.

In the unlikely event that the author did not send a complete manuscript and there are missing pages, these will be noted. Also, if material had to be removed, a note will indicate the deletion.



UMI 1585540

Published by ProQuest LLC (2015). Copyright in the Dissertation held by the Author.

Microform Edition © ProQuest LLC.

All rights reserved. This work is protected against unauthorized copying under Title 17, United States Code



ProQuest LLC.
789 East Eisenhower Parkway
P.O. Box 1346
Ann Arbor, MI 48106 - 1346

ABSTRACT

SKELETAL ANATOMY IN THE CHONDRICHTHYAN TREE OF LIFE

A thesis submitted in partial fulfillment of the requirements for the degree

MASTER OF SCIENCE

in

MARINE BIOLOGY

by

CALLIE CRAWFORD

November, 2014

at

THE GRADUATE SCHOOL OF THE COLLEGE OF CHARLESTON

Chondrichthyans (sharks, rays, skates, and chimaeras) are a diverse taxonomic clade inhabiting bodies of water all over the world. As a lineage, chondrichthyans split from the other jawed vertebrates 450 million years ago, the most basal split in the gnathostome vertebrate tree. Although they have been studied for centuries, knowledge about these animals lags behind that of many other vertebrate groups. This work uses Computed Tomography (CT) to explore morphological variation across phylogenetically diverse species of chondrichthyans. CT imaging is a nondestructive method for viewing internal structures of extant and fossilized specimens. After CT scan data acquisition, reconstruction software was used to manually segment the skeletal anatomical into constituent structures, creating 3-Dimensional representations of the structures. In most groups of vertebrate organisms, skeletal structures are made of calcified bone which has high radiopacity, leading to greater contrast between the skeleton and soft tissues. Chondrichthyans, by comparison, have skeletons composed of cartilage which is much less radiopaque than bone, resulting in lower contrast with surrounding tissues. Variations in the skeletal structures are discussed along with notes on calcification within the chondrichthyan orders. This work is presented as a summary of the variation observed in the skeletal anatomy, building upon previous works in chondrichthyan anatomy, expanding the current state of knowledge of the diversity in chondrichthyan fish skeletons. This project is part of a collaborative effort to develop a phylogenetic tree of life for modern chondrichthyans.

ACKNOWLEDGEMENTS

I thank my advisor, Dr. Gavin Naylor, for his substantial guidance, support, and patience throughout my time in the Graduate Program in Marine Biology at the College of Charleston. I would also like to thank my committee members, Dr. Shane Boylan, Dr. Andrew Clark, and Dr. Cheryl Wilga. Although they were not official members of my committee, I would like to extend a big thank you to Dr. John Maisey, Dr. Amy Balanoff, Dr. John Denton, Dr. Alan Pradel, and Dr. Mason Dean, for their help in identifying structures in the CT scans and general assistance in the completion of my thesis research.

This work could not have been completed without the extensive support from the many museums from which specimens were borrowed for CT scanning. I would like to specifically acknowledge Sandra Raredon and Shirleen Smith (USNM), Rob Robins (UF), Rick Feeney (LACM), and Peter Last (CSIRO) for their help in acquiring specimens. Additionally, thank you to Tracy Holden and Drew McQuisten at MUSC and Amy Balanoff and John Denton at the AMNH for their assistance with scanning the specimens and to Dr. U. J. Schoepf (MUSC) for permitting access to the new DSCT Scanner. The coverage of chondrichthyan diversity would not be nearly as complete without the additional CT scans shared by Dr. Adam Summers, Dr. Mason Dean, Dr. Kenshu Shimada, and Pepijn Kamminga.

Thank you to the members of the Naylor lab and to my classmates at CofC for their friendship and support. Finally, I wish to thank my family and friends for their support and encouragement.

This research was funded by the National Science Foundation (DEB Award 1132229) to Gavin Naylor and John Maisey for the chondrichthyan Tree of Life.

TABLE OF CONTENTS

ABSTRACT.....	i
COPYRIGHT PAGE.....	ii
ACKNOWLEDGEMENTS.....	iii
TABLE OF CONTENTS.....	iv
LIST OF FIGURES.....	vi
LIST OF TABLES.....	ix
Chapter	
1. INTRODUCTION.....	1
Induction in Science	
Chondrichthyans	
Chondrichthyan Anatomy	
Documented Anatomical Diversity	
CT Scanning	
Significance of Study	
2. MATERIALS AND METHODS.....	9
Specimen Selection	
CT Scanners	
CT Scanning	
Segmentation	
Institutional Abbreviations	
Skeletal Structures	
3. RESULTS.....	17
Introduction	
Chondrocranium	
Branchial Arches	

Pectoral Girdle	
Pelvic Girdle	
Vertebral Column	
Links to Life History	
4. DISCUSSION	30
Previous Works	
Additions from this Study	
Future Directions	
Conclusions	
FIGURES	36
TABLES	104
APPENDIX	
1. TABLE OF SCANNED SPECIMENS	108
2. SCANNING AND SEGMENTATION PROTOCOLS	113
LITERATURE CITED	114

LIST OF FIGURES

- Figure 1.** The Inquiry Wheel, Stages of Scientific Inquiry.
- Figure 2.** Dorsal and lateral views of an ideal specimen.
- Figure 3.** Examples of radiographs used to determine scanning candidacy.
- Figure 4.** Specimens prepared for scanning on two medical scanners at MUSC.
- Figure 5.** Mimics segmentation software with the scan of *Potamotrygon motoro*.
- Figure 6.** Initial thresholding stage and final completed segmentation.
- Figure 7.** Example of the anatomy portion of the chondrichthyan Tree of Life Project website.
- Figure 8.** Dorsal and later views of representative segmentations from each chondrichthyan order.
- Figure 9.** Hypothesis of phylogenetic relationships Adapted from Naylor *et al.* (2012)
- Figure 10.** Examples of two species with poor calcification.
- Figure 11.** Morphological variation in chondrocrania of the order Carcharhiniformes.
- Figure 12.** Morphological variation in chondrocrania of the order Lamniformes.
- Figure 13.** Morphological variation in chondrocrania of the order Orectolobiformes.
- Figure 14.** Morphological variation in chondrocrania of the order Squaliformes.
- Figure 15.** Morphological variation in chondrocrania of the order Rajiformes.
- Figure 16.** Morphological variation in chondrocrania of the order Myliobatiformes.
- Figure 17.** Morphological variation in chondrocrania of the order Torpediniformes.
- Figure 18.** Morphological variation in chondrocrania of the orders Heterodontiformes, Pristiformes, Pristiophoriformes, Squatiniformes, and Hexanchiformes.
- Figure 19.** Morphological variation in chondrocrania of the order Chimaeriformes.
- Figure 20.** Variation in the branchial structures of the Carcharhiniform sharks.
- Figure 21.** Variation in the branchial structures of the Lamniform sharks.
- Figure 22.** Variation in the branchial structures of the Orectolobiform sharks.
- Figure 23.** Variation in the branchial structures of the Squaliform sharks.
- Figure 24.** Variation in the branchial structures of the Rajiforms.

- Figure 25.** Variation in the branchial structures of the Torpediniformes.
- Figure 26.** Variation in the branchial structures of the Myliobatiforms.
- Figure 27.** Scapulocoracoid diversity in the order Carcharhiniformes.
- Figure 28.** Scapulocoracoid diversity in the order Lamniformes.
- Figure 29.** Scapulocoracoid diversity in the order Orectolobiformes.
- Figure 30.** Scapulocoracoid diversity in the order Squaliformes.
- Figure 31.** Scapulocoracoid diversity in the order Rajiformes.
- Figure 32.** Scapulocoracoid diversity in the order Torpediniformes.
- Figure 33.** Scapulocoracoid diversity in the order Rajiformes.
- Figure 34.** Scapulocoracoid diversity in the orders Heterodontiformes, Pristiformes, Pristiophoriformes, Squatiniformes, and Hexanchiformes.
- Figure 35.** Scapulocoracoid diversity in the order Chimaeriformes.
- Figure 36.** Pectoral fin variation in the Orectolobiforms.
- Figure 37.** Aplesodic and plesodic pectoral fins in families of Carcharhiniform sharks.
- Figure 38.** Aplesodic and plesodic pectoral fins in families of Lamniform sharks.
- Figure 39.** Pectoral fins of Squaliform sharks.
- Figure 40.** Pectoral fins of Squatiniformes and Pristiophoriformes.
- Figure 41.** Pectoral fins of Myliobatiforms.
- Figure 42.** Pectoral fins of Pristidae and the Rajiformes.
- Figure 43.** Pectoral fins of the Torpediniformes.
- Figure 44.** Pectoral fins of the Hexanchiforms.
- Figure 45.** Pectoral fins of the Chimaeriforms.
- Figure 46.** Morphological diversity of the puboischiadic bar in the order Carcharhiniformes.
- Figure 47.** Morphological diversity of the puboischiadic bar in the order Lamniformes.
- Figure 48.** Morphological diversity of the puboischiadic bar in the order Orectolobiformes.
- Figure 49.** Morphological diversity of the puboischiadic bar in the order Squaliformes.

- Figure 50.** Morphological diversity of the puboischiadic bar in the order Rajiformes.
- Figure 51.** Morphological diversity of the puboischiadic bar in the order Myliobatiformes.
- Figure 52.** Morphological diversity of the puboischiadic bar in the order Torpediniformes.
- Figure 53.** Morphological diversity of the puboischiadic bar in Heterodontiformes, Pristiformes, Pristiophoriformes, Squatiniformes, and Hexanchiformes.
- Figure 54.** Morphological diversity of the puboischiadic bar in the order Chimaeriformes.
- Figure 55.** Variations in the clarity of pelvic fin structures chondrichthyan orders.
- Figure 56.** Examples of vertebral columns with and without vertebral ribs.
- Figure 57.** Dorsal and lateral of the variations in calcification of the hexanchiform vertebral column.
- Figure 58.** Variations in the vertebral tube and synarcual of the chimaeriform fishes.
- Figure 59.** Examples of abnormal characteristics observed in the vertebral columns.
- Figure 60.** Examples of stomach contents in scanned chondrichthyans.
- Figure 61.** Four specimens with embryonic offspring visible in the CT scans.

LIST OF TABLES

Table 1. Characteristics of ideal scanning candidates

Table 2. Kernel and kV settings for the CT Scanners used in this study

Table 3. Skeletal structures observed in the segmented CT scans.

Chapter 1: Introduction

Induction in Science

Inductive reasoning in science is often used in exploratory research whereas deductive work is used to test a hypothesis. Medewar and Popper, vehemently objected to the use of induction in science, going so far as to say it has no place in science and only the hypothetico-deductive strategy should be used (Popper, 1959 and Medewar, 1996). Rothchild, on the other hand, includes both induction and deduction in his characterization of the scientific method and explains that there is no consensus on one scientific method or even one definition of science (Rothchild 2006). The hypothetico-deductive system is most similar to the generally accepted format of the scientific method, developing questions from previous observations and testing hypotheses to answer those questions (Rothchild 2006).

Reiff, Harwood, and Phillipson have proposed a new model of scientific investigation, The Inquiry Wheel (Reiff *et al.* 2002 and Robinson 2004) to replace the traditional framework. This model (Figure 1) moves away from linear scientific reasoning and into a wheel with continuous feedback among the constituent elements. The hub of the wheel is comprised of questions developed from past and current observations and the stages (Defining the problem, Forming the Question, Investigating the Known, Articulating the Expectation, etc.) at the tips of the spokes are visited throughout the investigation.

Questions that promote mechanistic understanding of systems can only be achieved after the relevant components have been identified and characterized. The first step in any such endeavor involves examining material and making observations. In the current work, the source material for the observations was collected and the results are new hypotheses or questions, not

answers to proposed hypotheses. This work centers on an academic interest investigating morphological transformations which may have influenced the diversification of modern elasmobranchs.

Chondrichthyans

About 450 million years ago, the vertebrate evolutionary tree split with one lineage giving rise to bony fishes, tetrapods, amniotes, and mammals while the other led to chondrichthyans (sharks, skates, rays and chimaeras) (Maisey *et al.* 1996). Due to their evolutionary independence, it is likely that both lineages developed different solutions to similar challenges and that each harbors lineage specific architectural attributes and innovations. Although substantial effort has been put into studying adaptations on the lineage leading to humans, relatively little is known about the corresponding innovations and adaptations on the lineage leading to chondrichthyans (Schindler *et al.* 2002, Libralato *et al.* 2005, and Myers *et al.* 2007).

Chondrichthyans are highly diverse and inhabit bodies of water all over the world from the tropics to polar seas; some even inhabit freshwater lakes and rivers (Compagno 1990; Martin 2005; Ebert & Winton 2010; Rosa *et al.* 2010; and White & Sommerville 2010). Although chondrichthyans first appear in the fossil record about 450 million years ago, modern elasmobranchs, the Neoselachii, represent a more recent diversification and date back to the Triassic about 200 million years ago with extensive diversification in the Jurassic and Cretaceous periods (Maisey 1984; Underwood 2006 and Maisey 2012). The chondrichthyan lineage survived mass extinctions from the Ordovician, Permian, Triassic, and Cretaceous periods (Raup & Sepkoski 1982 and Corrigan & Beheregaray 2009). Today, sharks are the most diverse group of large predatory animals and are important due to their role in structuring marine food webs and ecosystems (Libralato *et al.* 2005; Myers *et al.* 2007; Schindler *et al.* 2008). Although

chondrichthyans are currently a prominent topic in both research and popular-culture, knowledge about these animals lags behind that of many other vertebrate groups.

Chondrichthyan Phylogeny

Phylogenetic relationships among the approximately 1,200 currently recognized extant chondrichthyans remain poorly understood and many proposed relationships conflict with one another. Some relationships have been based exclusively on morphological observations (Compagno 1977; Maisey 1984; Thies & Reif 1985; Shirai 1996; and de Carvalho 1996) while others are primarily based on molecular sequence comparisons. Some molecular estimates focus on closely related taxa (Naylor 1992; Iglesias *et al.* 2005), while others look at higher taxonomic relationships (Dunn & Morrissey 1995; Kitamura *et al.* 1996; Douady *et al.* 2003; Maisey *et al.* 2004). Other researchers looked at many taxa among numerous distantly related groups (Naylor 2005; Vélez-Zuazo, and Agnarsson 2011; Aschliman *et al.* 2012; Naylor *et al.* 2012; and Sorenson, Santini, and Alfaro 2014). There is strong support for the conflicting topologies, leading to a difficult task in determining which is more likely to be the correct estimate.

Early phylogenetic estimates were based solely on morphology, both external and internal, and these observations or measurements were accepted as answers to the relationships (Muller & Henle 1839 (cited in White 1936; Naylor 2005; and White & Last 2012); Hasse 1879; Haswell 1884; Garman 1913; and White 1936). Morphology is still used in modern estimates (Nishida 1990; Shirai 1992 & 1996; de Carvahlo 1996; and Goto 2001); however, with the increasing availability of molecular tools; there has been a shift away from morphological standards. Over time, acceptance of phylogenetic estimates has moved from the original morphological data to molecular data. In some instances, instead of using anatomy as a standard to base the acceptance of molecular inferences, the molecular inferences have become the standard to which morphological data are judged (Hedges and Poling 1999; Brohman *et al.* 2002).

Currently, there is a lot of confidence in the molecular data, although, it is not always clear if this confidence is warranted as often times there is ambiguity in branch locations and branch lengths (Naylor *et al.* 2005, Naylor *et al.* 2012).

Genomic research is useful in the pursuit of explanations for the diversity observed in life. In order to explain this diversity, it must first be documented, and we must understand the extent and variation in the observations. In animals with smaller genomes, such as *Drosophila*, genome wide association studies (GWAS) use breeding experiments to gain knowledge of which genes are responsible for specific traits by focusing on the part or parts of the genome responsible for these traits using quantitative genetic approaches (Nuzhdin *et al.* 1997 and Harbison *et al.* 2013). In organisms with larger genomes, this process is many times more challenging and difficulties are further compounded by the increase in gene interactions. In these organisms, it is more straightforward to begin with a trait and move to the genes to see the variation. By collecting anatomical descriptions, countless questions for the genomic data to answer are being developed including questions about homology and convergence.

Ultimately, molecular data are expected to be used to explain the observed characteristics, including anatomical traits, however, not all of these have been documented for a large number of chondrichthyan species. While there is a large amount of information available in the genetic makeup of an organism, it is difficult to understand to which characteristics the genetic differences among species contribute. Knowledge of the morphological, functional, and behavioral traits that differ among species, genera, family, etc., give some examples of the manifestations of the genetic differences in the organism.

Chondrichthyan anatomy

According to Andreas Vesalius (in Benini and Bonar 1996 and Buckwalter 2000), knowledge of human anatomy could not be gained through the study of texts and reports on the

mythology of life but only through the dissection of human corpses (Benini and Bonar 1996). This belief holds true for the study of anatomy and physiology of all organisms. Comparative anatomy is an effective way to study evolutionary history and to better understand how lineages have responded to environmental changes and challenges. Through exploring the diversity of traits in a suite of related organisms and organizing the information into an evolutionary hierarchy, we can reveal potential schemes for how traits have changed over the course of time.

Despite over 150 years of study, there are still many chondrichthyan species whose skeletal anatomy has not been documented. There have been projects looking into the anatomy of single species or closely related species with the most comprehensive information on anatomical comparisons having been compiled in Samuel Garman's "The Plagiostomia (Sharks, Skates, and Rays)" (1913) which includes detailed illustrations from dissections of a relatively small number of species from various orders and families. Other researchers have publications exploring the diverse anatomical structures in many closely or distantly related species (Nishida 1999; Goto 2001; and Wilga *et al.* 2007), however few have worked on the entire skeleton of such a diverse collection of chondrichthyans as explored in the current study (Garman 1913; Shirai 1996).

Anatomical studies are sometimes used for understanding the functional biology (i.e. how organisms address challenges associated with locomotion, feeding, reproduction, etc.) (Lucifora and Vassallo 2002; Wilga *et al.* 2007; and Maia *et al.* 2012). The distribution of anatomical characters can then be used to estimate phylogenies and see trajectories of evolution in different groups of organisms. In other anatomical studies, the distributions are used to create phylogenetic estimates and can be used to develop hypothetical ancestral states of anatomical characters (Nishida 1990; Dean *et al.* 2007). Inferences based on functional morphology and phylogeny stem from different goals and essentially have conflicting approaches to explaining observed data. Functional morphology attempts to attribute the majority of character covariance to the functionality of the organism as a whole. The objective of phylogenetic inferences is to ascribe as

much of the covariance as possible to common history to give support for the relationship estimates.

Past works documenting anatomical diversity have often looked at closely related species such as Nishida's work on Myliobatiformes (1990) or Goto's work on Orectolbiformes (2001). One of the broadest studies on morphology and phylogeny of chondrichthyans was carried out by Shigeru Shirai (1992). Shirai developed a phylogeny which illustrated some relationships not shown before and although his sampling was strongly biased towards the squalians and batoids there was representation of the hexanchiform and Galeomorph sharks. Shirai extended his coverage to include more batoids and the galeomorph sharks in a later phylogeny by incorporating characters described by other researchers into his 1992 phylogeny. This newer phylogeny of the neoselachians maintained the unique relationship between squaliform sharks and batoids (Shirai 1996).

Documenting Anatomical Diversity

The focus of the work presented here is purely a documentation of skeletal anatomy observed through the segmentation of CT scans of a diverse selection of chondrichthyan fishes. This is a broad survey of the variations in skeletal traits, creating a preliminary point for further work with character matrices, ontogeny, phylogenetics, and functional biology using digital skeletons. The digital skeletons created here are accessible online at <http://sharkrays.org>. As this is a study of skeletal anatomy, there is no reference to musculature, nerves, ligaments, or soft tissues which are often used in morphologically based phylogenetic studies. The goal here is comparative anatomy of skeletal elements and the creation of a database of some of the diversity of skeletal structures seen in chondrichthyans.

While a large amount of anatomical data have been collected here, the data are not presented as character matrices. The coverage is broad, but not deep, with only one specimen per

species investigated. Intraspecific variation is not examined. Individuals studied here are assumed to be representative of their respective species, genus, and family. Although patterns are noted, a cladistics framework has not been developed. Patterns described here are constrained to family and generic levels as it is often easier to see clear patterns in more recent splits than in deeper relationships.

CT Scanning

As an alternative to gross dissections of specimens, we have used Computed Tomography (CT) to image the specimens and segment out the skeletal structures. CT is a 3-Dimensional (3D) imaging tool developed for medical purposes and used in a variety of fields including aviation security, forensic autopsy, and archaeology. Modern CT scanning techniques allow for the visualization of skeletal structures. To date, most of the skeletal information on elasmobranchs has been gained through dissection, which while revealing, involves specimen damage. In traditional dissection, it is often necessary to sequentially remove some structures to see others. This makes it challenging to reconstruct the spatial context of all of the constituent structures in their entirety. If a structure is cut or removed before it has been completely described or imaged, it may not be possible to replace the structure to its original location and orientation. As the digital data can be segmented over and over again, researchers can replace removed structures to check locations and articulations. The ability to replace structures and restart the digital dissection also makes it easier to check for structures or connections which that may have been omitted previously.

Even more importantly, dissection is not an option when studying rare species that must be kept intact. CT scanning provides a means to access the internal anatomy of such rare species, some of which are known only from one or a few specimens. We have had access to some type and holotype specimens which were collected over a century ago. CT enables the noninvasive

imaging of rare specimens without damaging body tissues or losing any information that dissection might jeopardize. This technology afforded us the opportunity to complete a broad sampling of chondrichthyans by borrowing specimens from museums around the world.

Significance of Study

The chondrichthyan lineage arose from the most basal split of the gnathostome vertebrate tree, this work provides a starting point to readily compare their skeletal morphology. Although there has been a lot of research focus on this lineage and they are currently a fixture in popular culture, there is still a lot unknown about them and continued research in all aspects of their biology are necessary.

This study builds upon past work on chondrichthyan anatomy, forming an atlas of 3-Dimensional morphological data for other studies to build upon. We hope the skeletal data provided herein will serve as a baseline for future work. We anticipate that the data may be useful reference material for examination of chondrichthyan development, the fossil record, and biomechanics, and a broader coverage of variation within the class. The data highlight areas needing greater coverage of extant diversity which will be important for determining relationships between extant and fossil forms.

Chapter 2: Methodology

Specimen Selection

Representatives of each of the currently accepted families were sought to explore skeletal variation. Specimens were borrowed from museum and institutional collections from around the world. Most of these specimens were first identified in online museum databases. Follow up discussions with curators and collection managers allowed us to determine the size, condition, and suitability for CT scanning of the specimen(s). While the initial goal was based on the premise that sampling representatives of each family would serve to capture the diversity of morphological variation in the group, it was subsequently determined that certain families were so morphologically diverse that multiple genera would be needed to capture representative diversity within family.

Ideal specimens for CT scanning are about one meter in length, straight and without visible cuts in the skeletal elements (Figure 2). Mature individuals are generally more calcified than immature ones, thus larger specimens were often expected better candidates for scanning than smaller ones. When possible, specimens were x-rayed in order to gauge whether the skeletal elements would be visible in a CT scan (Figure 3). Even when all characteristics of an ideal specimen were met, there were still instances where the specimen did not scan well and a second specimen was scanned in order to get the most complete skeleton. Additionally, some specimens which were expected to be poor candidates for scanning due to small size or deformities from being in a jar had unexpectedly high skeletal radiodensity. In these situations, the x-ray clarity was weighted more heavily than other characteristics including body condition and maturity. Selected specimens were brought to Hollings Marine Lab in Charleston, SC where they were held

in either 50% isopropyl alcohol or 70% ethanol depending on what they had been preserved in previously. Table 1 summarizes the characteristics of ideal scanning candidates.

CT Scanners

The majority of the data presented here were collected on three CT scanners. Two scanners are located at the Medical University of South Carolina (MUSC) in Charleston, SC, a Siemens Somatom Sensation 64 slice and a Siemens Somatom Force (Siemens Healthcare) (Figure 4). The third scanner, a GE Phoenix Vtome x S240 High Resolution scanner is located at the American Museum of Natural History (AMNH) in New York, NY. Some of the scans were collected by other researchers using CT scanners at the following facilities: the Siemens Somatom Sensation 64-slice at the *Royal Brompton Hospital, London, UK*; the *Toshiba Aquillion at the Toshiba Training Center, Orange County, CA*; the Siemens Somatom Sensation 64 slice at Children's Memorial Hospital, Chicago, IL; the Siemens Somatom Volume Zoom at Woods Hole Oceanographic Institute, Woods Hole, MA; and the Siemens Somatom 16-slice at UC Irvine Medical Center, Irvine, CA. Appendix I contains information for the source scanner for each specimen examined.

CT Scanning

The following applies to the scans completed as part of the current study, excluding those shared from other researchers unless otherwise noted. Specimens were sent to Hollings Marine Lab, Charleston, SC via postal service (Commonwealth Scientific and Industrial Research Organisation and Natural History Museum of Los Angeles County), were picked up in person and transported by car (University of Florida) or rail (Smithsonian Institution) to Charleston for scanning. Specimens were kept in metal holding tanks filled with either 50% Isopropyl alcohol or 70% Ethanol depending on the preservative used for the specimen at the museum of origin prior to coming to Charleston. All specimens brought the Charleston, SC were scanned on one of the

two medical scanners at MUSC (Siemens Somatom Force or Somatom Sensation 64-slice). Small specimens (<50cm TL) with good calcification but resolution too low in the medical scans for segmentation were sent to AMNH for scanning on their high resolution scanner.

In CT scanning, resolution is determined by the kernel and the X-Ray tube voltage (kV). The kernel is the reconstruction filter used in post processing. In general, lower kernel values create smoother images with lower noise but poorer edge definition and higher numbers increase the spatial resolution and have better edge definition with higher noise levels (Achenbach *et al.*, 2006). X-Ray tube voltage (kV) is generally kept low to reduce the radiation dosage a patient receives (van der Wall *et al.*, 2010). As our specimens were preserved, we were able to adjust the dosage to higher settings to get better contrast and reduced attenuation in the x-rays. The reconstruction kernel and kV of each scanner varied depending on the settings used by the CT technician working on each CT scanner (Table 2). On the MUSC scanners, each specimen was placed along the center-line of the CT scanner where resolution was highest and artifact lowest, and scans were performed using an imaging protocol optimized for each individual specimen by maximizing the tube current.

The quality and ease of segmentation is tightly tied to the visible contrast between study structures and other tissues in the organism. In most vertebrates, including humans for which CT scanning technology has been optimized, skeletal structures are made of calcified bone which is highly radiopaque. This results in a high contrast between the skeleton and soft tissues. The cartilaginous chondrichthyan skeleton, by comparison, is much less radiopaque than calcified bone, resulting in lower contrast between skeletal structures and the surrounding soft tissues. Distinguishing skeletal elements in such low-contrast circumstances is made even harder by noise artifacts.

Segmentation

CT scan data were saved to discs or hard drives and uploaded to the computers at Hollings Marine Lab to be segmented using MIMICS Research version 17.0 64-bit software (Materialise, Leuven, Belgium) and later processed using 3Matic Research version 9.0 64-bit software (Materialise, Leuven, Belgium), and MeshLab version 1.3.3 (Cignoni *et al.*, 2011). More detailed protocol is explained in Appendix II.

CT segmentation refers to the process of extracting 3D components from the raw CT scan slice data. In our case, the components are the constituent anatomical structures found in the cartilaginous skeletons of chondrichthyan fishes (Figure 5). The voxels (3-Dimensional pixels) in CT scan data have standardized Hounsfield units denoting density. Hounsfield units are linearly scaled to the radiodensity of tissues in the human body and allow thresholding to be used by algorithms in the MIMICS software to assist the manual segmentation. Segmentation is initiated by setting thresholds which select voxels of a certain Hounsfield unit or gray-scale value (Figure 6). Thresholding creates a mask which classifies all voxels within the selected Hounsfield range as the same color. Masks can be duplicated and cropped to contain only the area of interest.

Mimics Software contains a suite of tools for segmenting structures from the CT scans after thresholding to select the area of interest and to edit the masks for accurate segmentation. The tools used in this study were Region Growing, Edit Mask in 3D, Multiple Slice Edit, and Boolean Operations. During segmentation, edited structures are calculated as 3D objects to visualize them within Mimics to check accuracy of the segmentation and to locate areas requiring more editing. In Figure 6, the lower right view is the completed scan of the *Potamotrygon motoro* specimen calculated into 3D. The completed segmentations of each structure are saved as STereoLithography (STL) Files which are uploaded to the online database. An example of the skeleton viewer on the website is shown in Figure 7.

Thresholding

Thresholds are adjusted to visualize structures of different radiodensities. The lower bound can be reduced to select less radiodense voxels and increased to focus only on the subsets that are especially radiopaque. MIMICS has predefined a set thresholds for structures in the human body, some of which can be specified for child or adult stages. Example preset threshold levels include bone, enamel, soft tissue, muscle tissue, and prosthesis. Because these thresholds have been optimized for scans of humans, they don't always work well for animals with cartilaginous skeletons. As a result thresholds were manually selected based on the radiopacity of the structures. In each individual scan, multiple thresholds were found to be optimal for segmenting different structures. Each threshold creates a new mask which can be manipulated with the other tools in MIMICS. Narrower thresholds were generally adequate for more calcified structures such as the jaws, teeth, and vertebral column while less dense structures such as gill arches and fin radials often needed broader threshold ranges to capture the finer parts of the structures.

Medical scans would often require fewer than five different thresholds to segment the entire specimen, whereas high resolution scans could sometimes require more than ten thresholds to accurately segment all of the structures. In some poorly calcified areas, most commonly the pectoral radials, multiple thresholds were required. In these instances, the two segmented parts would later be merged together in 3Matic. Multiple thresholds were often required for areas with a lot of noise artifact.

Once thresholds were selected, multiple tools in MIMICS were used to segment each structure. The whole segmentation process could take upwards of 60 hours to complete per specimen, depending on the calcification of structures and clarity of articulations. Some very well calcified specimens required only about 10 hours to complete the segmentation.

Region Growing

Region Growing is a tool which is often useful for removing noise artifacts from the scans. It is also used to select continuous structures; essentially allowing a new mask to “grow out” from the selection point and continue to include connected voxels in the mask defined by the original threshold. Floating structure such as the pelvic and pectoral girdles are generally easily separated from the rest of the scan using this tool, taking care to include the distal segments when they are not abutting the proximal segments. When using Region Growing to remove noise, it is important to look throughout the scan to catch any missed parts of a structure, as areas with low calcification manifesting as hole-like artifacts are not uncommon in CT scans of cartilaginous fishes. Although Region Growing is one of the easier tools to use, in order to check the accuracy of the new mask, one must calculate the 3D model from the mask.

Edit Mask in 3D

Another tool that proved especially useful for segmenting chondrichthyan skeletons was Edit Mask in 3D (3D Edit). This tool allows the user to work in 3D to select and remove noise or structures which are not of interest at the time. One benefit to 3D Edit is the ability to visualize changes made in real time. 3D Edit can also be used to separate structures from one another. Separations are often useful in the branchial structures when the whole gill basket can be edited at once, and the floating structures can be separated into their own masks without having to start over with the original mask of the whole animal. Edit mask in 3D is fairly straight forward and is very powerful as long as articulations are clear and easily discernible. In cases where the articulations are tight or indistinct, another tool, Multiple Slice Edit, is more effective.

Multiple Slice Edit

Multiple Slice Edit proved to be an invaluable tool for cleaning up edges of structures and accurately separating two structures at articulation points. The connections between the palatoquadrate and meckel's cartilage or synarcual and scapulocoracoid are two examples of articulations where Multiple Slice Edit was used to obtain an accurate segmentation. In many animals, articulations are so tight, that the CT scan data, even at high resolution, does not show clear enough distinctions between structures for there to be enough space for Region Growing or 3D Edit to be used to accurately separate the structures. In Multiple Slice Edit, the segmenter has the opportunity to work voxel by voxel to select parts to remove or add to the structure.

Boolean Operations

Boolean Operations is a tool which can save a lot of time. Once a structure has been segmented, Boolean Operations can be used to subtract that structure from the rest of a mask, removing the need to cut it out of the rest of the scan a second time. Boolean Operations can also be used to unite two masks of the same threshold range. This is particularly useful when part of a structure has been inadvertently cut away when using one of the other tools. This tool also has an intersect function which is useful when noise is an issue in some areas of a scan at a certain threshold but not others. Once structures have been removed from the threshold, a narrower threshold can be used to remove noise, leaving only the structures which still need to be segmented.

Institutional abbreviations

Specimens for this work were borrowed from the following museum and institutional collections: **AMNH**, American Museum of Natural History (New York, NY); **BMNH**, British Museum of Natural History (London, UK); **BPBM**, Bernice Pauahi Bishop Museum (Honolulu,

Hawai'i); **CSIRO**, Commonwealth Scientific and Industrial Research Organisation (Hobart, Tasmania, Australia); **FMNH**, Field Museum of Natural History (Chicago, IL); **GMBL**, Grice Marine Biological Laboratory (Charleston, SC); **HUMZ**, Hokaido University Museum (Hokkaido, Japan); **LACM**, Natural History Museum of Los Angeles County (Los Angeles, CA); **MCZ**, Museum of Comparative Zoology at Harvard University (Cambridge, MA); **SIO**, Scripps Institute of Oceanography, San Diego, CA; **UF**, University of Florida (Gainesville, FL); **USNM**, United States National Museum, Smithsonian Institution (Washington, DC). Abbreviations are from the “Standard symbolic codes for institutional resource collections in herpetology and ichthyology: an Online Reference” (Sabaj, 2014). The specimens used for the segmentations presented here are listed in Appendix I.

Skeletal Structures

Table 3 is a comprehensive list of the skeletal structures segmented from the CT scans from the different groups of chondrichthyans, divided into structures found in sharks, batoids, and holocephalans. Most of these structures are visible in the figures while some are obscured by other structures and are only visible with removal of concealing structures or rotation of the segmented skeleton. Additionally, a small number of structures marked as present in the groups were only identifiable in one or a few specimens examined. Conversely, some structures which were expected to be found in the scans but were not visible in the segmentations, such as the anal fin in *Callorhinchus* and *Neoharriotta*, were not included.

Chapter 3: results

The completed segmentations of cartilaginous skeletons examined are listed in Appendix I. Representative segmentations from each order are shown in Figure 8. The phylogeny proposed by Naylor *et al.* (2012) has been used for aligning the taxonomic groups for the morphological comparisons presented (Figure 9). The original mission was to cover as much diversity as possible with one specimen per described family. Some families have great diversity in morphology and required increased coverage in order to represent the diversity. For example, the family Etmopteridae is represented by both the genera *Trigonognathus* and *Etmopterus*. Genera and species coverage was also increased in families where anatomical transitions are of greater interest. In the family Sphyrnidae, all species except for the Great Hammerhead (*Sphyrna mokarran*) were scanned in order for an undergraduate student to explore variation in post cranial anatomy.

Heterogeneity due to age, developmental stage, condition, size, and degree of calcification precluded using one set system for all segmentations. Heterogeneity of calcification was observed both among and within specimens. In general, we found that immature animals tend to be less calcified and thus more difficult to segment. As a result, some of segmentations carried out for taxa for which only juvenile specimens were available may be less accurate than those for which better calcified larger animals were used.

Carcharhiniformes and Orectolobiformes were generally easier to segment using data collected from both medical and high resolution scanners. While there was still variation among these two groups in terms of calcification, the majority showed good contrast in the scans allowing a better understanding of positioning and shape of articulations in both the larger animals and the smaller ones. In contrast with these well calcified animals, two species of ray,

Plesiobatis daviesi and *Hexatrygon bickelli*, were scanned but could not be segmented due to poor calcification (Figure 10). This difficulty in obtaining CT scan data with enough contrast to segment these species has been observed by other researchers (Mason Dean, pers. Comm.) and their soft skeleton was noted by Nishida (1990). The following provides a breakdown of observations from the segmentations organized by anatomical region, highlighting differences among taxa in addition to information on observations linked to the life history of some species.

Chondrocranium

The chondrocrania of chondrichthyans exhibit extensive diversity both in shape and calcification patterns (Figures 11-19).

Carcharhiniform sharks have a wide variety of chondrocranium shape (Figure 11). Some of the scyliorhinids have more squared chondrocrania while that of *Scoliodon* is markedly narrow and elongate with long pre- and postorbital processes while the closely related sphyrnids have very wide heads compared to head length. The preorbital and postorbital processes in the majority of Carcharhiniformes are more delicate looking than those in other shark orders. The rostral cartilage patterns observed in this order also show great variation from completely undetectable in the scans to a well-developed tripodial rostrum as seen in *Triaenodon* and *Scoliodon* (Figure 11.11-12).

The chondrocrania of the lamniform sharks, with the exception of *Mitsukurina* are generally dorso-ventrally compressed with some exhibiting large and robust rostral cartilage extensions (Figure 12). In *Mitsukurina*, the rostral cartilage is long and fragile (Figure 12.1). Both specimens of *Mitsukurina owstoni* examined showed breaks in the rostral cartilage.

The chondrocrania of the Orectolobiformes were well calcified and did not show the hole-like artifacts observed in some specimens in other orders (Figure 13). Like the

Carcharhiniformes, this family shows extensive variation among families with some more aquiline while others appeared robust and square.

Chondrocrania were poorly calcified in some of the deep sea Squalan sharks, including scans of specimens from Etmopteridae, Centrophoridae, and Somniosidae (Figure 14). The poor calcification was observed in both high resolution and medical scans. In other families, such as the Dalatiidae, there was no evidence of reduced calcification in this structure (Figure 14.12).

The Rajiformes exhibit extensive variation in rostral shape. Many species have long and sturdy rostral cartilages while a few have reduced rostral cartilage (Figure 15). With the exclusion of Platyrrhinidae, the chondrocrania of the Myliobatiformes lack a rostrum and are more boxlike than the other batoids (Figure 16). The Torpediformes generally have narrow chondrocrania except for *Narke japonica*, whose chondrocranium was proportionately much wider than the other three species examined (Figure 17).

The chondrocrania in the Hexanchiformes have pronounced antorbital and postorbital processes (Figure 18.5-7). Like the batoids, this order has a range of size and shape of rostral cartilages. The Chimaeriformes all have generally similarly shaped chondrocrania, with one striking difference between the families being the length of the rostral cartilage (Figure 19). Portions of the lateral line associated with the chondrocranium of the chimaeras were readily visible and could often be identified and segmented (Figure 8.13).

Branchial Arches

The branchial arches were often difficult structures to segment. As with most structures, very large or mature specimens often had better calcification in the branchial structures, leading to cleaner and more accurate segmentations. The form of the branchial arches were consistent across groups with a few exceptions. The Carcharhiniformes shark branchial baskets could be separated into two groups by general robustness, Scyliorhinidae and Proscyllidae as one group

and all other families together forming another group (Figure 20). In the Lamniformes, *Carcharias taurus*, *Odontaspis ferox*, and *Carcharodon carcharias*, did not have visible branchial rays whereas the other Lamniformes examined did (Figure 21). In *Lamna ditropis*, the branchial rays are dense while in the others, they are more spread out (Figure 21.5). In Orectolobiformes, the branchial arches appear more robust than the other shark orders (Figure 22). In Squaliformes, *Dalatias licha*, *Oxynotus caribbeus*, and *Squalus acanthias* also had more robust gill arches, although not as robust as the Orectolobiformes (Figure 23).

The majority of batoids had branchial arches that did not show much contrast from the surrounding tissues, thus, the constituent structures could not be separated. In these cases, the threshold had to be lowered considerably which concomitantly increased noise artifacts making segmentation especially challenging (Figure 24). Some skate specimens were scanned on both the medical and high resolution scanners in an attempt to get better resolution on the branchial structures. Although the resolution was greater on the high resolution scanner, the detail of the gill structures was still poor.

In the Myliobatiformes, two families, Platyrrhinidae and Zanobatidae, lacked traits shared by the other specimens scanned from this order. Both of these families exhibited a shorter and broader basibranchial while the other Myliobatiformes have elongated and narrow basibranchials and they were lacking the ventral extension from the basibranchial-ceratobranchial articulation (Figure 25). The electric rays, Torpediniformes, exhibited a very wide range of shape and robustness of all gill structures (Figure 26).

Pectoral Girdle

Scapulocoracoid

Representative variation observed in the scapulocoracoids of chondrichthyans is shown in Figures 27-35. In the Carcharhiniformes, Lamniformes, and Squaliformes, there are specimens

with spaces between the left and right sides of the scapulocoracoid. These breaks in continuation of the structures may be developmental in some cases or characteristic of the structure in others. In the orders without such spaces, the coracoid bars were much more robust.

Specimens with dorso-ventrally flattened scapulocoracoids generally have lower fins nearly parallel to the horizontal plane, including the batoids and orectolobiform sharks (Figures 29, 31-33 and 34.2). Those with deeper scapulocoracoids, such as mustelids and lamniforms, often have fins orientated at greater angles relative to horizontal with the propterygium originating higher on the coracoid (Figures 27-28).

In sharks, the scapulocoracoid is not attached to the vertebral column (Figures 27-30). In the batoids, the articulation between the synarcual and the scapulocoracoid is variable across taxa (Figures 31-33). The connection between the synarcual and the scapulocoracoid has two patterns. In the skates the connection is blunt with the suprascapula creating a T-shape whereas in the guitar fishes and wedgefishes, it is forked (Figure 31). Most of the Myliobatiformes have a ball and socket connection except for *Zanobatus schoenleinii* and *Platyrrhinoidis triseriata* which have the blunt connection and forked connections, respectively, as seen in the Rajiformes (Figure 32). The Torpediniformes, do not have a connection between the synarcual and scapulocoracoid (Figure 33). In *Pristis clavata*, there was no visible connection between the scapulocoracoid and the synarcual. This has previously been documented as an unknown state by Aschliman *et al.* (2012) (Figure 34.2).

The scapulocoracoid of the Chimaeriformes are shark-like but with thick and squared coracoids, unlike the curved and often thin coracoids of most sharks (Figure 35). The connection to the synarcual in the chimaeras is blunt while the entire scapulocoracoid remains narrow.

Basal Cartilages and Fin Rays

The Orectolobiformes exhibited variation in the degree of calcification of the pectoral fins, specifically in the basal cartilages and pectoral radials (Figure 36). In three genera, *Ginglymostoma*, *Stegostoma*, *Nebrius*, the pectoral radials were not visible at all while the basal cartilages were greatly reduced. In *Ginglymostoma*, no basal cartilages could be segmented. The reduced calcification observed here may be due to the age of the specimen as the closely related *Nebrius* had a small calcification of the basal cartilages (Figure 36). In contrast, both *Hemiscyllium* and *Chiloscyllium*, both from the family Hemicilliidae had robust pectoral radials (Figure 36). The pectoral fins of *Brachaelurus waddi*, *Orectolobus maculatus*, and *Parascyllium collare* were well developed, but not as robust as those in Hemicylliidae. The scapulocoracoids of the Orectolobiformes were well calcified in all scanned specimens. Along with some of the Orectolobiformes, the specimen of *Heterodontus francisci* also had reduced pectoral radials, likely attributable to the young age of the specimen.

Within the carcharhiniform sharks, the pectoral fins could easily be labeled aplesodic or plesodic. Aplesodic fins have truncated pectoral fin rays which may allow for greater maneuverability whereas plesodic fins have longer fin rays stiffening and streamlining the fins (Maia *et al.* 2012). Plesodic fins were seen in the faster swimming pelagic forms (Carcharhinidae, Sphyrnidae, etc) and the aplesodic form in the more benthic families (Scyliorhinidae, Proscylliidae, etc) (Figure 37). The basal cartilages in this order varied greatly in form with some well calcified such as specimens in the family Sphyrnidae and others poorly visible, including some of the scyliorhinids.

As with the Carcharhiniformes, the lamniform sharks had both aplesodic and plesodic pectoral fins. Aplesodic fins were observed in *Carcharias taurus*, *Mitsukurina owstoni*, *Odontaspis ferox*, and *Pseudocarcharias kamoharai*, while the *Alopias superciliosus*, *Carcharodon carcharias*, *Isurus oxyrinchus*, *Lamna ditropis* had plesodic fins (Figure 38).

The squaliform sharks exhibited a wide range of fusing patterns in the basal cartilages. Some species had three distinctly separate basal cartilages. Others exhibited fusing between all three structures, while others had fusing between the mesopterygium and propterygium, or between the mesopterygium and metapterygium (Figure 39). Many species did not have visible pectoral fin rays and those which were visible were considered aplesodic (Figure 39).

Pristiophoriformes and Squatiniformes both have basal cartilages that appear to be intermediate between shark and batoid morphology. *Pristiophorus nudipinnis* is more similar to sharks with the basal cartilages all directed posteriorly while *Squatina nebulosa* appears more batoid-like with the propterygium extending anteriorly. Both of these species have basal cartilage attachments to the scapulocoracoid that are more similar to those seen in sharks. They also do not have visible fin rays extending from the propterygium, instead they extend from the mesopterygium and metapterygium (Figure 40).

Myliobatiformes exhibited a lot of variation among the pectoral fins including size, shape, and position of the mesopterygium, degree of roundedness of the edges of the pectoral fins, and the presence or absence of cephalic lobes or cephalic fins (Figure 41). In most Myliobatiforms, there is an anterior extension of the propterygium and adjoining radials which support the snout. This extension was not observed in those families with cephalic lobes or cephalic fins (Mobulidae, Myliobatidae, and Rhinopteridae), nor was it seen in Platyrhinidae.

The majority of Rajiformes examined have the anterior tips of the propterygium broadly separated (Figure 42), however in two species, *Irolita waitii* and *Dactylobatus armatus*, the propterygium tips appeared narrowly separated (Figure 42.7). The pectoral fin of Pristidae is similar to that of the Rhinobatidae and Rhynchobatidae in both basal cartilages and fin rays (Figure 42.1).

Within the Torpediniformes, the basal cartilages of Hypnidae were distinct from those seen in the other families, with the propterygium and metapterygium being longer and the

mesopterygium being reduced (Figure 43). Hypnidae had the most visible pectoral fin rays while the other families had poorly calcified fin rays (Figure 43).

The hexanchiforms exhibited two patterns of basal cartilage calcification, one with the three basal cartilages as completely separate structures, and the other with the fusion between the propterygium and mesopterygium with the metapterygium separate. The frill shark, *Chlamydoselachus anguineus* and the bigeyed six gill shark, *Hexanchus nakamurai*, had separate basal cartilage structures while the sharpnose seven gill shark, *Heptranchias perlo*, exhibited fusion between the propterygium and metapterygium. The pectoral fin rays of the two Hexanchidae specimens had similar patterns while the fin rays of the frill shark were not very well calcified, but still appear to be narrower than those in the other two species (Figure 44).

The Chimaeriformes exhibited two trends. The Callorhynchidae has fin rays extending from the metapterygium and continuing in parallel beyond the end of the metapterygium while both Rhinochimaeridae and Chimaeridae have fin rays that continue around the posterior tip of the metapterygium (Figure 45). All three chimaera families have an enlarged anterior radial which articulates with the propterygium. Unlike the majority of sharks and batoids, the chimaeras do not possess three pectoral basal cartilages. They possess two, a propterygium and a metapterygium along with an enlarged anterior radial articulating with the propterygium (Didier, 1995).

Pelvic Girdle

Puboischiadic bar

The carcharhiniform puboischiadic bar exhibits substantial morphological variation across taxa (Figure 46). The Proscylliidae and most scyliorhinid sharks have fairly straight bar-like puboischiadic bars, some without a post pelvic process, and others with one or two. The size of the lateral prepelvic processes varies within scyliorhinids. Other Carcharhiniformes have more

curved puboischiadic bars, some less bar-like and more robust. The houndsharks in the family Triakidae exhibited the most extreme curvature among the Carcharhiniiformes examined (Figure 46.10).

The lamniform sharks had more plate-like puboischiadic bars although all had a recurved posterior edge. The puboischiadic bars of *Carcharias taurus* (Figure 47.2) and *Pseudocarcharias kamoharai* (Figure 47.4) were narrower than the other lamniforms. The scans representing *Carcharodon carcharias* (Figure 47.6) and *Lamna ditropis* (Figure 47.7) were derived from juvenile specimens. As a result their puboischiadic bars were not fully calcified.

The puboischiadic bars of the Orectolobiformes were more uniform in shape. Most of them were straight bar-like structures (Figure 48). The zebrashark, *Stegostoma fasciatum*, in the family Stegostomatidae was the only orectolobiform exhibiting substantial curvature (Figure 48.7). The main differences within this order are in the shape and size of the lateral prepelvic postpelvic processes. Heterodontiformes possesses a puboischiadic bar similar to those seen in the Orectolobiformes, but with more curvature (Figure 53.1).

In the squaliform sharks, the puboischiadic bars have slight curvature and are between the bar-like shape of the Orectolobiformes and the plate-like shape of the Lamniformes (Figure 49). The squaliforms exhibit all three states of postpelvic processes (zero, one, or two).

Pristiophoriformes and Squatiniformes are not easily aligned with any of the other orders. Both species lack the iliac process seen in batoids, keeping in line with their closer relationships to the sharks (Figure 53.3-4).

The batoids exhibit a wide range of shapes in the puboischiadic bar. However, all possess iliac processes of varying length (Figures 50-52 and Figure 53.2). Within the Rajiformes, there is a distinct separation in shape and robustness of the puboischiadic bars between the group described as Rhinopristiformes by Naylor *et al.* (2012) (Figure 50.1-3 and Figure 53.2) and the other Rajiformes (Figure 50.4-8).

The prepelvic processes are greatly extended in some of the Myliobatiformes, while others have either small prepelvic processes or smooth rounded anterior edges (Figure 51). Platyrrhinidae is the only myliobatiform with a straight puboischiadic bar which is reminiscent of the shape typical for the Rajiformes (Figure 51.2). No representatives in this order have the postpelvic processes seen in some of the sharks and the Rajiformes.

The iliac processes of the Torpediniformes are well developed (Figure 52). In Narcinidae and Narkidae, the iliac processes are large and curved whereas they are more similar to the other batoids in Hypnidae and Torpedinidae. This order also possesses extended lateral prepelvic processes.

The Hexanchiformes all have shield-like puboischiadic bars (Figure 53.5-6). *Chlamydoselachus anguineus* has a very elongate puboischiadic bar while those of *Hexanchus nakamurai* and *Heptranchias perlo* have nearly equal lengths and widths.

The puboischiadic bars of the Chimaeriformes are similar to their scapulocoracoids with elongated lateral processes extending posteriorly and dorsally (Figure 54). In all specimens except for *Neoharriotta carri* (Figure 54.5), the left and right sides of the puboischiadic bar are unconnected. This conflicts with Didier (1995) who states that all chimaeriforms except for Callorhynchidae have puboischiadic bars connected at the symphysis. The lack of connection observed in the specimens studied here may be due to the age of the specimens or other factors which could have caused reduced calcification.

Basal cartilages and Fin rays

Comparisons among the pelvic fin structures were made difficult by the mix of male and female specimens scanned and segmented. Fin ray counts and metapterygium shape can vary greatly between the two sexes. With these differences, conclusions drawn from the variations among specimens could not be accurately attributed to differences between species and sexual

dimorphisms within species. Additionally, pelvic fin rays exhibited marked variation in calcification, making it especially difficult to draw conclusions from the medical scans. Figure 55 shows a comparison of well calcified and poorly calcified pelvic fins in various chondrichthyan orders.

Vertebral column

For the majority of specimens scan resolution prevented accurate vertebral counts from being completed. In some batoids the vertebrae appear to be fused at the tail even in the high resolution scans, further contributing to the difficulty of accurate counts.

Excluding Hexanchiformes, Heterodontiformes, and Chimaeriformes, all orders contained at least one scanned specimen with vertebral ribs with enough calcification to be visible in the segmentations (Figure 56). Lack of visibility of ribs in scans does not definitively mean they are not present, only that they were not visible in the representative specimens examined. For example, in the three etmopterids examined, two *Etmopterus* (*E. splendidus* and *E. shekoi*) and *Trigonognathus kabeyai*. Ribs were visible on the two *Etmopterus* but not on the *Trigonognathus* (Figure 56.7-9). It is also worth noting, that no vertebral ribs were seen in the specimen of *Heterodontus francisci* examined, however, they are reported as being present, extending from the first 30 vertebrae in Daniel, (1922).

While most orders had a mixture of specimens with and without vertebral ribs, all of the Torpediniformes examined had vertebral ribs although rib length varied among specimens. In Torpedinidae, Narkidae, and Narcinidae, the anterior vertebral ribs are short and the posterior ribs are much longer. In contrast, the vertebral ribs of Hypnidae are longer along the entire length of the vertebral column. In Torpedinidae, the dorsal tips of the lateral stays of the synarcual are broader while in the other three families they are narrower and more rounded.

The scan of the frill shark, *Chlamydoselachus anguineus*, showed a unique calcification pattern in the vertebral column. The vertebrae were most easily segmented towards the head and tail, but there was a decrease in calcification towards the middle of the body. The vertebrae immediately anterior and posterior to the area of reduced calcification are reduced in size, only creating a half circle compared to the whole circle vertebrae in closer proximity to the head and tail (Figure 57.1). Another hexanchiform shark, *Hexanchus nakamurai*, had vertebrae with reduced calcification throughout the vertebral column (Figure 57.2) while a third Hexanchiform, *Heptranchias perlo*, had a well-calcified vertebral column (Figure 57.3). The vertebral column of *Echinorhinus brucus* was similar to that in *Hexanchus nakamurai* (Figure 56.7).

The vertebral column of the chimaeras exhibited a wide range of calcification patterns. Some species had solid vertebral columns which were very well calcified whereas others had reduced calcification throughout the vertebral column or just at the distal ends (Figure 58). Most of the Chimaeras had a short synarcual which was deeper than it was long, except the synarcual of *Rhinochimaera atlantica*, which was longer and the dorsal extension with which the dorsal spine articulates beginning about midway along the synarcual base (Figure 58.6).

In several of the scans there are locations in the vertebral columns with abnormal characteristics. At the start of the last quarter of the vertebral column of *Centroscymnus owstoni*, there are two vertebrae which appear to be fused (Figure 59.1). Similarly, in *Bythaelurus canescens*, there are multiple locations midway down the vertebral column with enlarged vertebrae (Figure 59.2). In the middle of the vertebral column of *Rhizoprionodon terraenovae*, there is a section of vertebrae with increased girth (Figure 59.3).

Links to Life History

Predation

Some scans provided us with opportunities to see what made up the last meal the animal had consumed prior to being collected (Figure 60). The stomach contents have variously included parts of fish, most likely bait used to catch the specimen, and whole animals including bony fish, crustaceans, and other chondrichthyans. Other specimens had gut contents that had been digested to such an extent that they were no longer identifiable. One specimen, *Squatina nebulosa*, which was caught in a trawl net, had small fish and shrimp in the mouth; these were likely pushed into the mouth of the animal during capture but could also be an instance of predation (Figure 60.12).

Reproduction

In four of the scans which had been completed at the time of writing, the specimens were mature females within which developing embryos or egg cases could be identified (Figure 61). Specimens with developing offspring had structures that could be identified as eggs or egg cases, however most did not have visible skeletons of the offspring within these structures. In the specimen of *Sphyrna corona* 22 embryos were identified by the number of visible vertebral columns associated with paired lenses (Figure 61.4). Past work on this species suggests a litter size of only two pups (Compagno, 1984). Other species with eggs or egg cases visible were *Anacanthobatis folirostris*, *Bythaelurus canescens*, and *Aptychotrema vincentiana*.

Chapter 4: Discussion

Previous Work

Previous studies of chondrichthyan anatomy have generally been restricted to comparisons among closely related species or a small number of distantly related taxa (Garman, 1913, Nishida, 1990; Shirai, 1992 & 1996; de Carvahlo 1996; and Goto, 2001). The data presented here are intended to provide a balanced taxon sampling across all of the extant lineages. We have strived to bring attention to the rich source of underappreciated information that has evolved in parallel with bony fishes and tetrapods by presenting 3D detailed data of the variation in skeletal morphology exhibited in these animals.

Additions from this Study

At the time of writing, skeletal anatomy had been segmented for one or more specimens in 13 Orders, 55 Families, 88 Genera, and 97 Species. The families currently without representation are Cetorhinidae, Megachasmidae, Rhincodontidae, Pseudotriakidae, Hexatrygonidae and Plesiobatidae. Continuation of the scanning and segmentation is expected to result in coverage of nearly every currently described genus, some genera with an abundance of diversity in skeletal morphology will have multiple representatives in an effort to cover that diversity. Coverage of genera is dependent upon locating whole body specimens of mature or large individuals which meet the requirements for scanning outlined in Chapter 2. The completed digital skeleton reconstructions are publicly available through the Tree of Life website, <http://sharksrays.org>.

Increased calcification generally leads to an increase in the radiopacity of the skeletal structures. There are multiple potential causes for the reduced calcification observed in different

specimens. These include the method of preservation used, habitat, depth, and age of the specimen at capture. In general, larger, adult specimens had greater calcification than juveniles or embryos.

Calcification trends were observed in various orders and families. Some groups, such as the deep sea squaliform sharks have generally well calcified skeletons except for the chondrocrania many of which had areas with reduced calcification. The unexpected reduction in calcification created hole-like artifacts even when very broad threshold ranges were used during segmentation. In some cases, such as the scan of *Trigonognathus kabeyi* (Figure 14.7) these artifacts made it difficult to visualize the general shape of the chondrocrania.

Some batoids, such as the electric rays, often had very robust and well calcified gill structures while others, including the Anacanthobatids, had poorly calcified gill structures which failed to show up clearly without extensive noise artifacts even when scanned with the high resolution scanner at the AMNH. The reduced calcification observed in the chondrocrania and branchial arches of some specimens, particularly those which were scanned on the high resolution scanner, is likely due to the young age of these specimens. The size restrictions for the high resolution scanner at the AMNH are more restrictive than those on the medical scanners, requiring animals to be smaller and likely younger if they are to be scanned at high resolution.

Drawing conclusions from segmentations of scans from animals whose skeletal elements were not clearly visible is difficult. In some instances, structures that have been well documented by other researchers through dissection and staining approaches were not visible in our CT scans (i.e. ribs in *Heterodontus* and pectoral radials in some orectolobiforms) (Daniel 1922 and Goto 2001). Lack of visibility in CT scans should not be taken as proof that a structure does not exist. It can sometimes only mean that the structure was not sufficiently calcified to be distinguished from background noise in the scan.

Future Directions

Increased Coverage

The research presented in this thesis has nearly complete representation at the family level. While this has revealed extensive anatomical diversity among chondrichthyans, our reliance on single representatives for each family likely under-represents the total anatomical diversity. There are several families, for example *Sphyrna*, that contain considerable diversity at the genus level. The continuation of the chondrichthyan Tree of Life project will attempt to obtain representation at the generic level to augment the current study. As with families, there are constraints on genera. Representatives of some genera will be difficult and potentially impossible to cover at this time due to the size of the specimens or the lack of whole body specimens in museum collections.

In addition to expanding generic level coverage, we plan to explore the differences both among and within species. There is undoubtedly interspecific variation by gender and developmental stages (Feduccia & Slaughter 1974; Ellis & Shackley 1995; Summers *et al.* 2004). Further work should give us a greater understanding of such individual variation and in doing so, will likely help increase our understanding of the primary drivers of differences in patterns of calcification, such as influence of specimen age.

We anticipate that the data collected in this study will prove especially useful both for those interested in estimating phylogenetic relationships from anatomical data and those interested in exploring morphological evolution in chondrichthyan fishes. Such studies will allow us to examine the incidence of morphological character diversification and convergence. Such an analysis has not been attempted in the current study as it was considered beyond the scope of the current work. The current study is strictly a baseline survey that will be foundational, but not sufficient for a formal morphological phylogenetic study of the group. A denser sampling of trait

variability within species and over ontogenies will be required before such a study can be attempted. We anticipate that this will be pursued in the future.

More High-Resolution Scans

The majority of CT scan data collected for the work presented here have been collected using Medical grade CT scanners. A small selection of scan data have been collected with a high-resolution scanner. Short time requirements and wider size ranges make using the medical scanners more efficient, although, the resolution is dramatically reduced, even with the addition of the new Dual-Source Multidetector CT scanner.

Recent work at the American Museum of Natural History, AMNH, has reduced the time required to complete full high-resolution scans by adjusting the settings on the high resolution scanner. When we first began using the high-resolution scanner, each specimen required 5-6 hours to scan in addition to time required to format the scans to be read by the segmentation software. The new time requirement is less than an hour for many specimens. The new settings require good calcification as they were developed for osteological studies. Unfortunately, batoids with wide “wingspans” do not lend themselves to the faster scanning protocols as their width requires the use of a tiling function which precludes the use of the new settings. Further advances may remedy this as well. Size restrictions for the high-resolution scanner continue to restrict the specimens which could be scanned in high resolution.

Cartilage Staining

The age of a specimen appears to have a large impact on the quality of the scan data. Younger specimens tend to be less calcified in many areas of the skeleton, reducing the already low radiopacity of the cartilage. Two species of ray, *Plesiobatis daviesi* and *Hexatrygon bickelli*, yielded particularly poor scans. Both are large, deep water rays with relatively soft and flexible

skeletons. These two species are likely to be good candidates for staining techniques. There are multiple staining techniques used in CT scanning including Potassium and Iodine stains which increase the radiopacity of the cartilaginous elements (Metscher *et al.* 2009; Gignac & Kley 2014; Descamps *et al.* 2014; and Davis 2014). Some methods permanently stain the cartilage and use highly toxic chemicals which may create problems for future work on the specimens (Descamps *et al.* 2014), however others are reversible (Metscher *et al.* 2009; Gignac & Kley 2014 and Davis 2014). As many specimens used for this CT scanning work are rare and are borrowed from museum collections, nondestructive staining methods are preferred.

MRI

While CT scans are especially well suited to the exploration of skeletal morphology of chondrichthyans, soft tissue cannot be cleanly segmented with these data. Magnetic Resonance Imaging (MRI) is generally preferred for soft tissue visualization, including muscles, liver, spiral valve, brain, kidneys, etc, in addition to the skeletal structures. Currently, segmenting MRI data is more time consuming than CT scan segmentation and requires a different suite of computational tools within the Mimics Software. MRI segmentations also require more extensive smoothing to the structures than is generally the case for CT scans, likely causing a reduction in the accuracy of the structure segmentations.

Conclusions

Using CT scan segmentation, digital models of the skeletal anatomy of chondrichthyan fishes can be created without the necessity of dissecting specimens, thus preserving the specimens for future work on other structures and systems not visible in CT scans. The non-destructive nature of CT scanning allowed us access to many rare and fragile specimens from various museum collections.

Data presented here represent a preliminary collection of observations in the diversity of skeletal anatomy in chondrichthyan fishes. These data do not contain enough coverage of variation for proper studies of the diversification of morphological characters. However, with a greater sampling of specimens to cover potential individual variation within a species, these data could be used for those types of studies and currently form an important foundation for these future studies.

Within Reiff's Inquiry Wheel (2002), the segmented skeletons represent the source of observations from which problems are defined and questions for further research are formed. The current study sets the stage for future projects which may investigate the relationships between calcification levels and life history traits, or the effect of preservation methods on the radiopacity of cartilaginous skeletons. The continuation of segmentations to coverage of nearly every described genus will lead to more observable trends and thus further questions to be investigated.

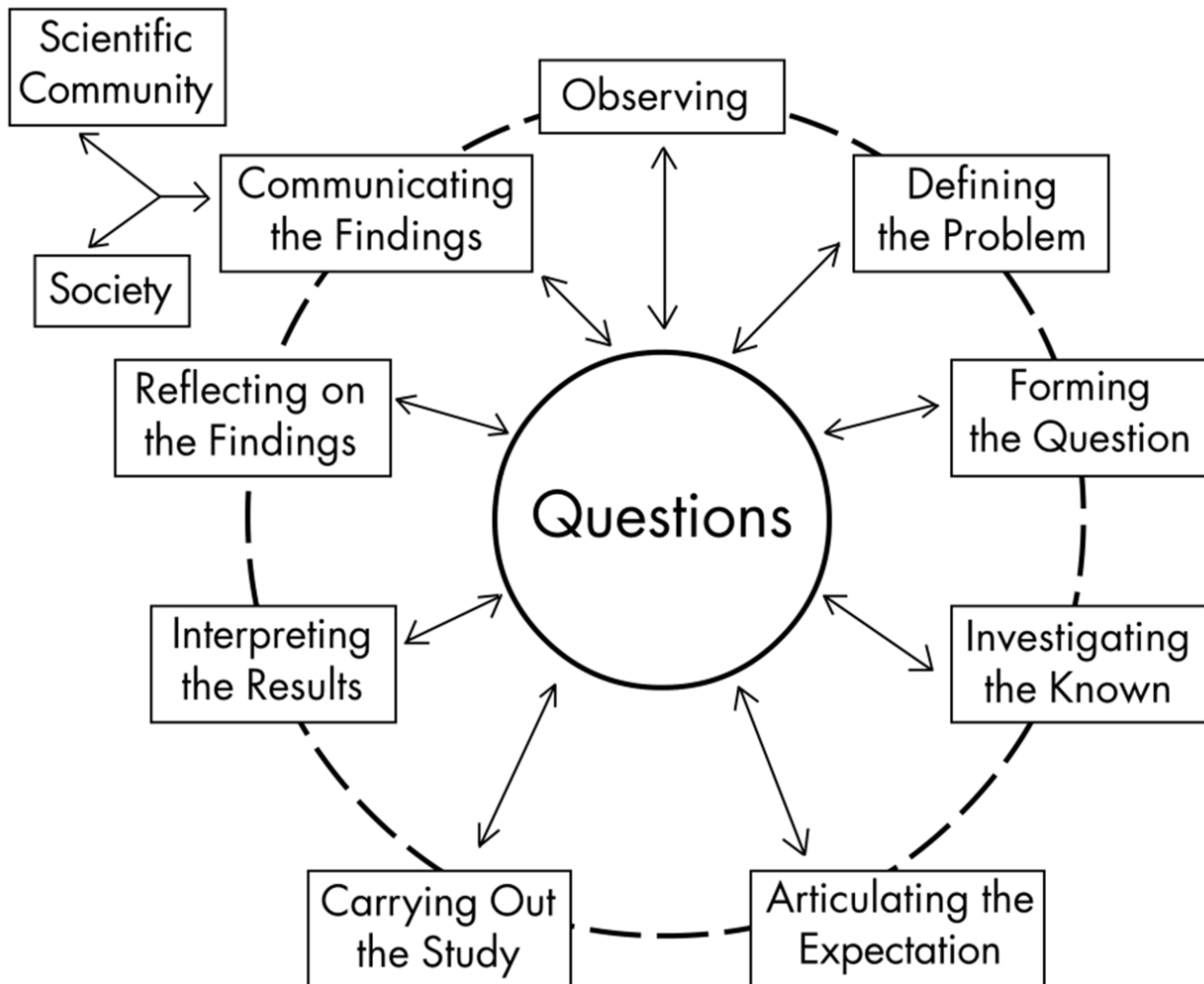


Figure 1. The Inquiry Wheel, Stages of Scientific Inquiry (from Williams, 2004 after Reiff, Harwood, and Phillipson, 2004).

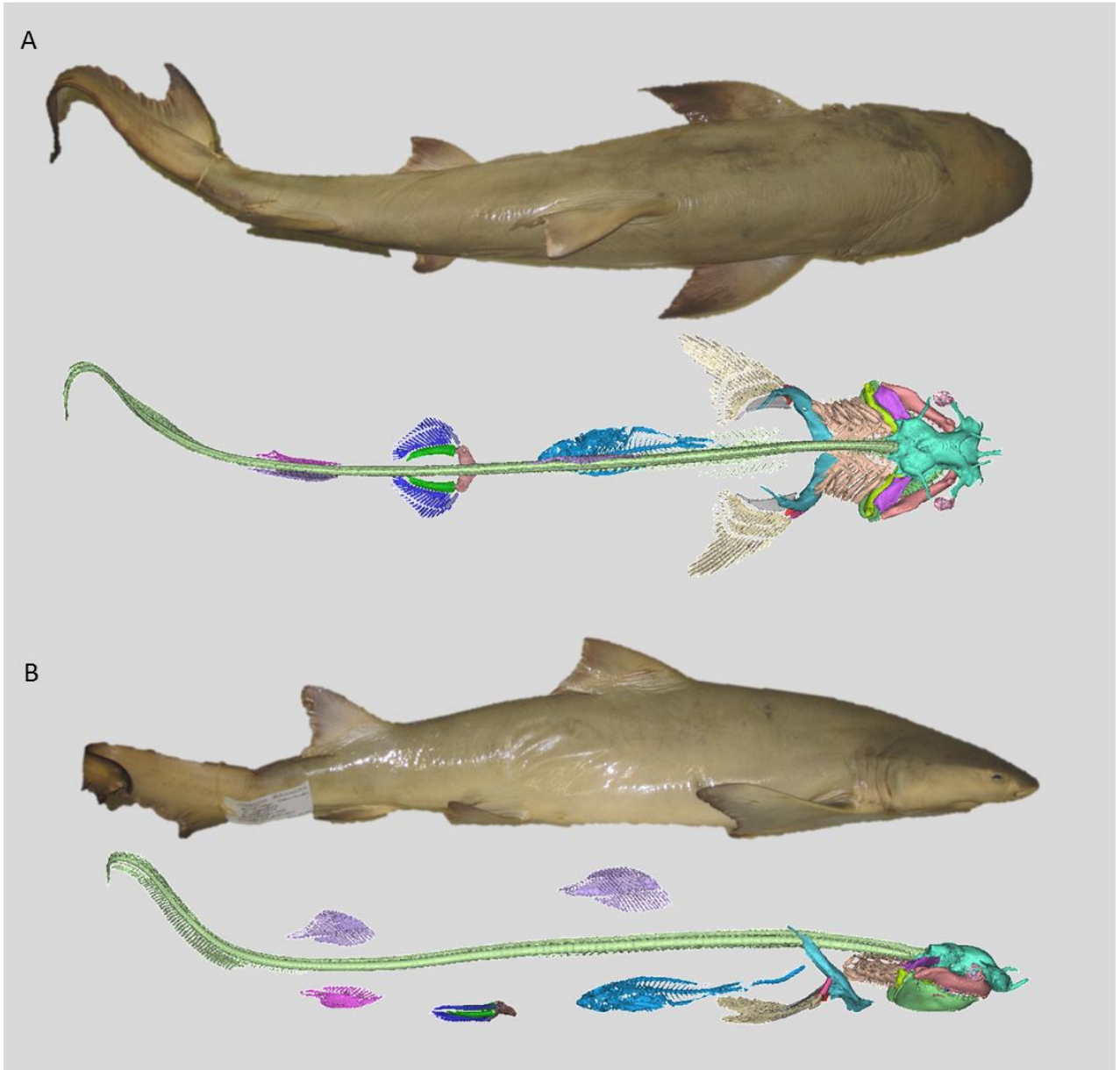


Figure 2. Dorsal (A) and lateral (B) views of an ideal specimen, as outlined in Table 1, with the completed segmentations in the same views.



Figure 3. Examples of radiographs used to determine scanning candidacy; A, *Glaucostegus typus*; B, *Platyrhinoidis triseriata*; C, *Eusphyra blochii*; D, *Stegostoma fasciatum*.

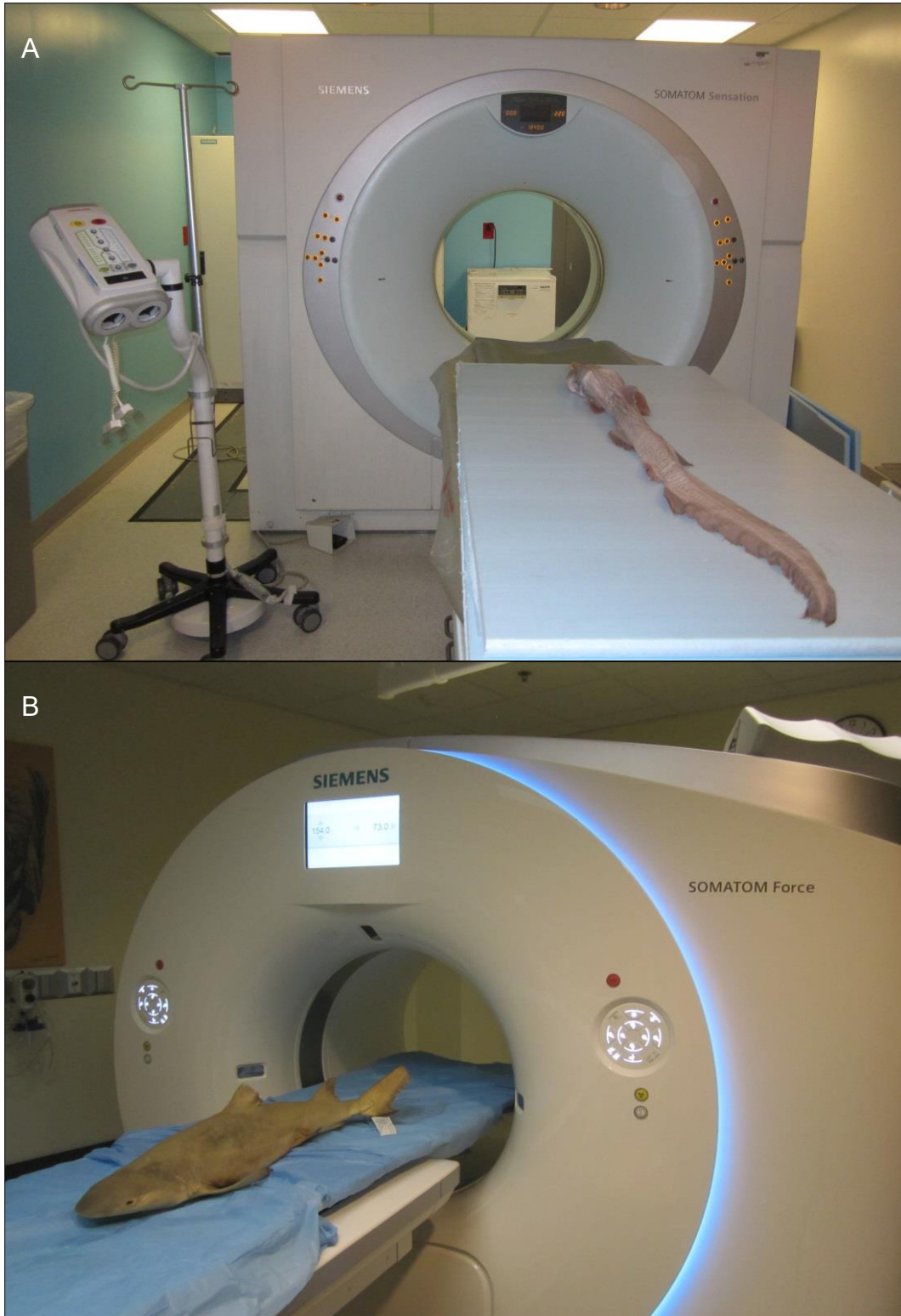


Figure 4. Specimens prepared for scanning on the Somatom Sensation, SSCT scanner (A) and Somatom Force, DSCT scanner (B) located at the Medical University of South Carolina.

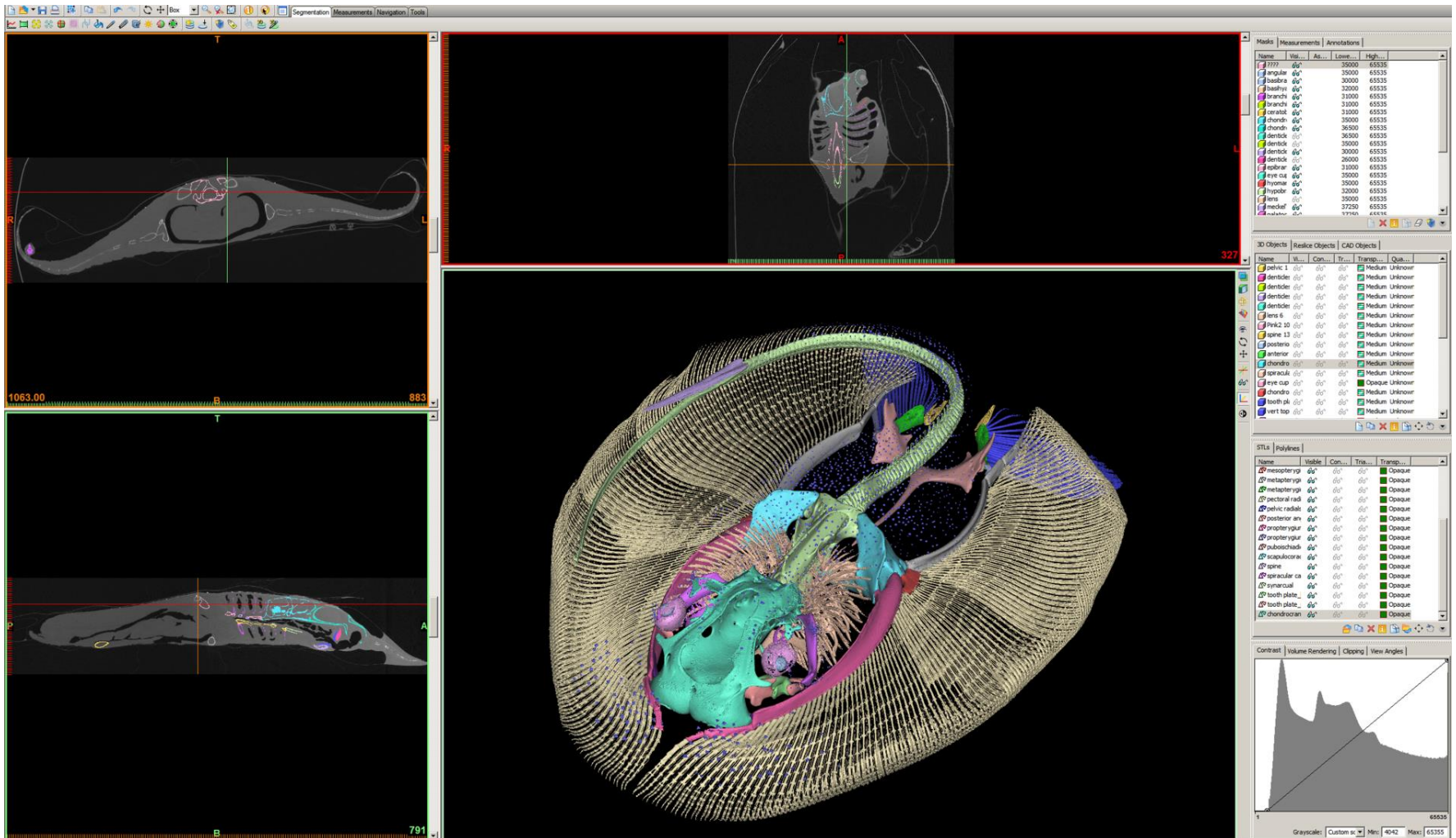


Figure 5. Mimics segmentation software with the scan of *Potamotrygon motoro*.

A



B

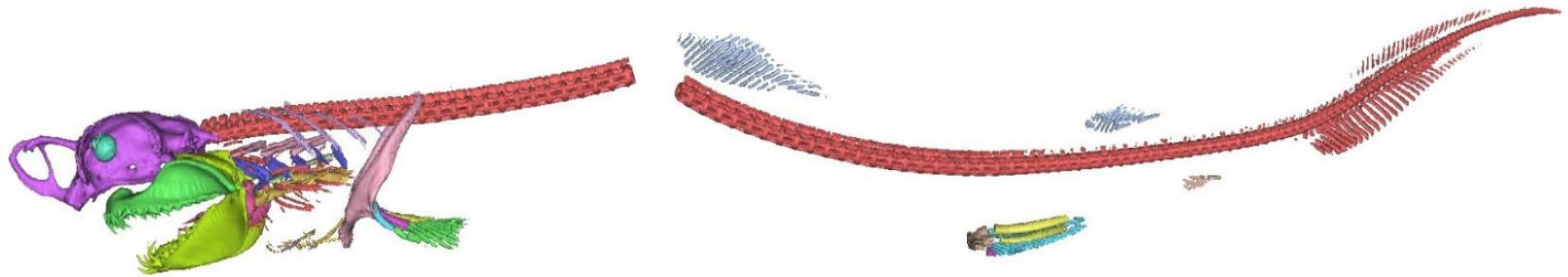
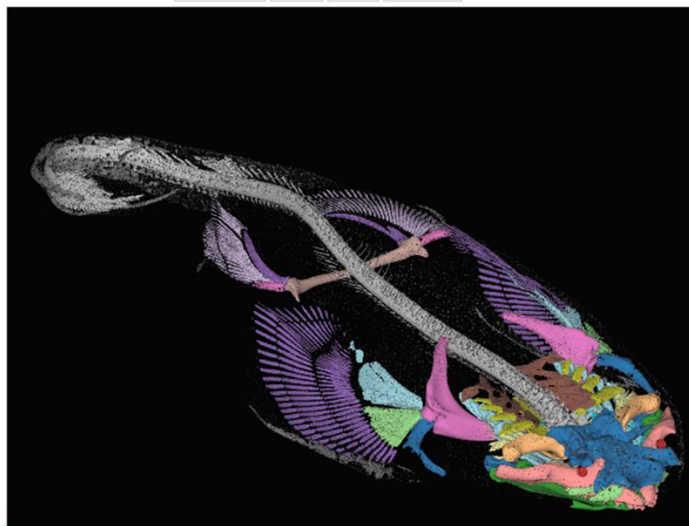
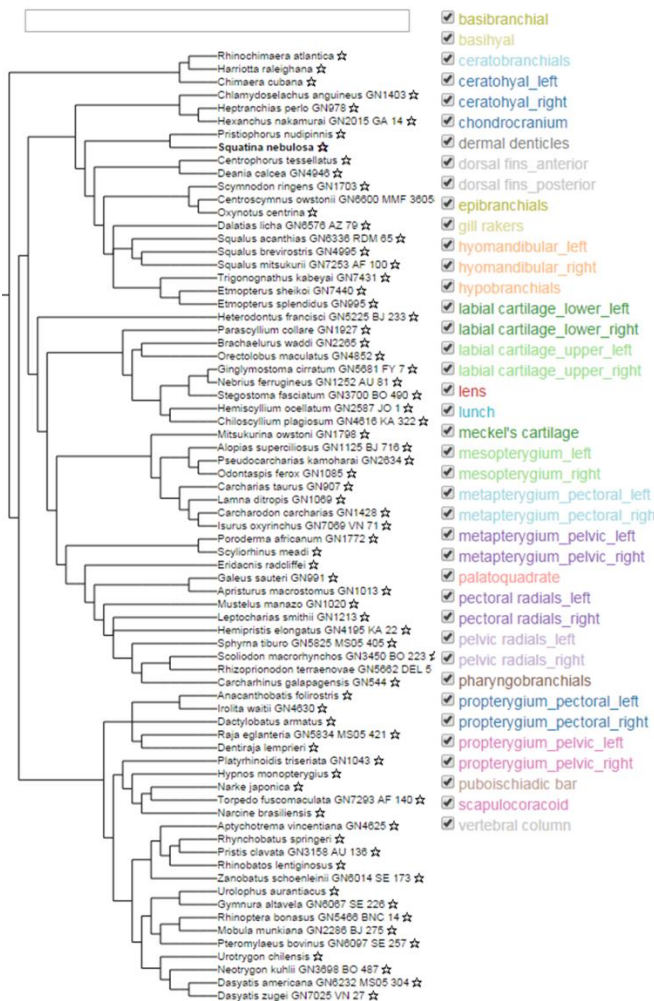


Figure 6. Initial thresholding stage (A) and final completed segmentation (B) of a specimen of *Pseudocarcharias kamoharai*.

Chondrichthyes: Tree of Life

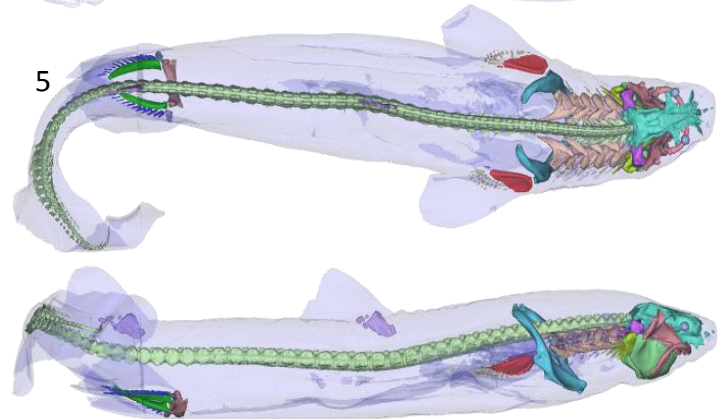
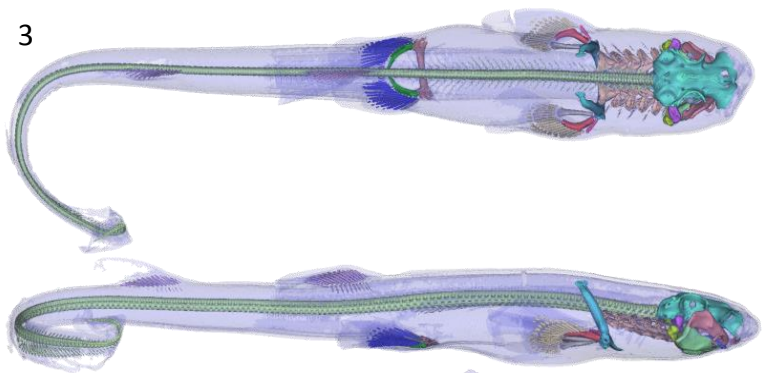
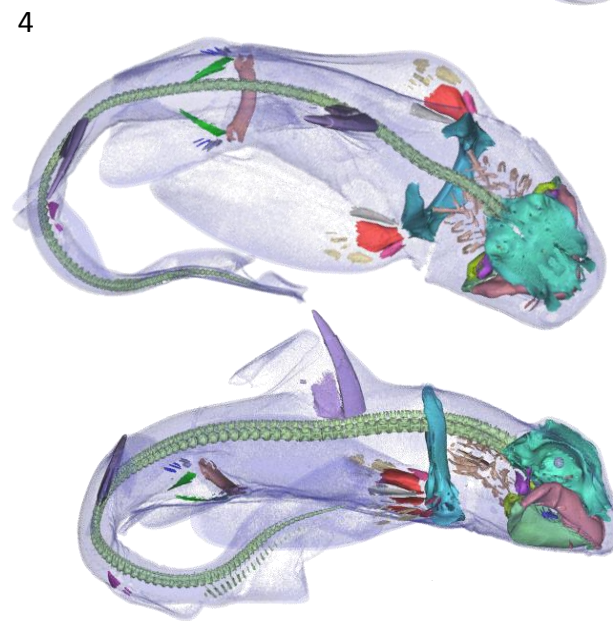
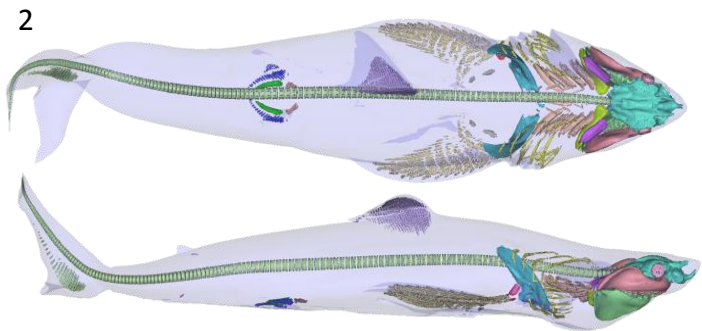
Phylogeny Atlas DNA Anatomy

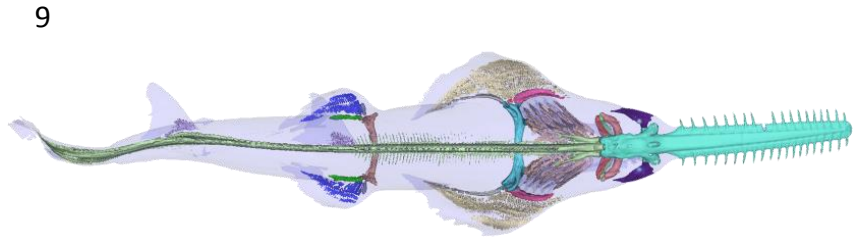
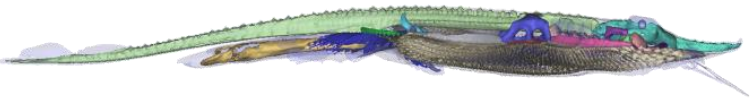
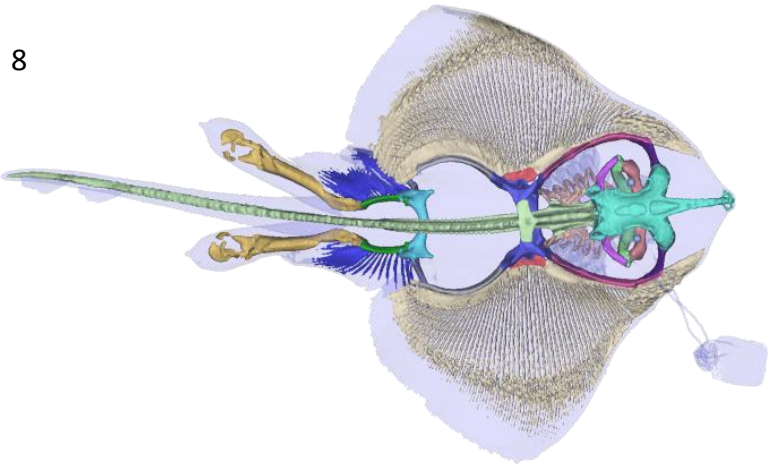
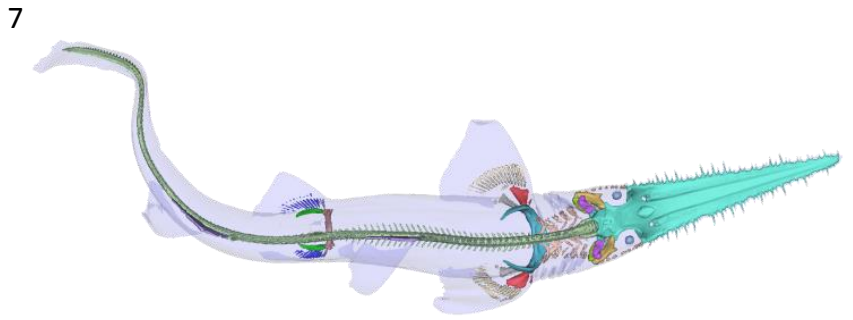
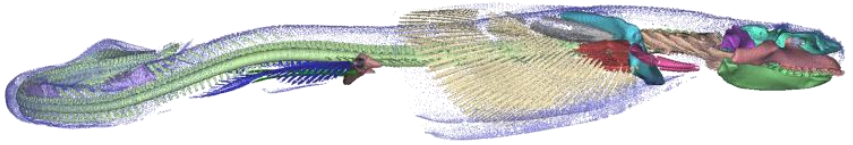
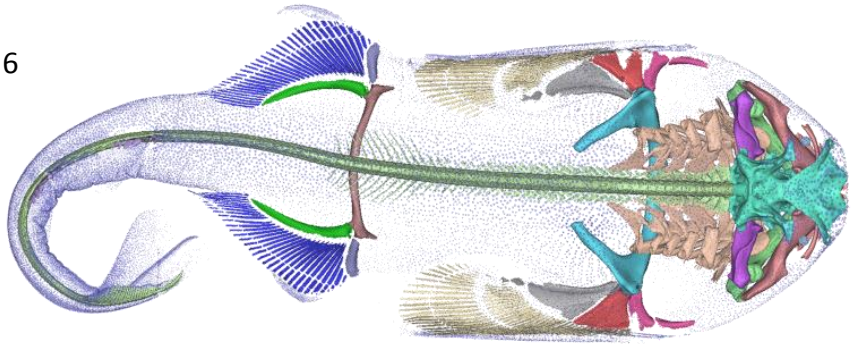
Contact: Gavin Naylor



Lock Delete Focus Colours

Figure 7. Example of the anatomy portion of the chondrichthyan Tree of Life Project website with the completed segmentation of *Squatina nebulosa*.





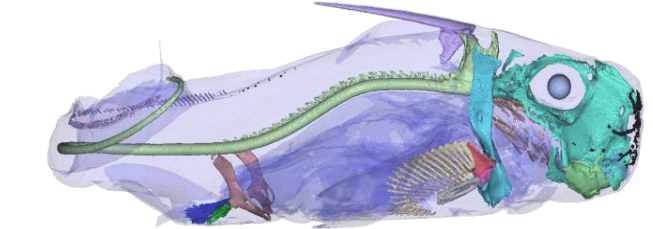
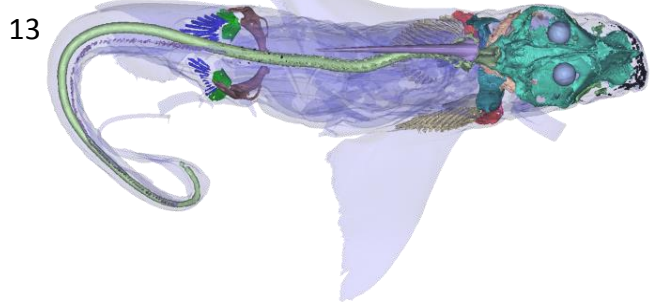
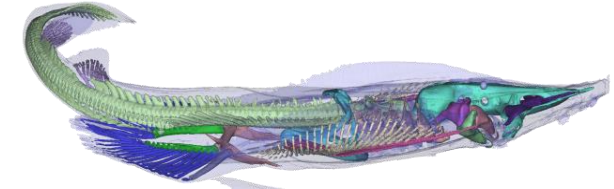
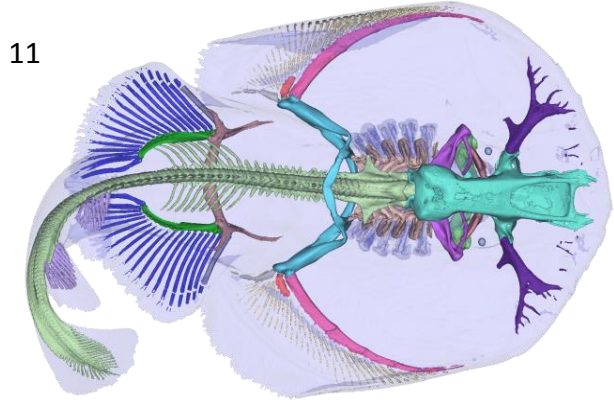
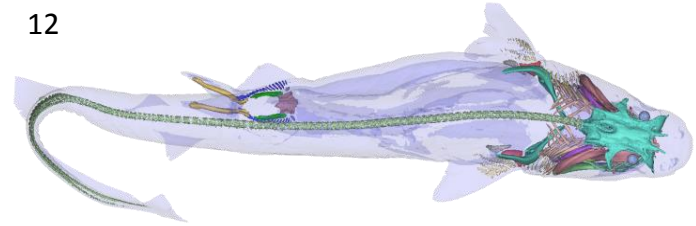
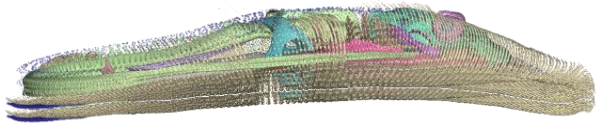
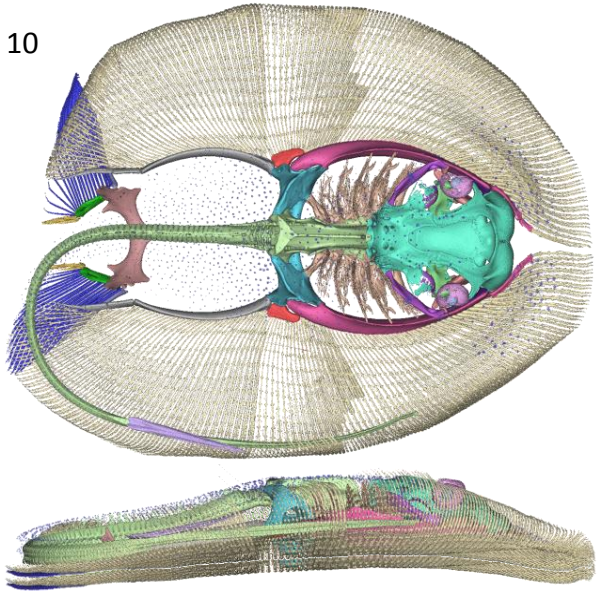


Figure 8. Dorsal and later views or representative segmentations from each chondrichthyan order. 1, Charcharhiniformes (*Rhizoprionodon terraenovae*); 2, Lamniformes (*Carcharodon carcharias*); 3, Orectolobiformes (*Chiloscyllium plagiosum*); (D) Heterodontiformes (*Heterodontus francisci*); 5, Squaliformes (*Dalatias licha*); 6, Squatiniformes (*Squatina nebulosa*); 7, Pristiophoriformes (*Pristiophorus nudipinnis*); 8, Rajiformes (*Raja eglanteria*); 9, Pristiformes (*Pristis clavata*); 10, Myliobatiformes (*Potamotrygon motoro*); 11, Torpediniformes (*Narcine brasiliensis*); 12, Hexanchiformes (*Hexanchus nakamurai*); 13, Chimaeriformes (*Hydrolagus novaezealandiae*). Skeletal element color coding: dark purple, antorbitals; black, lateral line (only visible in chimaera); turquoise, chondrocranium; pink, eye cup; pale blue, lens; coral, palatoquadrate; shamrock green, meckel's cartilage; blue, basihyal; green-yellow, ceratohyals; purple, hyomandibula; peach, branchial arches, yellow, extrabranchials; cyan, scapulocoracoid; magenta, pectoral propterygium; red, mesopterygium; gray, pectoral metapterygium; pale yellow, pectoral radials; pale red, puboischiadic bar; lilac, pelvic propterygium; green, pelvic metapterygium; deep blue, pelvic radials; orange, claspers; lavender, dorsal fins; fuchsia, anal fin; pale green, synarcual and vertebral column; transparent blue, skin.

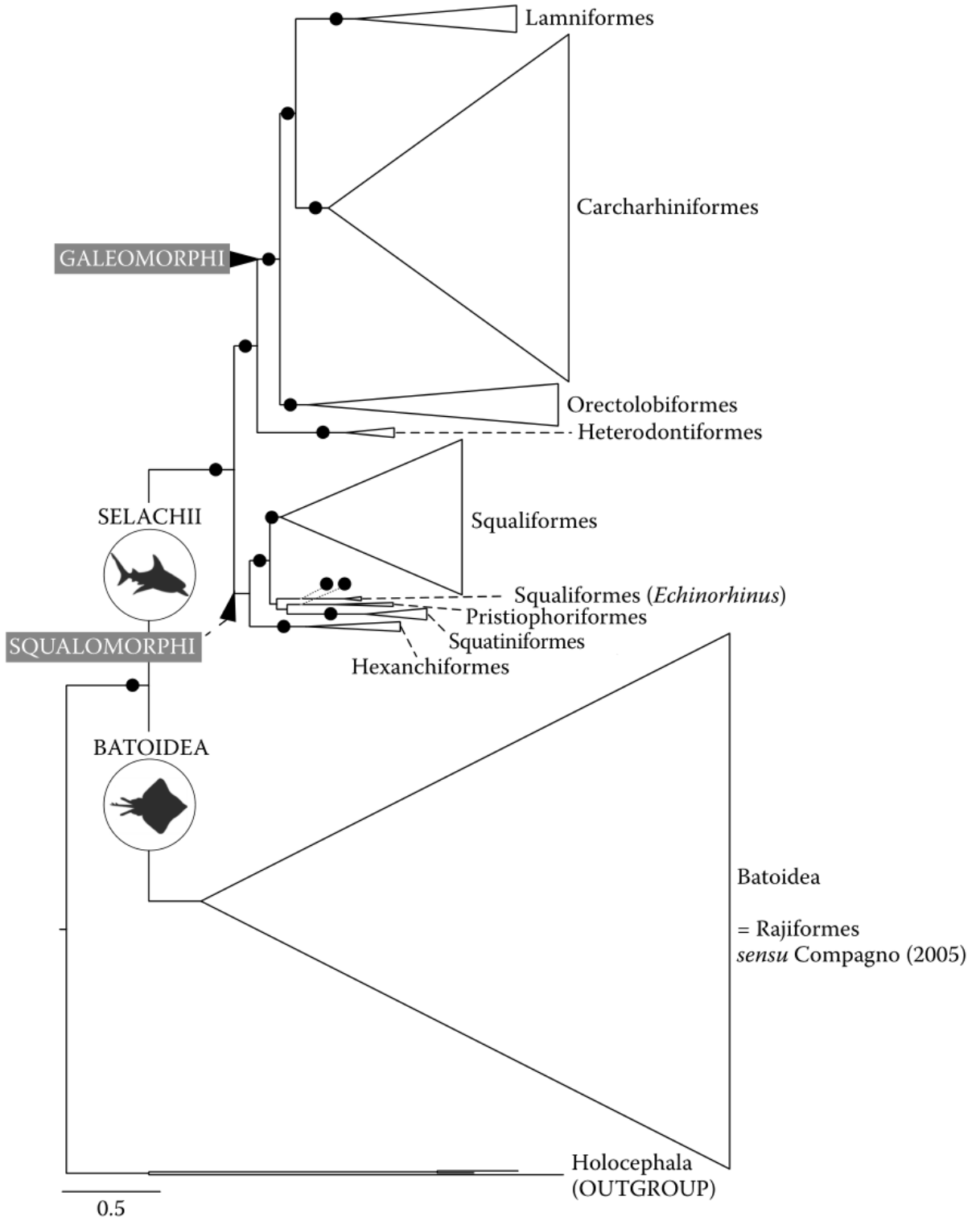


Figure 9. Hypothesis of phylogenetic relationships in Chondrichthyes based on Mitochondrial DNA analyses; Modified from Naylor *et al.* (2012)

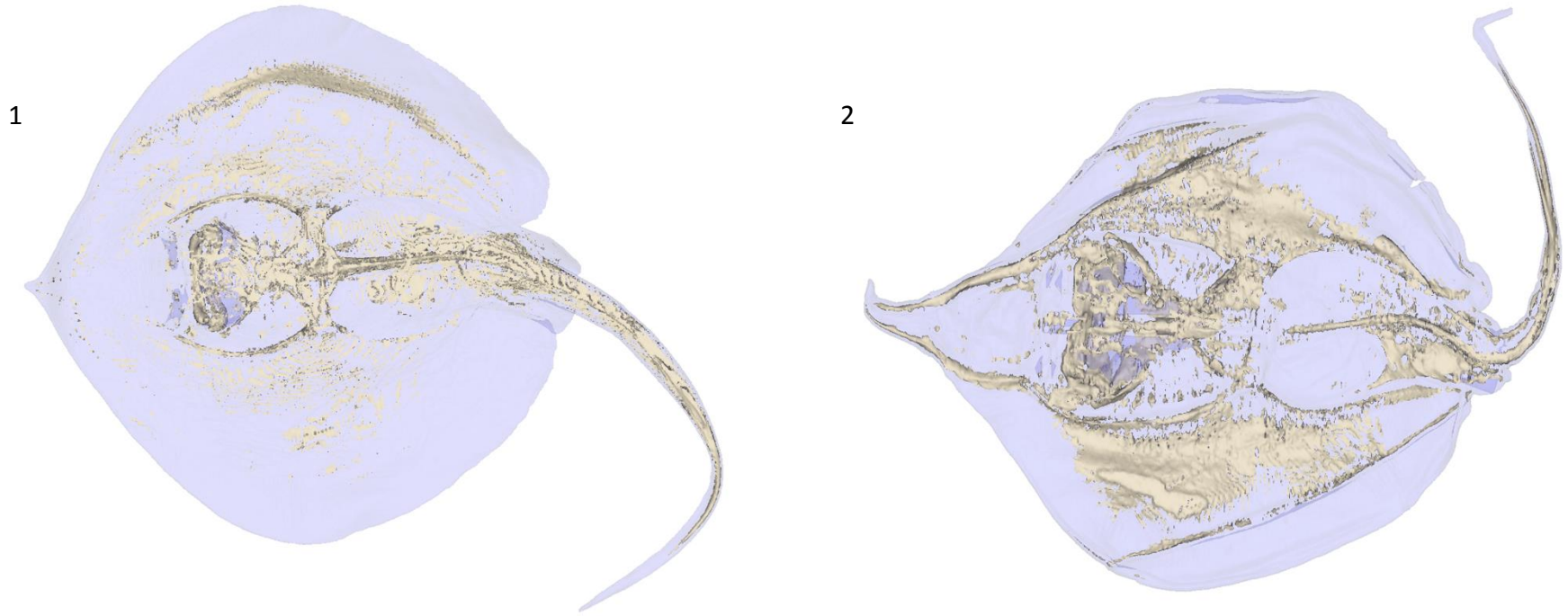


Figure 10. Examples of two species with poor calcification; 1, *Plesiobatis daviesi* and 2, *Hexatrygon bickelli*.

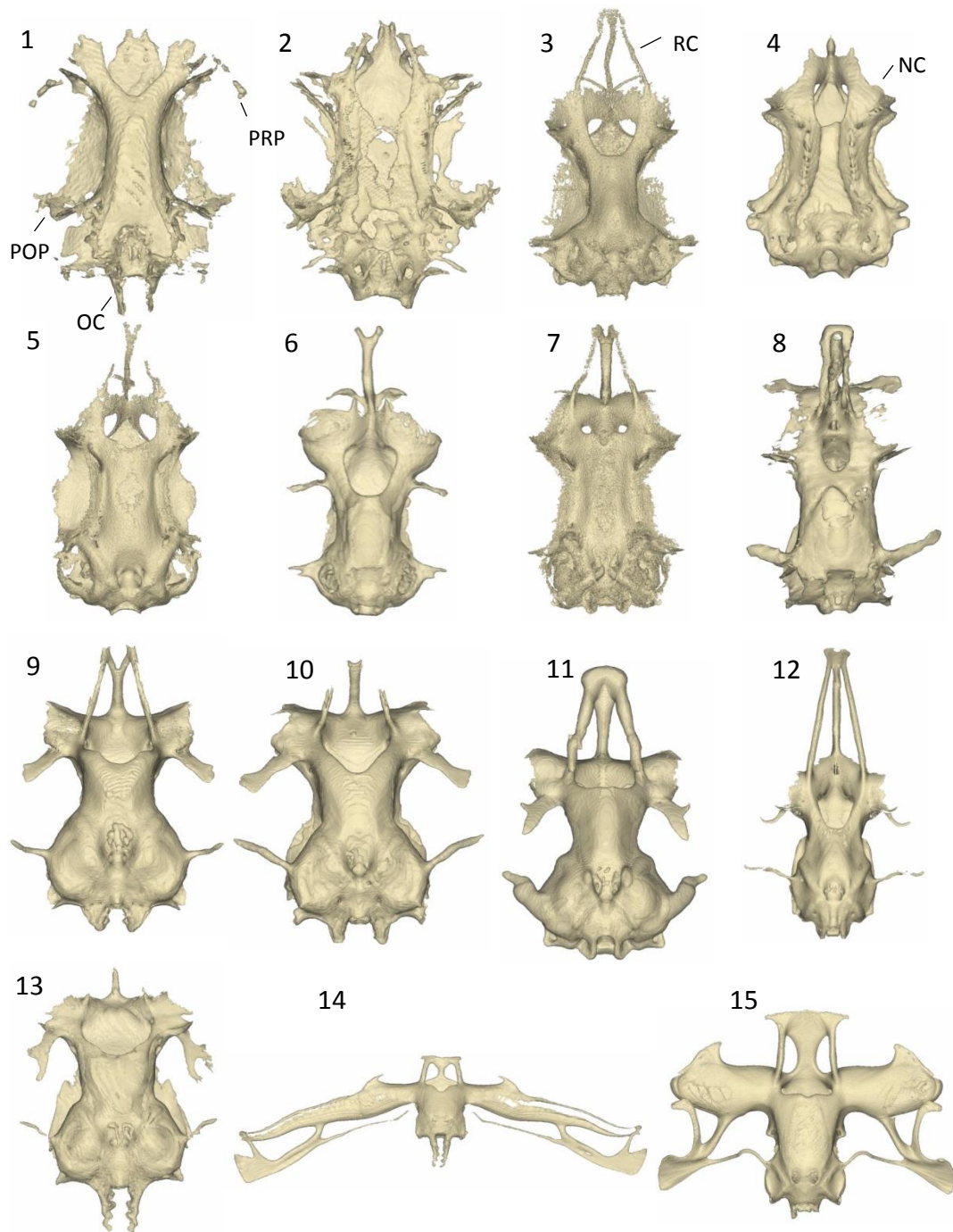


Figure 11. Chondrocrania from chondrichthyans showing morphological diversity across the order Carcharhiniformes. 1-4, Scyliorhinidae (*Bythaelurus waddi*, *Cephaloscylium isabellum*, *Galeus sauteri*, and *Schroederichthys chilensis*); E Proscyllidae (*Eridacnis radcliffei*); 6, Leptochariidae (*Leptocharias smithii*); 7, Triakidae (*Mustelus manazo*); 8, Hemigaleidae (*Hemipristis elongatus*); 9-13, Carcharhinidae (*Carcharhinus galapagensis*, *Negaprion brevirostris*, *Rhizoprionodon terraenovae*, *Scoliodon macrorhynchus*, and *Trianodon obesus*); 14-15, Sphyrnidae (*Eusphyra blochii* and *Sphyrna tiburo*). NC, nasal capsule; OC, occipital condyle; POP, postorbital process; PRP, preorbital process; RC, rostral cartilage.

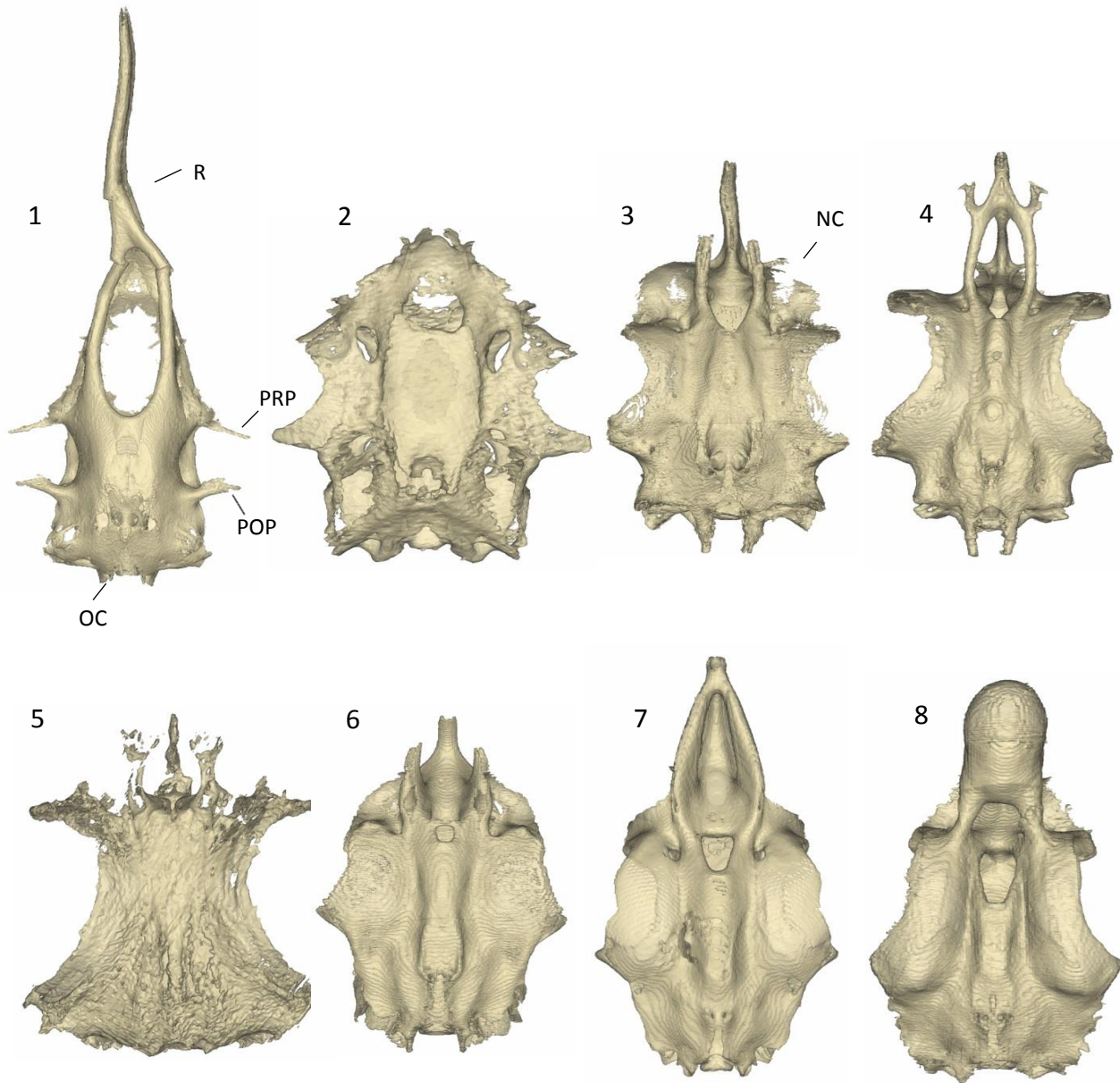


Figure 12. Chondrocrania from chondrichthyans showing morphological diversity across the order Lamniformes. 1, Mitsukurinidae (*Mitsukurina owstoni*); 2-3, Odontaspidae (*Carcharias taurus* and *Odontaspis ferox*); 4, Pseudochariidae (*Pseudocarcharias kamoharai*); 5, Alopiidae (*Alopias superciliosus*); 6-8, Lamnidae (*Carcharodon carcharias*, *Isurus oxyrinchus* and *Lamna ditropis*). NC, nasal capsule; OC, occipital condyle; POP, postorbital process; PRP, preorbital process; RC, rostral cartilage.

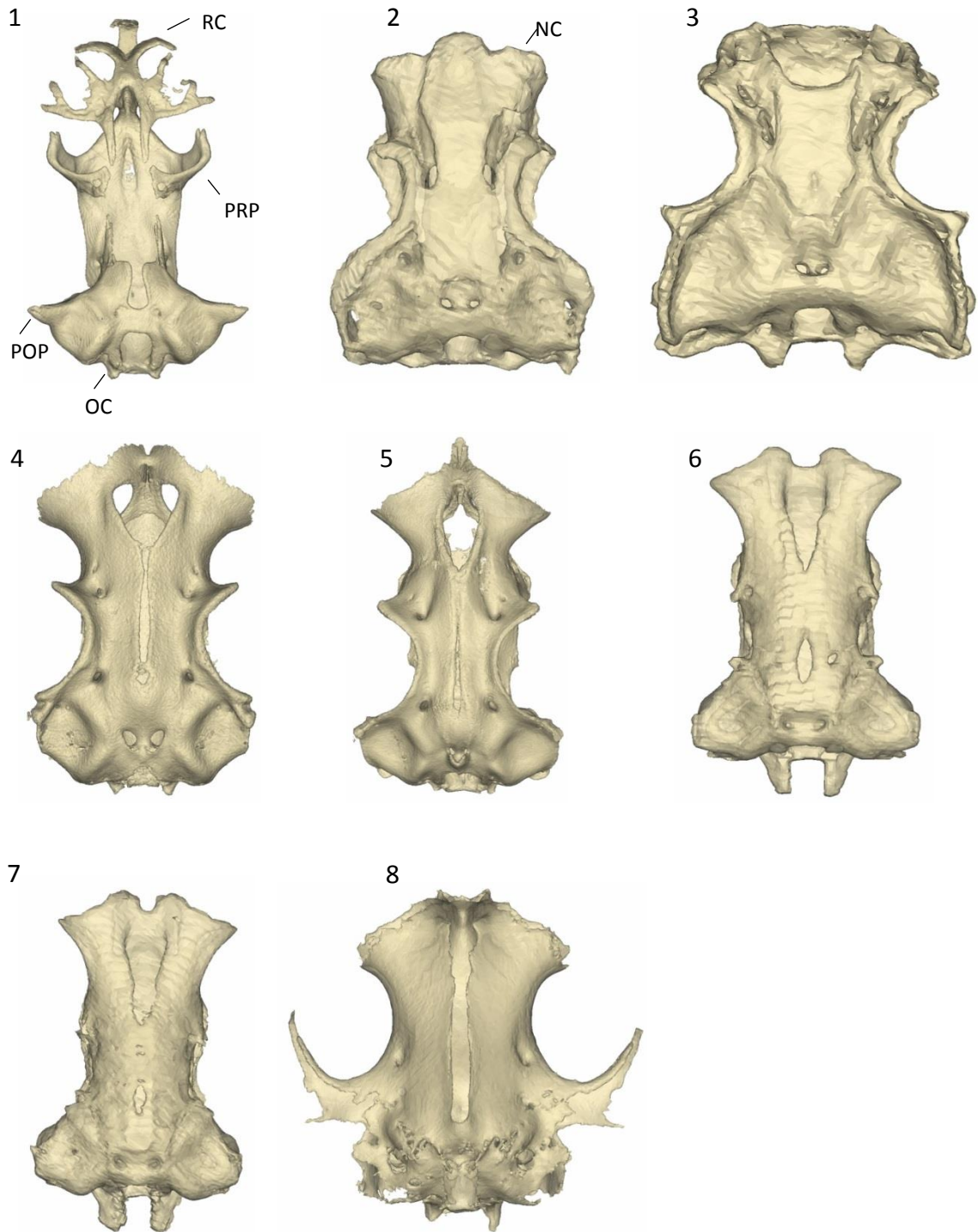


Figure 13. Chondrocrania from chondrichthyan showing morphological diversity across the order Orectolobiformes. 1, Parascylliidae (*Parascyllium collare*); 2, Brachaeluridae (*Brachaelurus waddi*); 3, Orectolobidae (*Orectolobus maculatus*); 4-5, Hemiscylliidae (*Chiloscyllium plagiosum* and *Hemiscyllium ocellatum*); 6-7, Ginglymostomatidae (*Ginglymostoma cirratum* and *Nebrius ferrugineum*); 8, Stegostomatidae (*Stegostoma fasciatum*). NC, nasal capsule; OC, occipital condyle; POP, postorbital process; PRP, preorbital process; RC, rostral cartilage.

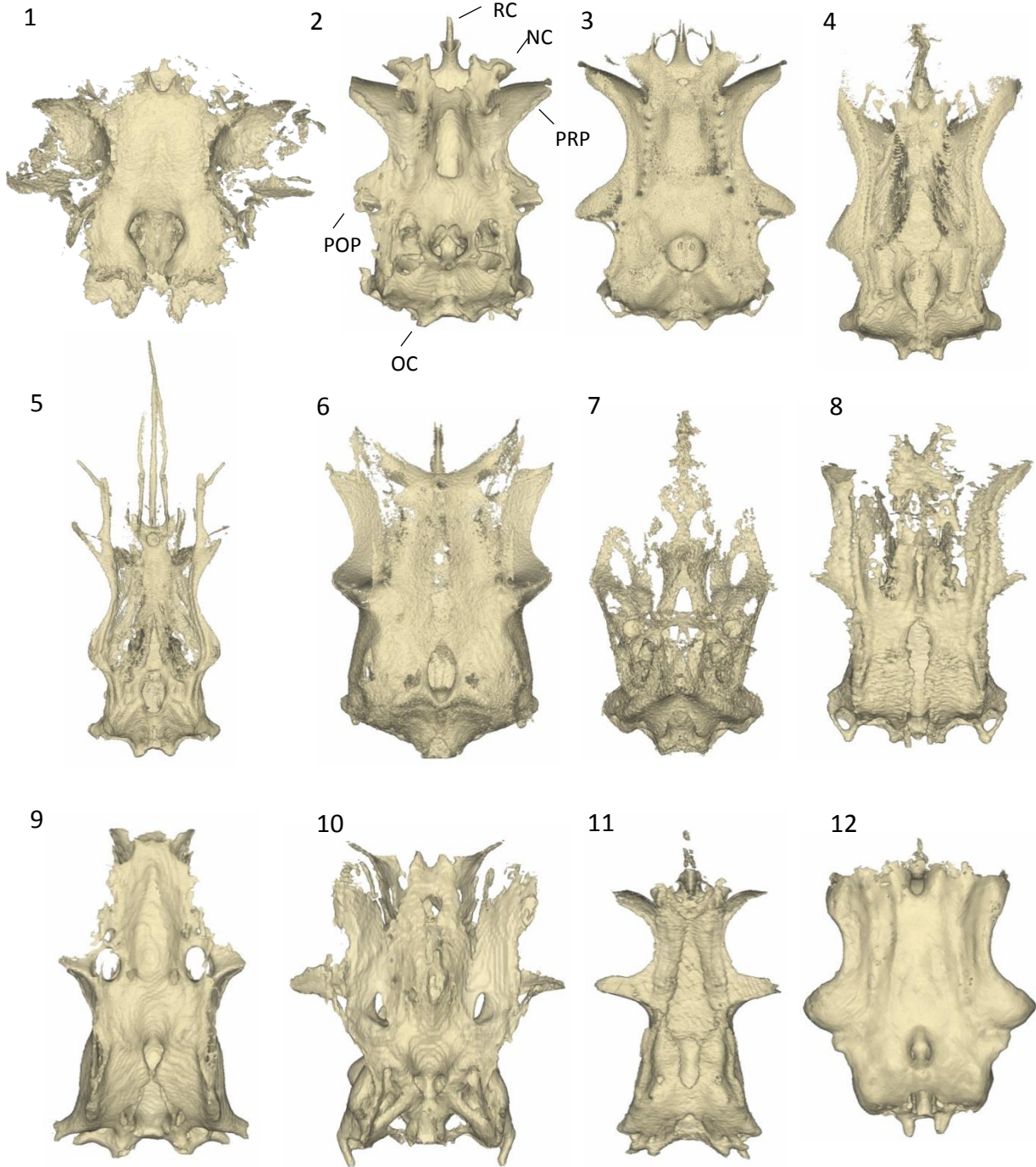


Figure 14. Chondrocrania from chondrichthyan showing morphological diversity across the order Squaliformes. 1, Echinorhinidae (*Echinorhinus brucus*); 2-3, Squalidae (*Squalus acanthias* and *Squalus brevirostris*); 4-5, Centrophoridae (*Centrophorus tessellatus* and *Deania calcea*); 6-7, Etmopteridae (*Etmopterus sheikoi* and *Trigonognathus kabeyai*); 8-10, Somniosidae (*Centroscymnus owstoni*, *Scymnodon rigens* and *Zameus squamulosus*); 11, Oxynotidae (*Oxynotus centrina*); 12, Dalatiidae (*Dalatias licha*). NC, nasal capsule; OC, occipital condyle; POP, postorbital process; PRP, preorbital process; RC, rostral cartilage.

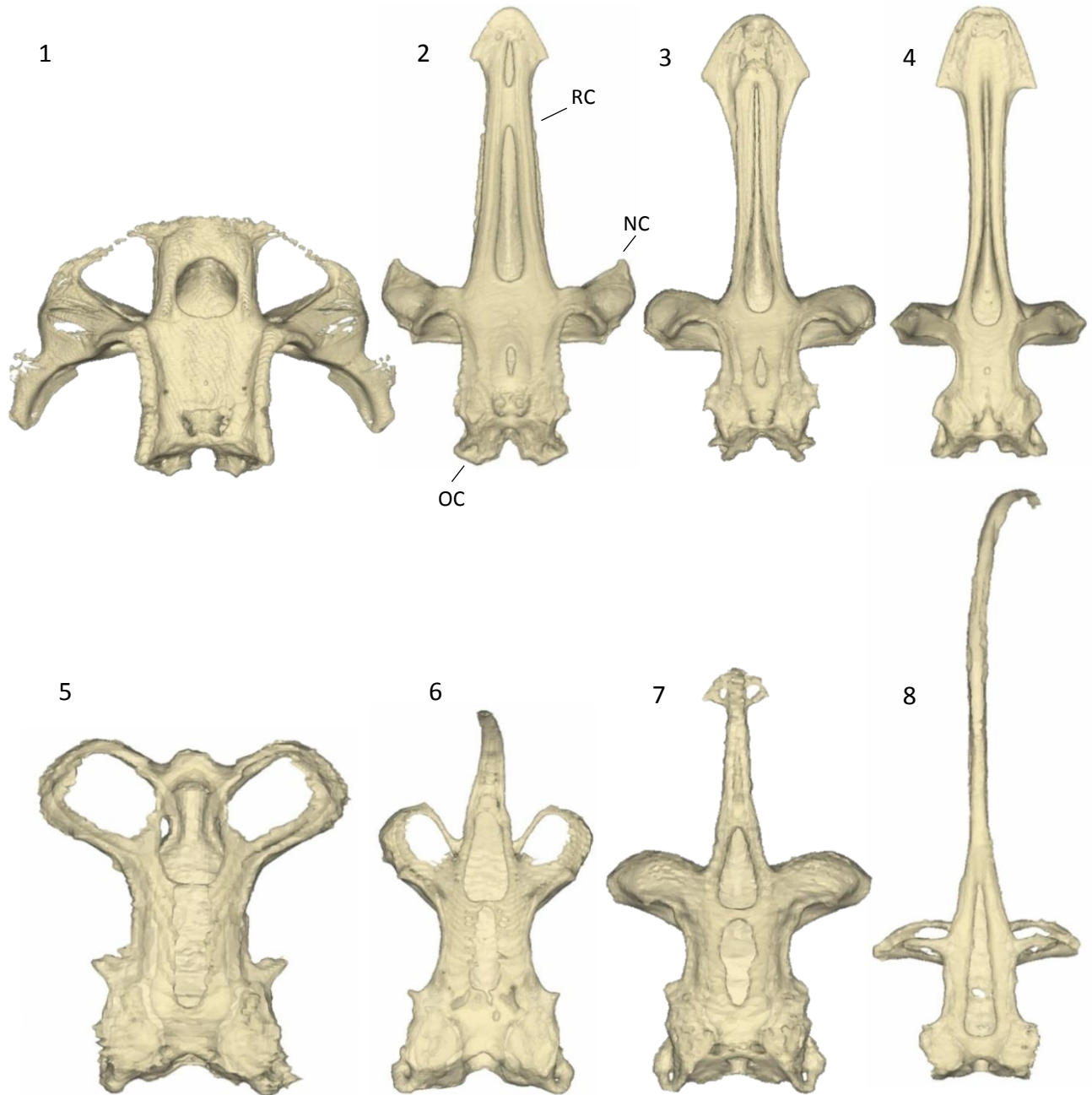


Figure 15. Chondrocrania from chondrichthyans showing morphological diversity across the order Rajiformes. 1, Rhinidae (*Rhina ancylostoma*); 2, Rhynchobatidae (*Rhynchobatus springeri*); 3-4, Rhinobatidae (*Aptychotrema vincentiana* and *Rhinobatos lentiginosus*); 5, Arhynchobatidae (*Irolita waitii*); 6-7, Rajidae (*Dactylobatus armatus* and *Raja eglantaria*); 8, Anacanthobatidae (*Anacanthobatis folirostris*). NC, nasal capsule; OC, occipital condyle; RC, rostral cartilage.

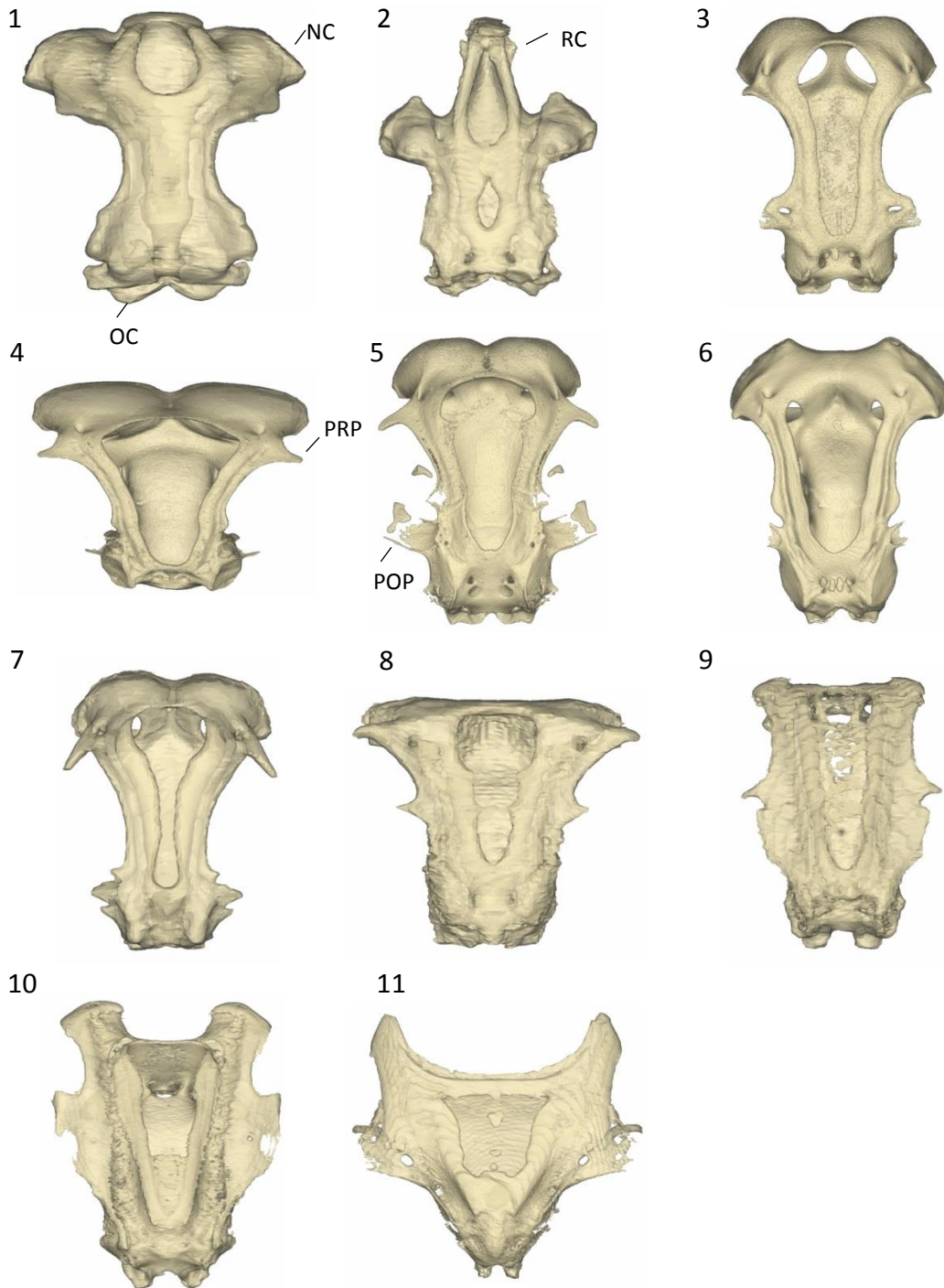


Figure 16. Chondrocrania from chondrichthyans showing morphological diversity across the order Myliobatiformes. 1, Zanobatidae (*Zanobatus schoeleini*); 2, Platyrhinidae (*Platyrhinoidis triseriata*); 3, Urolophidae (*Urolophus aurantiacus*); 4, Urotrygonidae (*Urotrygon chilensis*); 5, Potamotrygonidae (*Potamotrygon motoro*); 6-7, Dasyatidae (*Dasyatis zugei* and *Neotrygon kuhlii*); 8, Gymnuridae (*Gymnura altaveala*); 9, Myliobatidae (*Pteromylaeus bovinus*); 10, Rhinopteridae (*Rhinoptera bonasus*); 11, Mobulidae (*Mobula munkiana*). NC, nasal capsule; OC, occipital condyle; POP, postorbital process; PRP, preorbital process; RC, rostral cartilage.

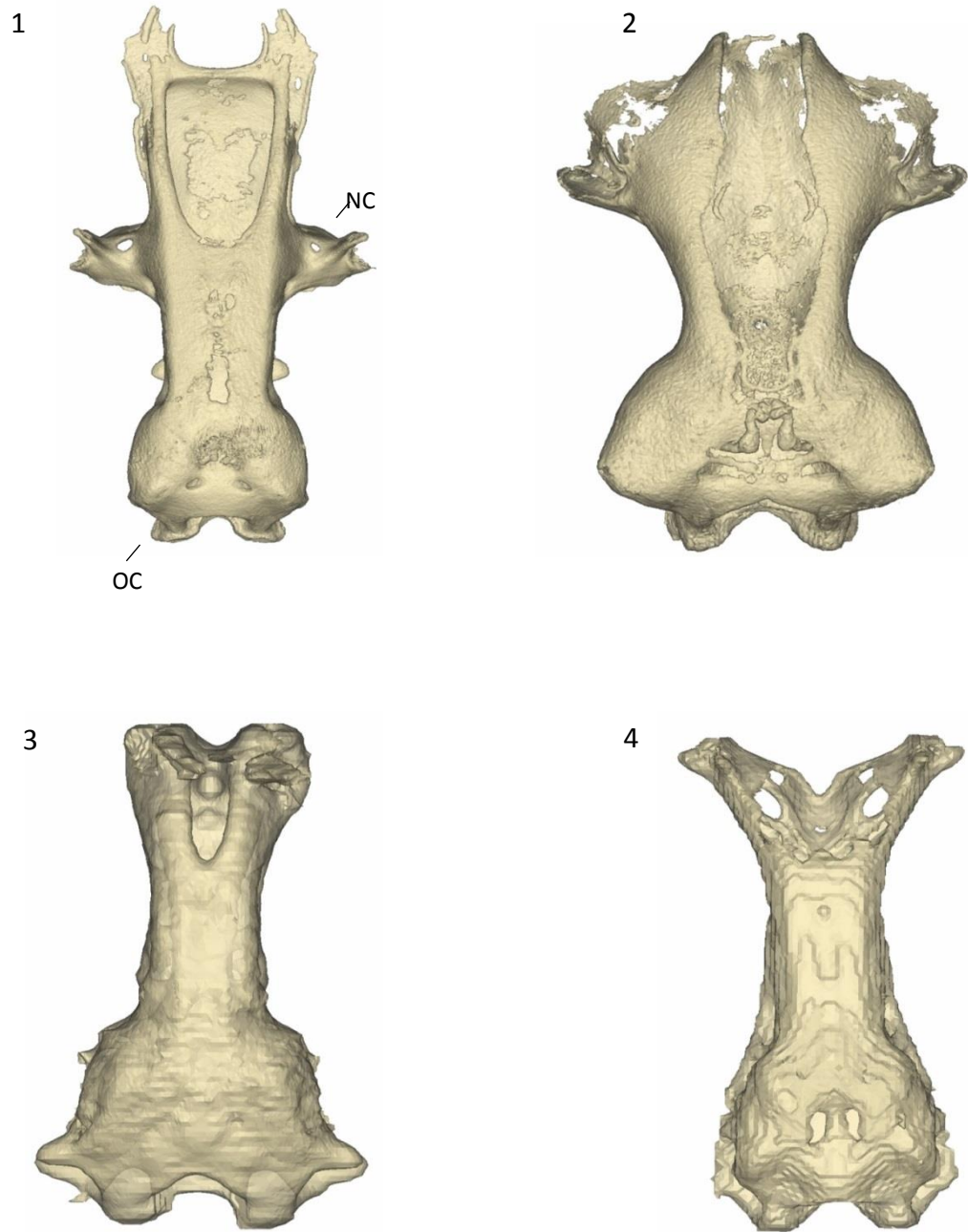


Figure 17. Chondrocrania from chondrichthyans showing morphological diversity across the order Torpediniformes. 1, Narcinidae (*Narcine brasiliensis*); 2, Narkidae (*Narke japonica*); 3, Hypnidae (*Hypnos monoptyerius*); 4, Torpedinidae (*Torpedo fuscomaculata*). NC, nasal capsule; OC, occipital condyle.

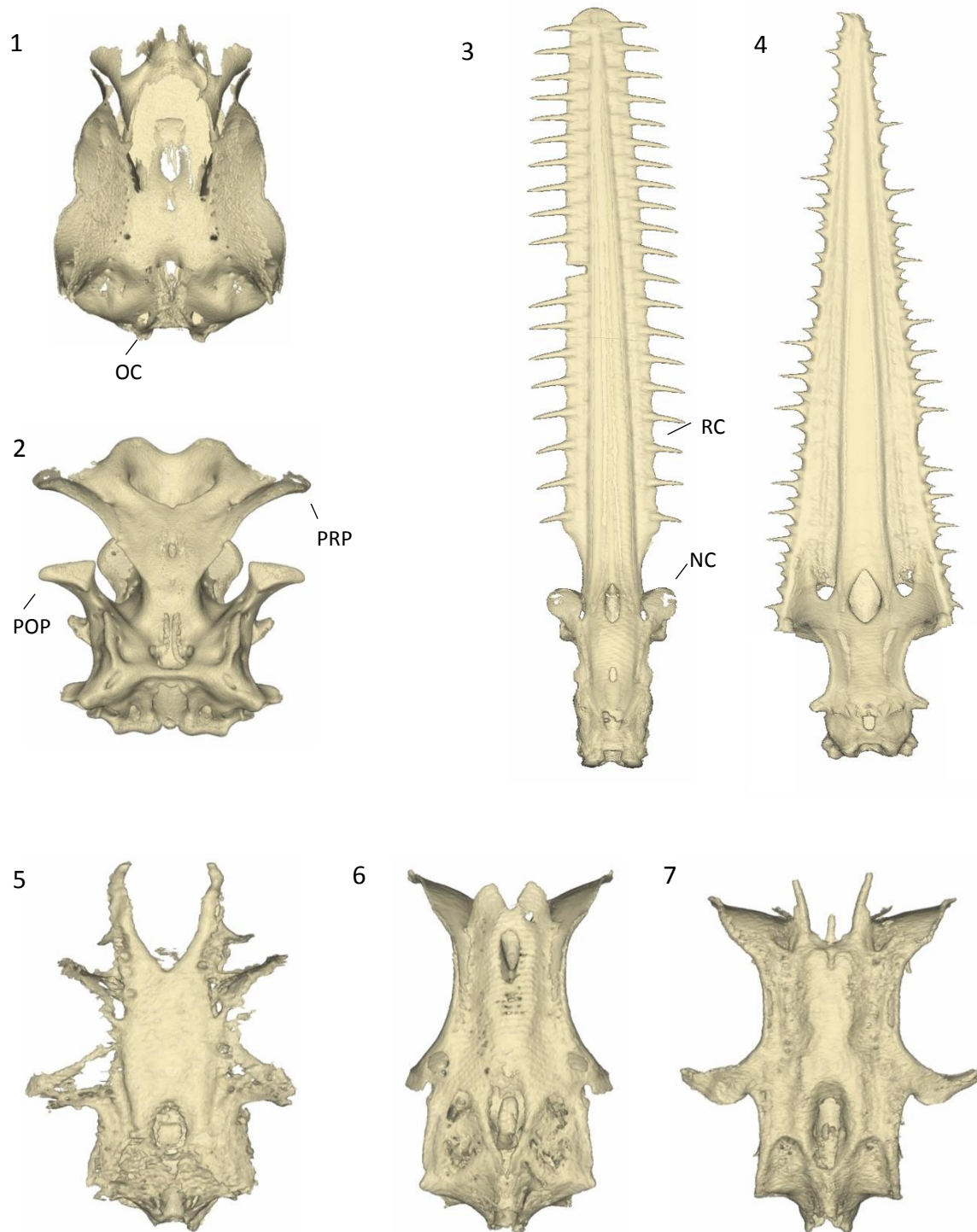


Figure 18. Chondrocrania from chondrichthyans showing morphological diversity across the orders: 1, Heterodontiformes (*Heterodontus francisci*); 2, Squatiniformes (*Squatina nebulosa*); 3, Pristiformes (*Pristis clavata*); 4, Pristiophoriformes (*Pristiophorus nudipinnis*); 5-7, Hexanchiformes (*Chlamydoselachus anguineus*, *Hexanchus nakamurai* and *Heptanchias perlo*). NC, nasal capsule; OC, occipital condyle; POP, postorbital process; PRP, preorbital process; RC, rostral cartilage.

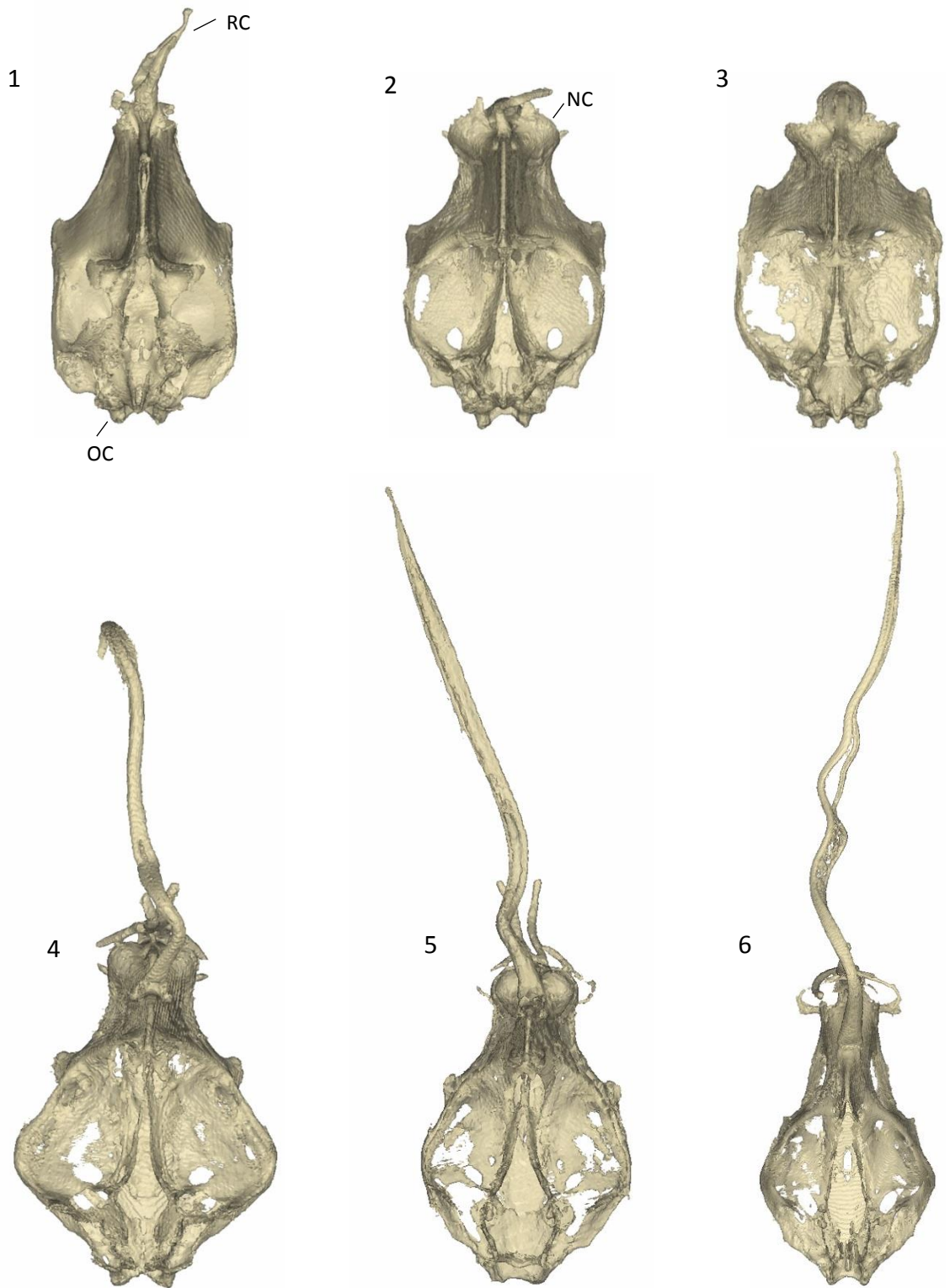


Figure 19. Chondrocrania from chondrichthyans showing morphological diversity across the order Chimaeriformes. 1, Callorhynchidae (*Callorhynchus milii*); 2-3, Chimaeridae (*Chimaera cubana* and *Hydrolagus novaezealandiae*); 4-6, Rhinochimaeridae (*Harriotta raleighana*, *Neoharriotta carri*, and *Rhinochimaera atlantica*). NC, nasal capsule; OC, occipital condyle; RC, rostral cartilage.

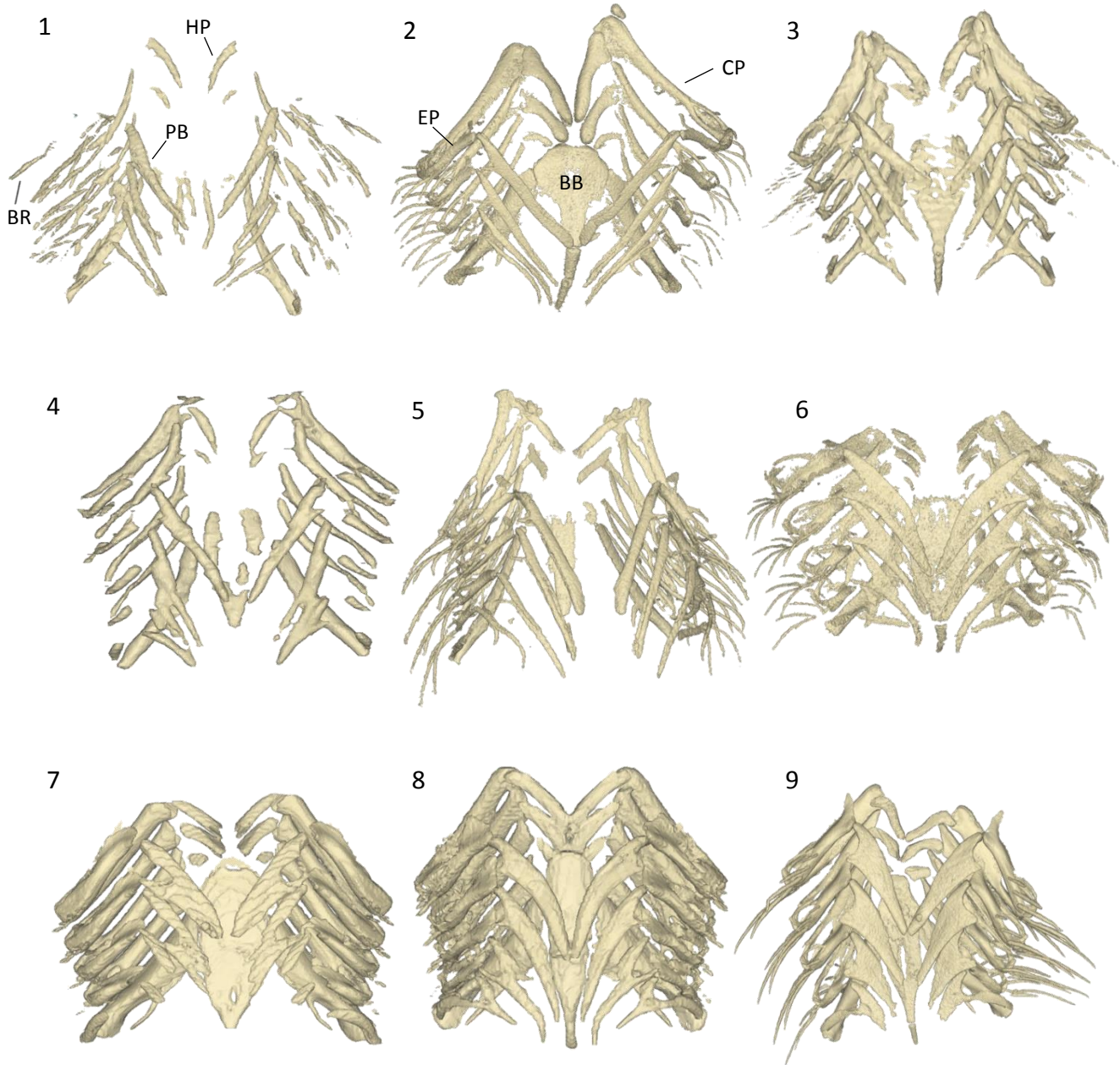


Figure 20. Variation in the branchial structures of the Carcharhiniform sharks; 1, *Bythaelurus canescens*; 2, *Galeus sauteri*; 3, *Schroederichthys chilensis*; 4, *Scyliorhinus meadi*; 5, *Eridacnis radcliffei*; 6, *Mustelus manazo*; 7, *Negaprion brevirostris*; 8, *Rhizoprionodon terreaovae*; 9, *Sphyrna tiburo*. BB, basibranchial; BR, branchial rays; CP; ceratobranchials; EB, epibranchials; HP, hypobranchials; PB, pharyngobranchials.

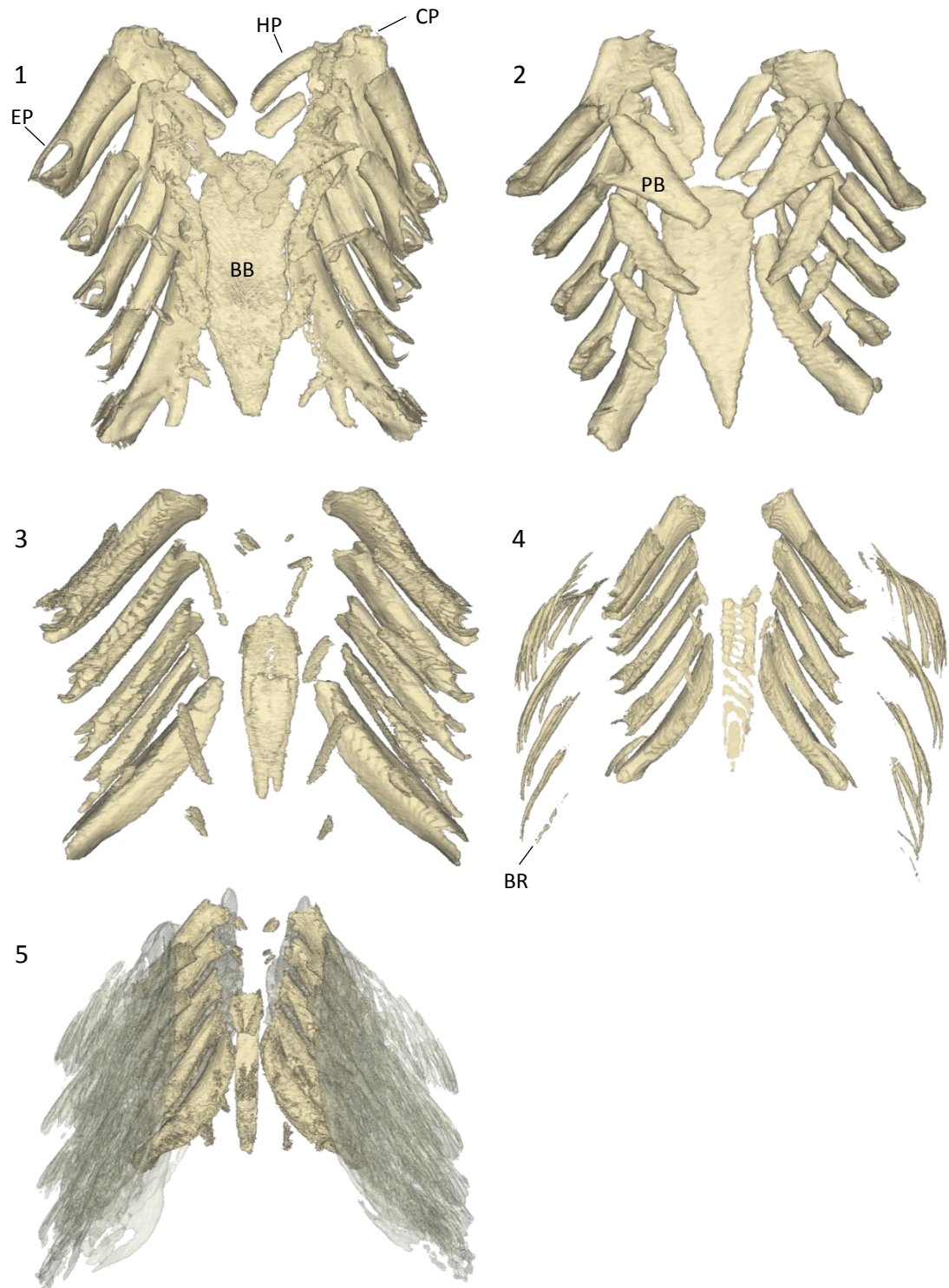


Figure 21. Variation in the branchial structures of the Lamniform sharks; 1, *Carcharias taurus*; 2, *Odontaspis ferox*; 3, *Carcharodon carcharias*; 4, *Isurus oxyrinchus*; 5, *Lamna ditropis*. BB, basibranchial; BR, branchial rays; CP; ceratobranchials; EB, epibranchials; HP, hypobranchials; PB, pharyngobranchials.

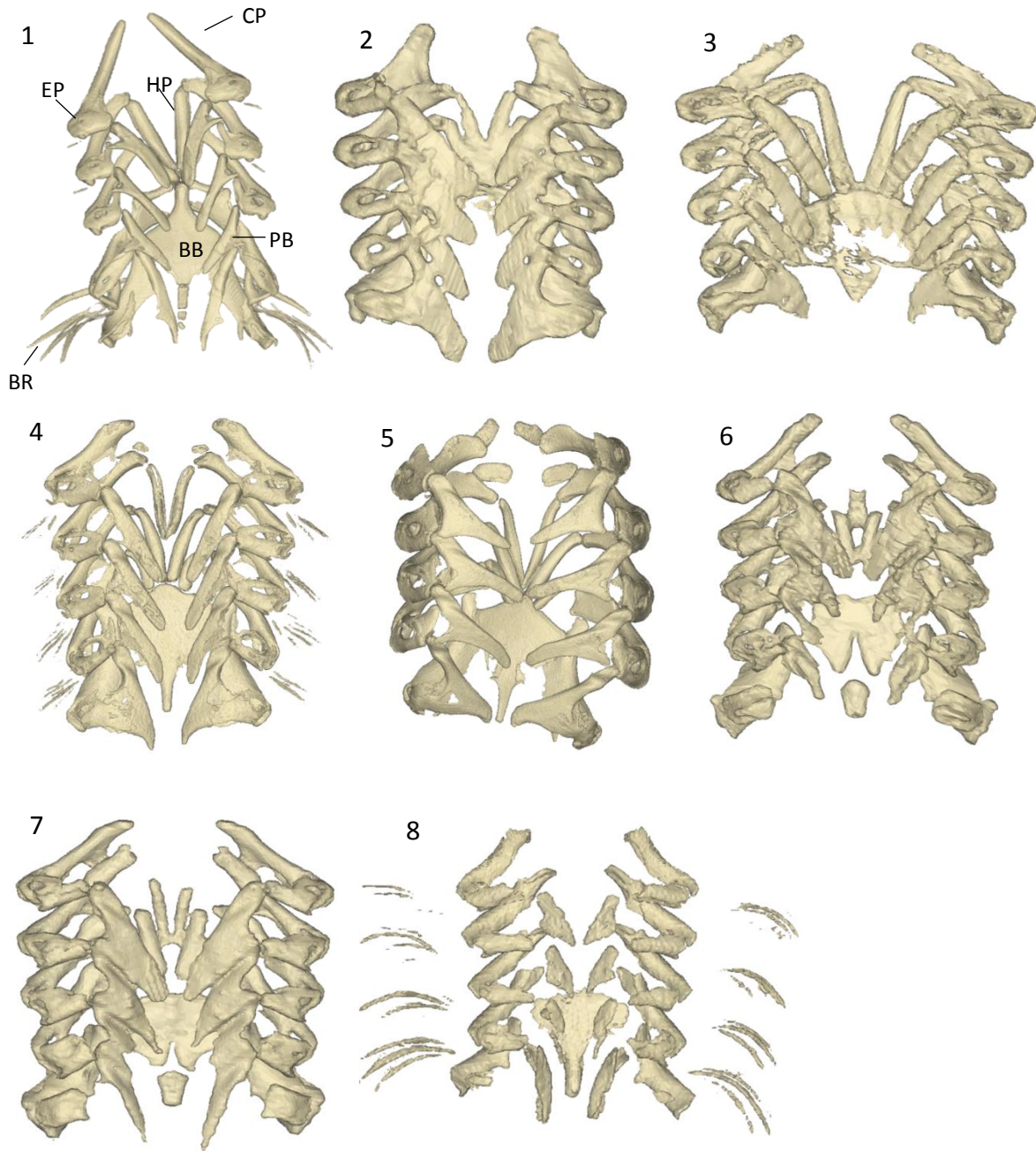


Figure 22. Variation in the branchial structures of the Orectolobiform sharks; 1, *Parascyllium collare*; 2, *Brachaelurus waddi*; 3, *Orectolobus maculatus*; 4, *Chiloscyllium plagiosum*; 5, *Hemiscyllium ocellatum*; 6, *Ginglymostoma cirratum*; 7, *Nebrius ferrugineum*; 8, *Stegostoma fasciatum*. BB, basibranchial; BR, branchial rays; CP; ceratobranchials; EB, epibranchials; HP, hypobranchials; PB, pharyngobranchials.

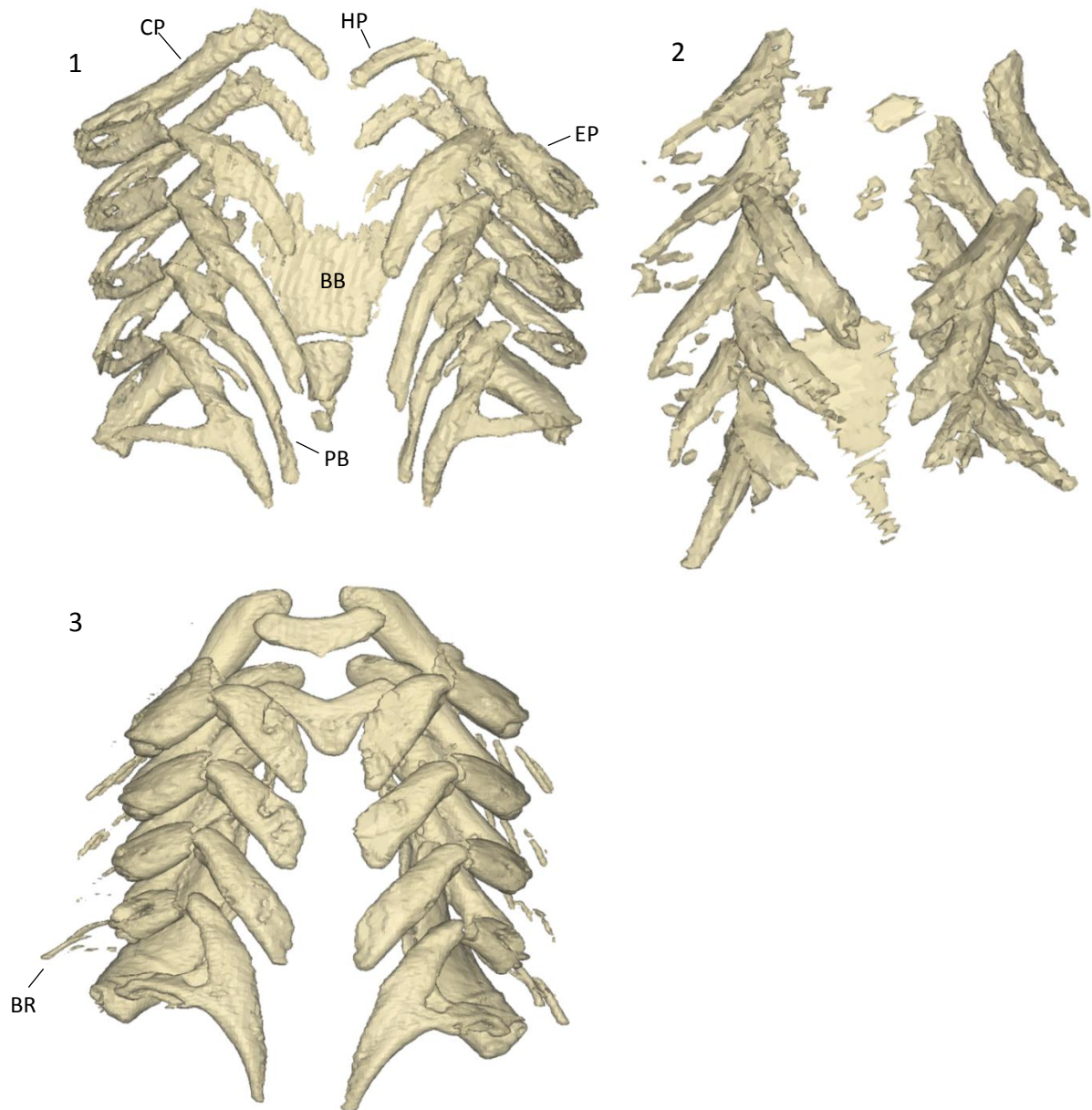


Figure 23. Variation in the branchial structures of the Squaliform sharks; 1, *Squalus brevirostris*; 2, *Oxynotus centrina*; 3, *Dalatias licha*. BB, basibranchial; BR, branchial rays; CP; ceratobranchials; EB, epibranchials; HP, hypobranchials; PB, pharyngobranchials.

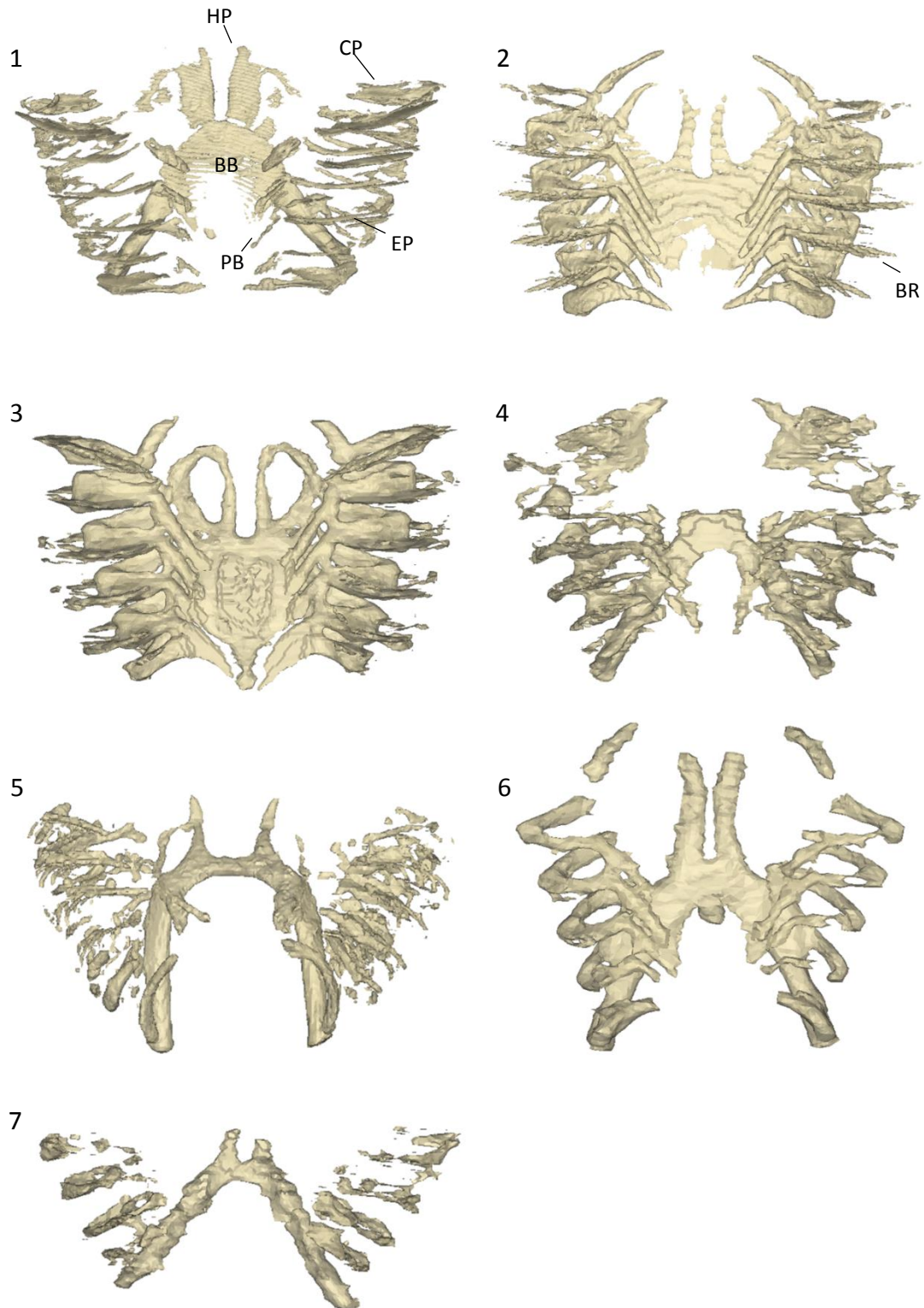
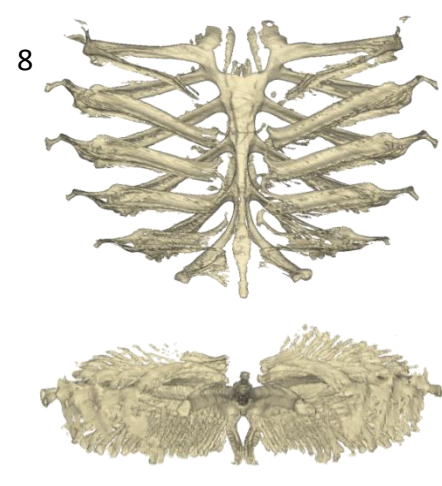
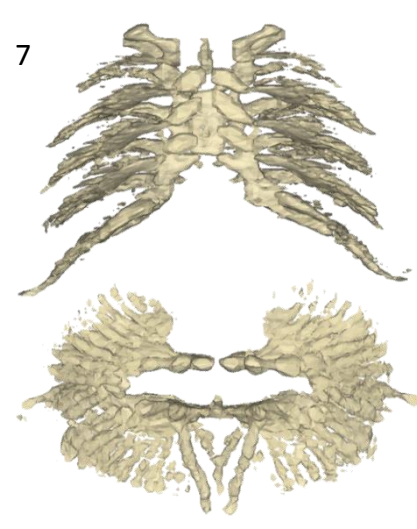
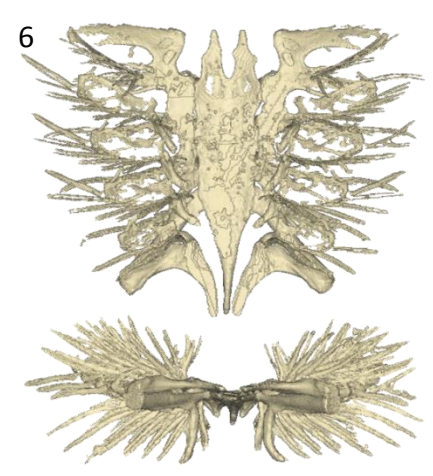
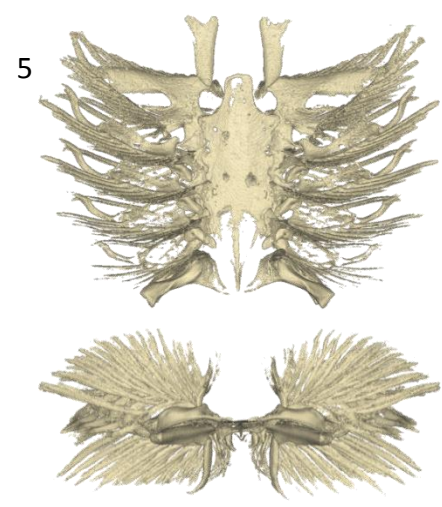
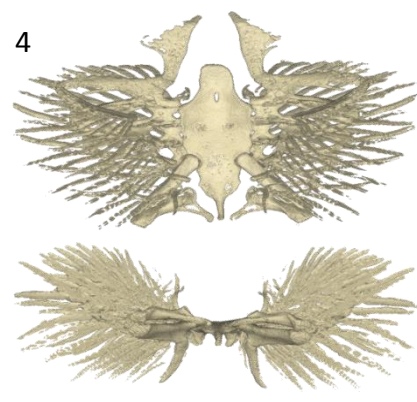
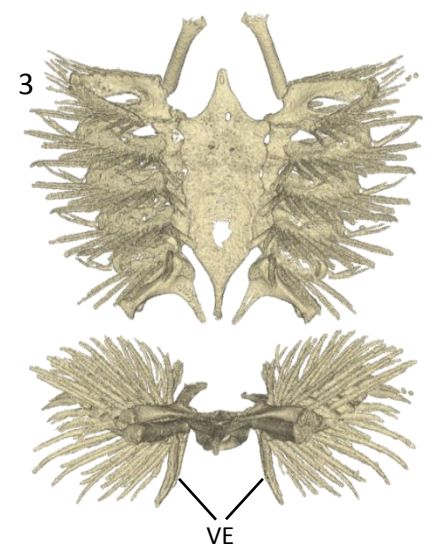
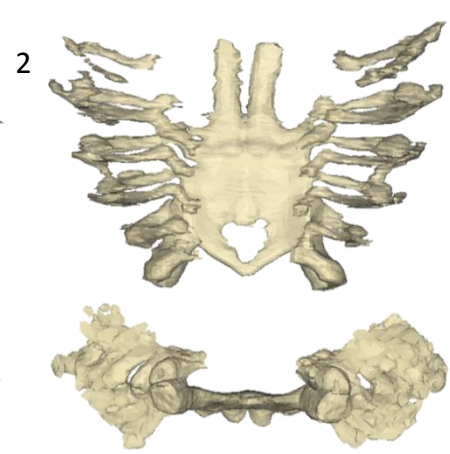
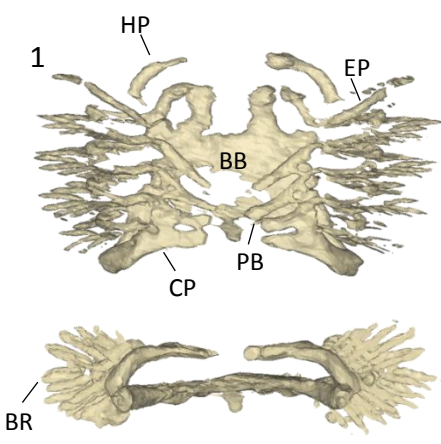


Figure 24. Variation in the branchial structures of the Rajiforms; 1, *Rhina ancylostoma*; 2, *Aptychotrema vincentiana*; 3, *Rhinobatos lentiginosus*; 4, *Irolita waitii*; 5, *Dactylobatus armatus*; 6, *Raja eglanteria*; 7, *Anacanthobatis folirostris*. BB, basibranchial; BR, branchial rays; CP, ceratobranchials; EB, epibranchials; HP, hypobranchials; PB, pharyngobranchials.



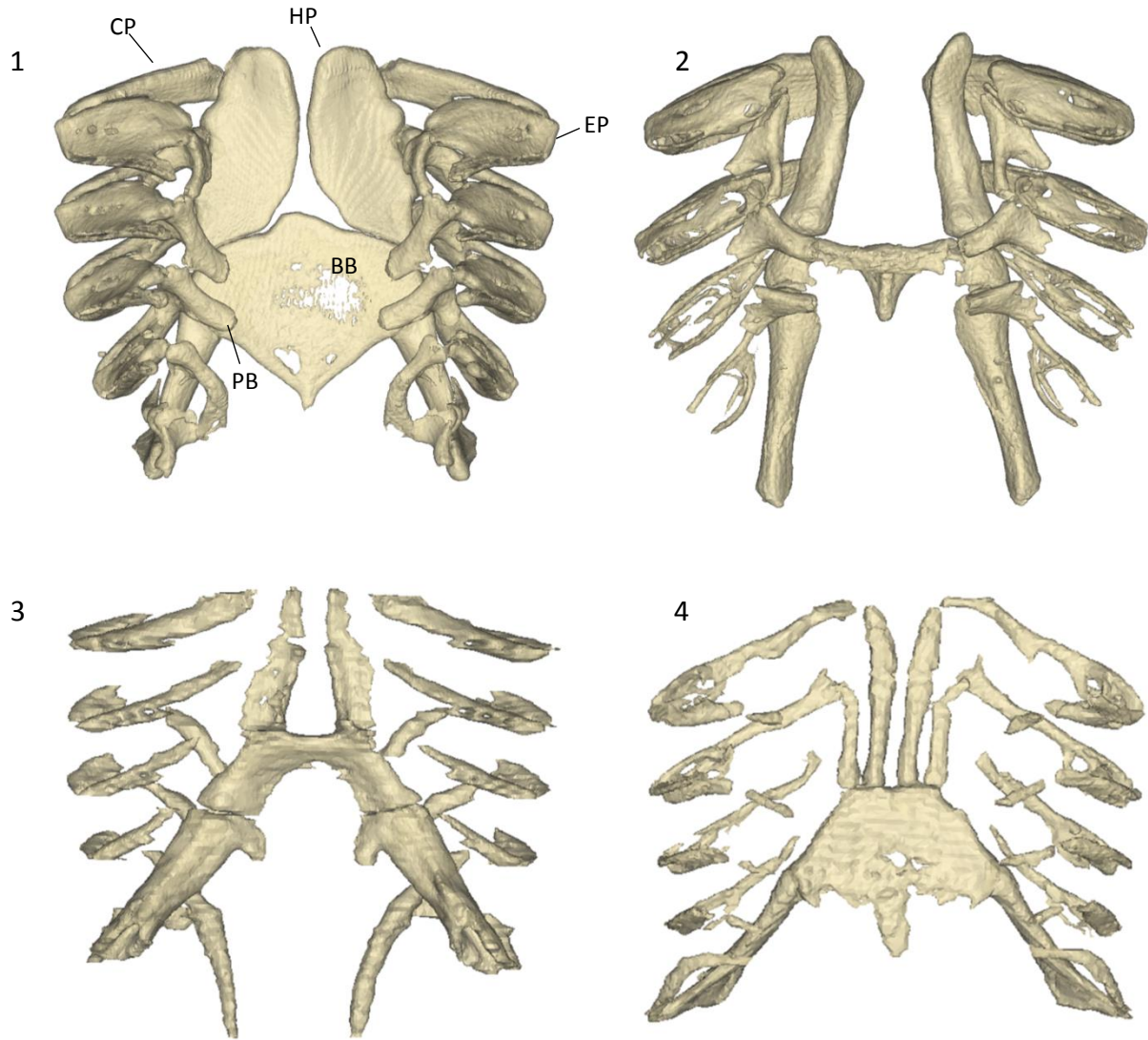
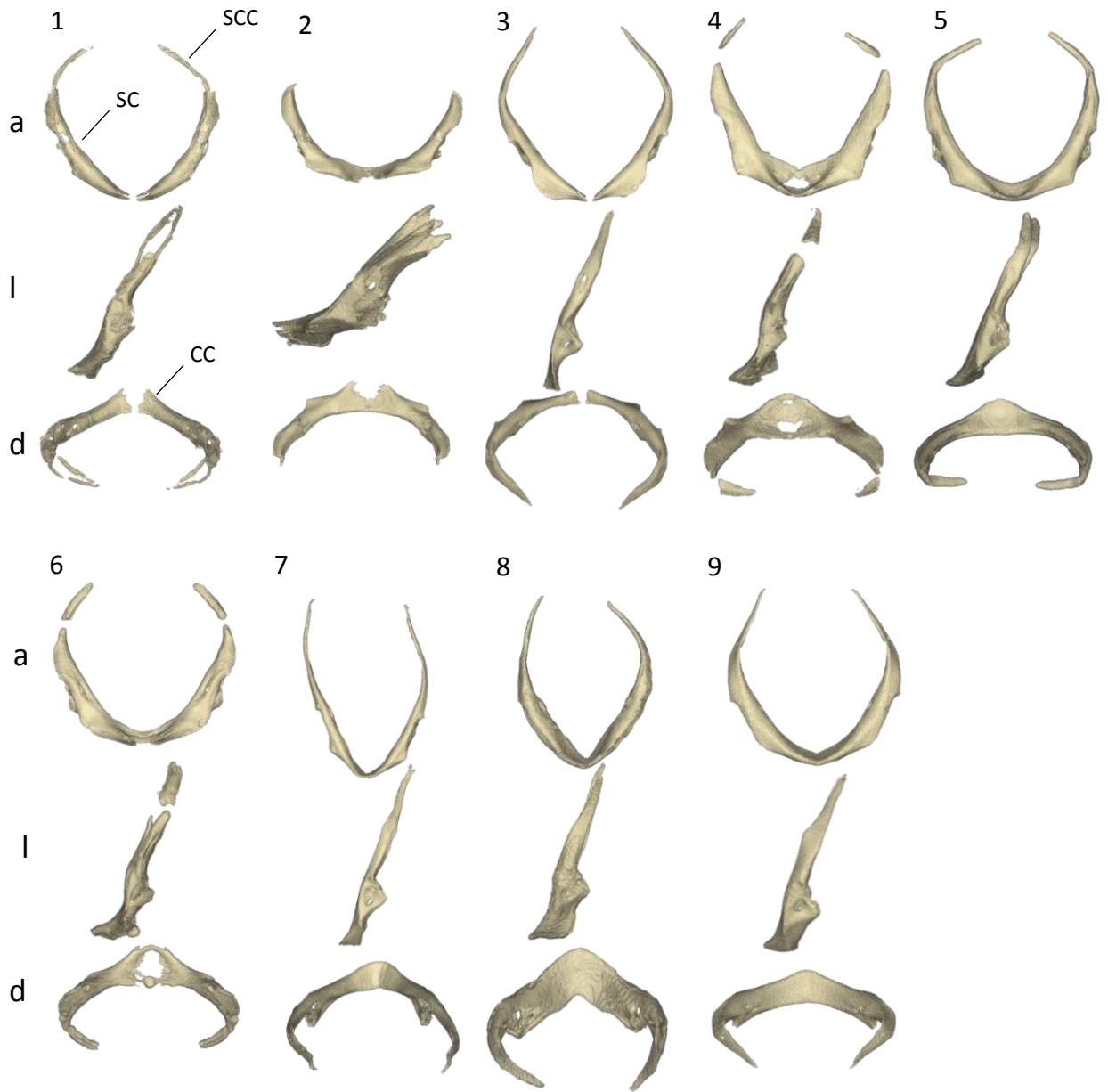


Figure 26. Branchial baskets of the Torpediniformes; 1, *Narcine brasiliensis*; 2, *Narke japonica*; 3, *Hypnos monoptyerygius*; 4, *Torpedo fuscomaculata*. BB, basibranchial; CP; ceratobranchials; EB, epibranchials; HP, hypobranchials; PB, pharyngobranchials.

Figure 25. Dorsal (upper) and posterior (lower) views illustrating the variation in the branchial structures of the Myliobatiforms with emphasis on the ventral extensions from the basibranchial-ceratobranchial articulation; 1, *Platyrhinoidis triseriata*; 2, *Zanobatus schoeleini*; 3, *Urolophus aurantiacus*; 4, *Urotrygon chilensis*; 5, *Potamotrygon motoro*; 6, *Dasyatis zugei*; 7, *Pteromylaeus bovinus*; 8, *Mobula munkiana*. BB, basibranchial; BR, branchial rays; CP; ceratobranchials; EB, epibranchials; HP, hypobranchials; PB, pharyngobranchials; VE, ventral extension.



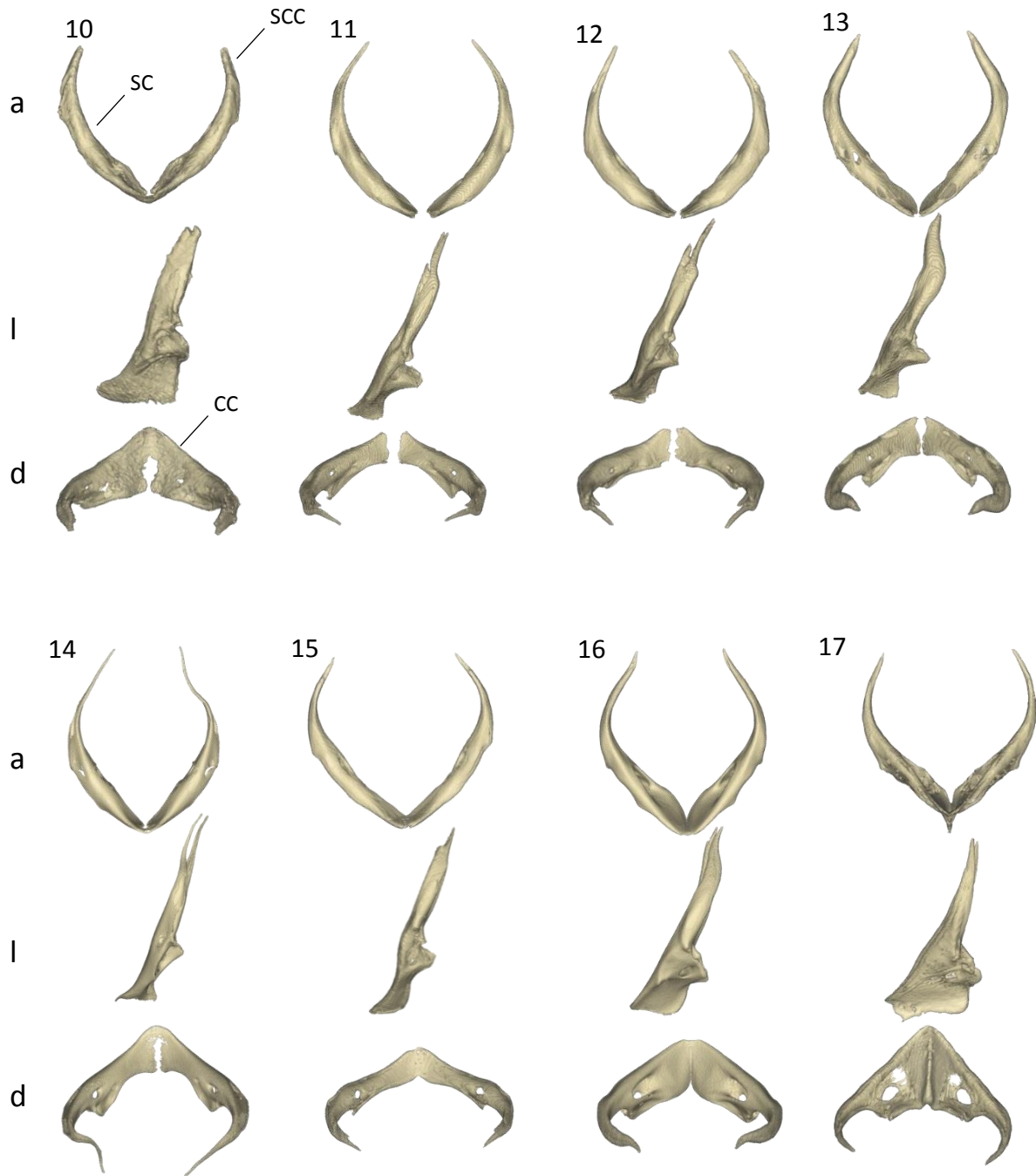


Figure 27. Chondrichthyan scapuolacoracoids showing morphological diversity across the order Carcharhiniformes in three views, Anterior (a), Lateral (l), and Dorsal (d). 1-6, Scyliorhinidae (*Bythaelurus waddi*, *Cephaloscylium isabellum*, *Galeus sauteri*, *Poroderma africanum*, *Schroederichthys chilensis*, and *Scyliorhinus meadi*); 7, Proscylliidae (*Eridacnis radcliffei*); 8, Leptochariidae (*Leptocharias smithii*); 9, Triakidae (*Mustelus manazo*); 10, Hemigaleidae (*Hemipristis elongatus*); 11-15, Carcharhinidae (*Carcharhinus galapagensis*, *Negaprion brevirostris*, *Rhizoprionodon terraenovae*, *Scoliodon macrorhynchus*, and *Triaenodon obesus*); 16-17, Sphyrnidae (*Eusphyrna blochii* and *Sphyrna tiburo*). CC, coracoid; SC, scapular; SCC, suprascapula.



Figure 28. Chondrichthyan scapuolocoracoids showing morphological diversity across the order Lamniformes in three views, Anterior (a), Lateral (l), and Dorsal (d). 1, Mitsukurinidae (*Mitsukurina owstoni*); 2-3, Odontaspidae (*Carcharias taurus* and *Odontaspis ferox*); 4, Pseudochariidae (*Pseudocarcharias kamoharai*); 5, Alopiidae (*Alopias superciliosus*); 6-8, Lamnidae (*Carcharodon carcharias*, *Isurus oxyrinchus* and *Lamna ditropis*). CC, coracoid; SC, scapular; SCC, suprascapula.



Figure 29. Chondrichthyan scapuolacoracoids showing morphological diversity across the order Orectolobiformes in three views, Anterior (a), Lateral (l), and Dorsal (d). 1, Parascylliidae (*Parascyllium collare*); 2, Brachaeluridae (*Brachaelurus waddi*); 3, Orectolobidae (*Orectolobus maculatus*); 4-5, Hemiscylliidae (*Chiloscyllium plagiosum* and *Hemiscyllium ocellatum*); 6-7, Ginglymostomatidae (*Ginglymostoma cirratum* and *Nebrius ferrugineum*); 8, Stegostomatidae (*Stegostoma fasciatum*). CC, coracoid; SC, scapular; SCC, suprascapula.

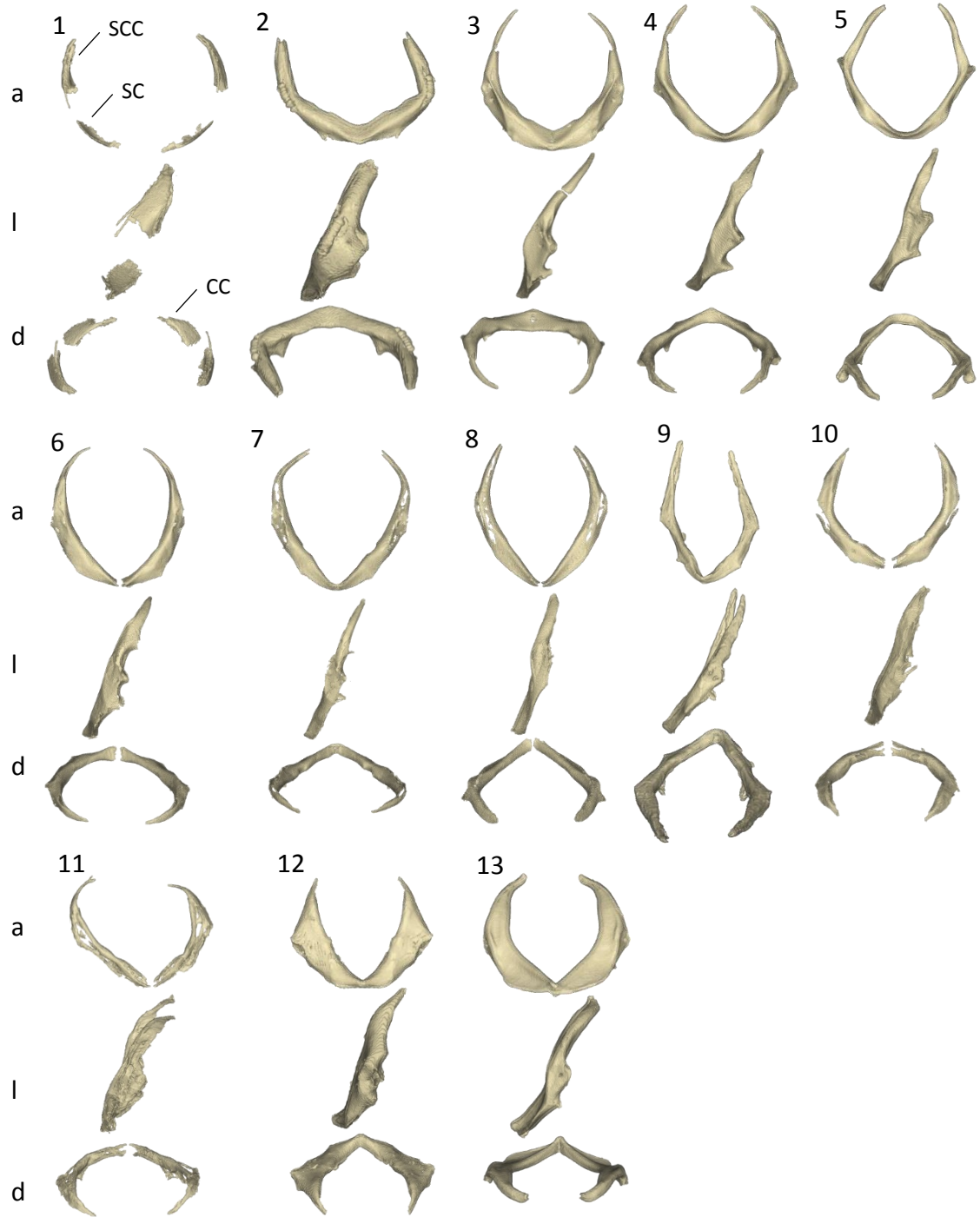


Figure 30. Chondrichthyan scapuolacoracoids showing morphological diversity across the order Squaliformes in three views, Anterior (a), Lateral (l), and Dorsal (d). 1, Echinorhinidae (*Echinorhinus brucus*); 2-3, Squalidae (*Squalus acanthias* and *Squalus brevirostris*); 4-5, Centrophoridae (*Centrophorus tessellatus* and *Deania calcea*); 6-8, Etmopteridae (*Etmopterus sheikoi*, *Etmopterus splendidus*, and *Trigonognathus kabeyai*); 9-11, Somniosidae (*Centroscymnus owstoni*, *Scymnodon rigens* and *Zameus squamulosus*); 12, Oxynotidae (*Oxynotus centrina*); 13, Dalatiidae (*Dalatias licha*). CC, coracoid; SC, scapular; SCC, suprascapula.

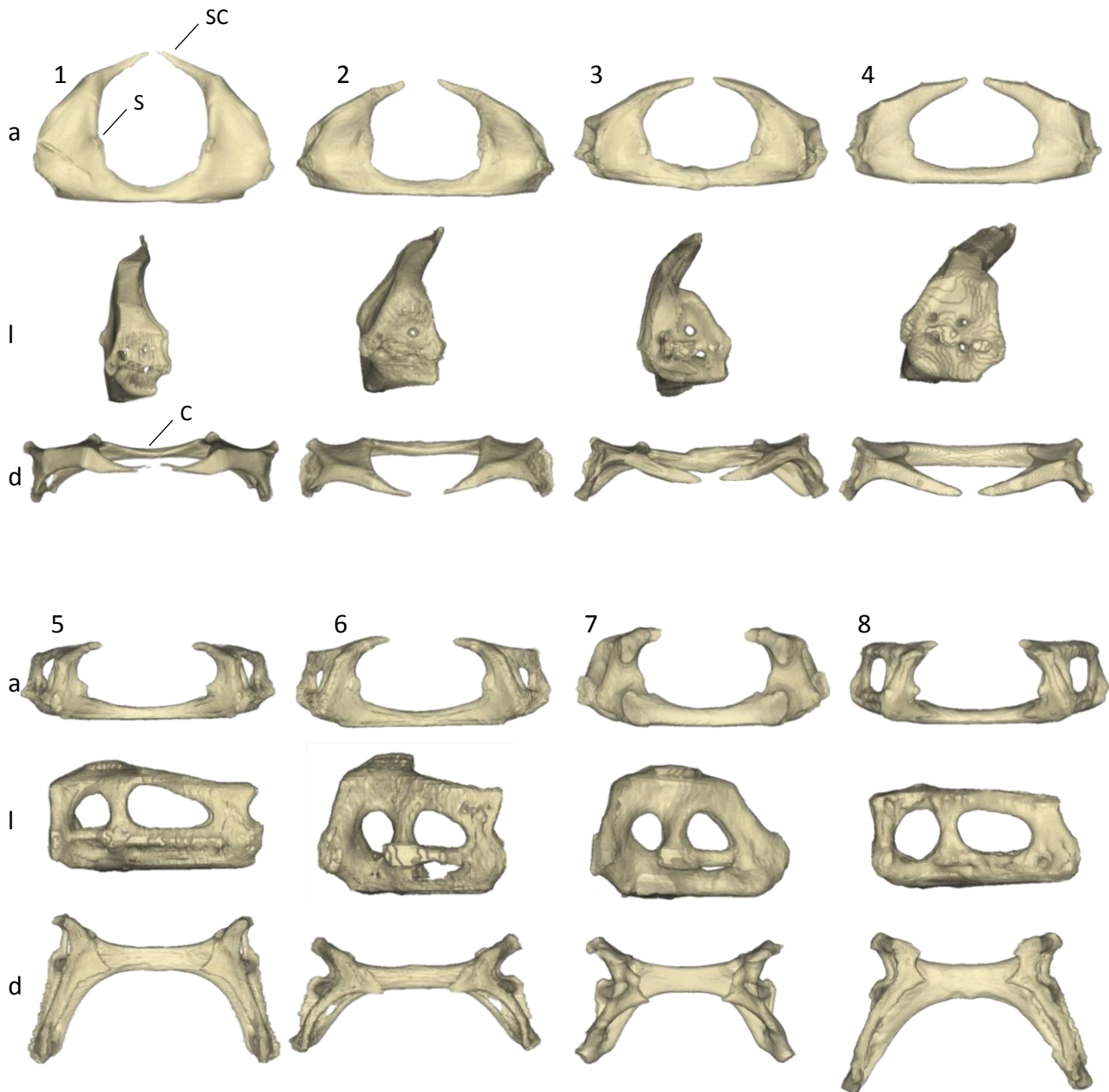
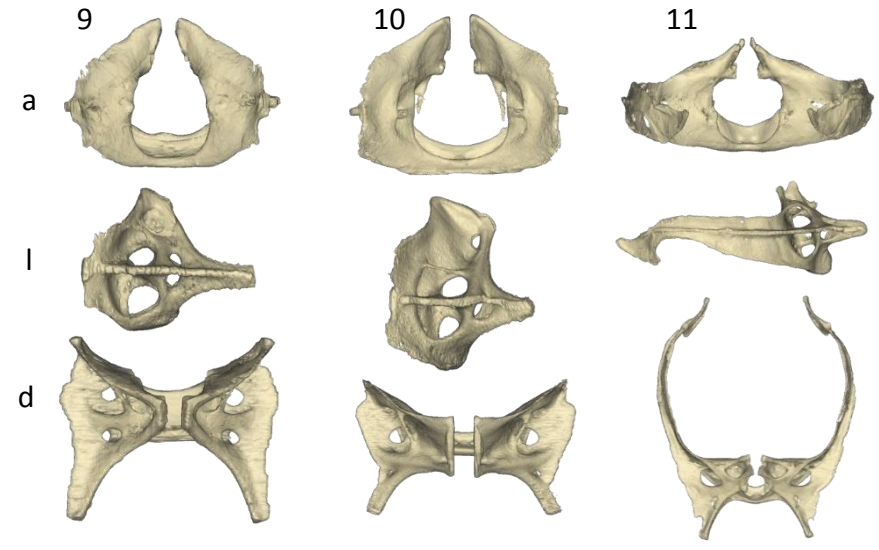
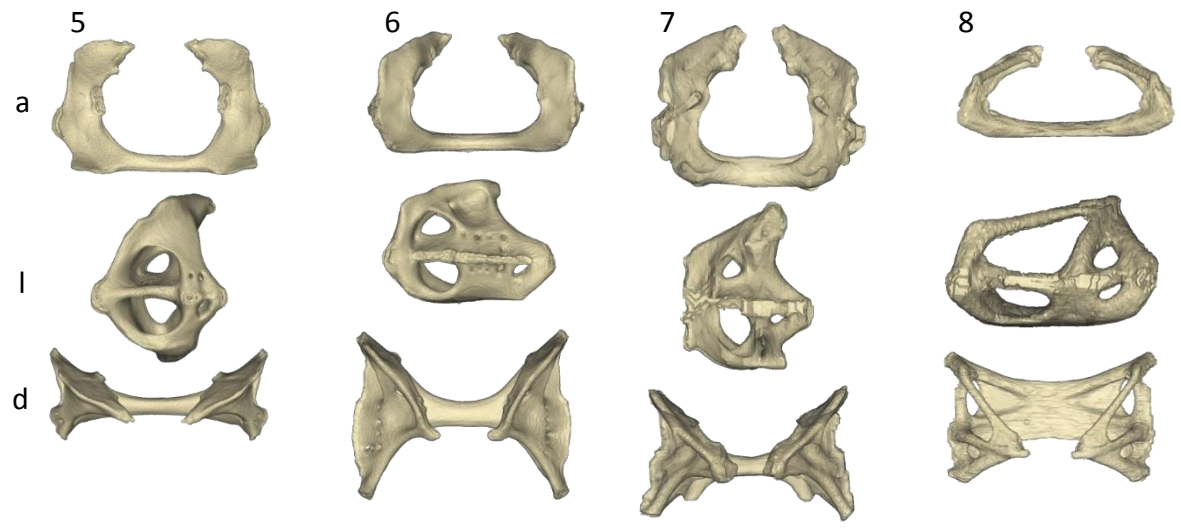
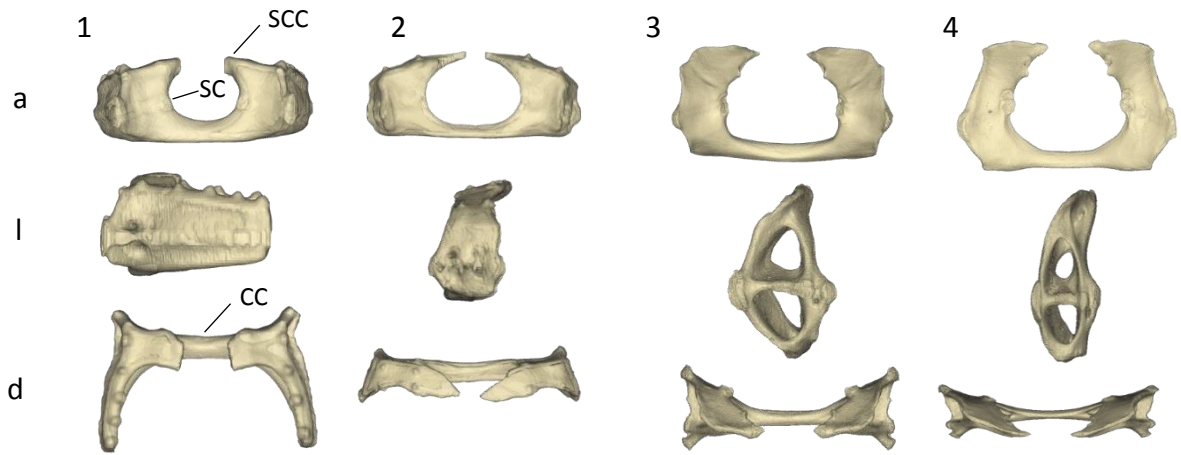


Figure 31. Chondrichthyan scapuolacoracoids showing morphological diversity across the order Rajiformes in three views, Anterior (a), Lateral (l), and Dorsal (d). 1, Rhinidae (*Rhina ancylostoma*); 2, Rhynchobatidae (*Rhynchobatus springeri*); 3-4, Rhinobatidae (*Aptychotrema vincentiana* and *Rhinobatos lentiginosus*); 5, Arhynchobatidae (*Irolita waitii*); 6-7, Rajidae (*Dactylobatus armatus* and *Raja eglantaria*); 8, Anacanthobatidae (*Anacanthobatis folirostris*). CC, coracoid; SC, scapular; SCC, suprascapula.



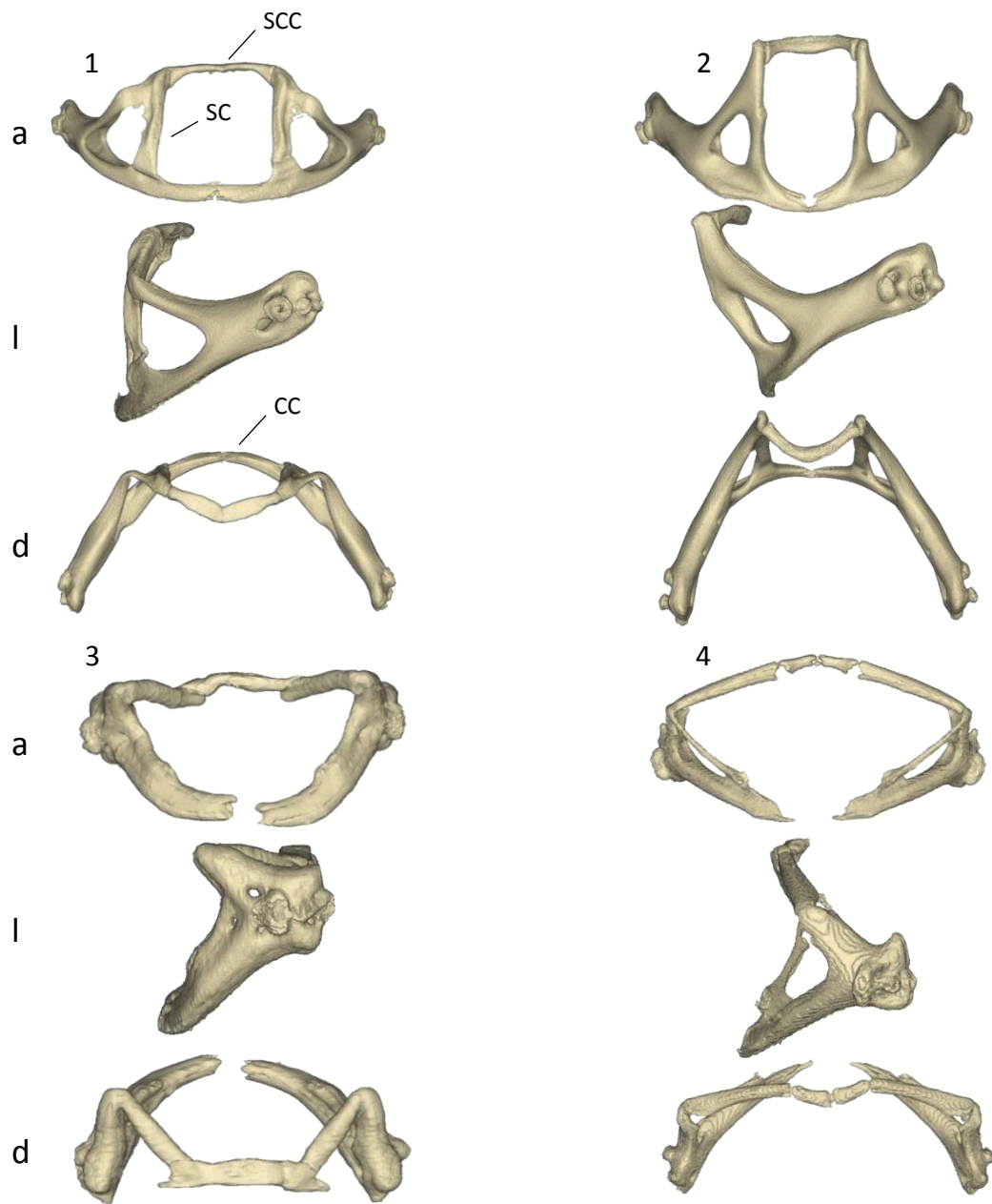


Figure 33. Chondrichthyan scapuolacoracoids showing morphological diversity across the order Torpediniformes in three views, Anterior (a), Lateral (l), and Dorsal (d). 1, Narcinidae (*Narcine brasiliensis*); 2, Narkidae (*Narke japonica*); 3, Hypnidae (*Hypnos monopterygius*); 4, Torpedinidae (*Torpedo fuscomaculata*). CC, coracoid; SC, scapular; SCC, suprascapula.

Figure 32. Chondrichthyan scapuolacoracoids showing morphological diversity across the order Rajiformes in three views, Anterior (a), Lateral (l), and Dorsal (d). 1, Rhinidae (*Rhina ancylostoma*); 2, Rhynchobatidae (*Rhynchobatus springeri*); 3-4, Rhinobatidae (*Aptychotrema vincentiana* and *Rhinobatos lentiginosus*); 5, Arhynchobatidae (*Irolita waitii*); 6-7, Rajidae (*Dactylobatus armatus* and *Raja eglantaria*); 8, Anacanthobatidae (*Anacanthobatis folirostris*). CC, coracoid; SC, scapular; SCC, suprascapula.

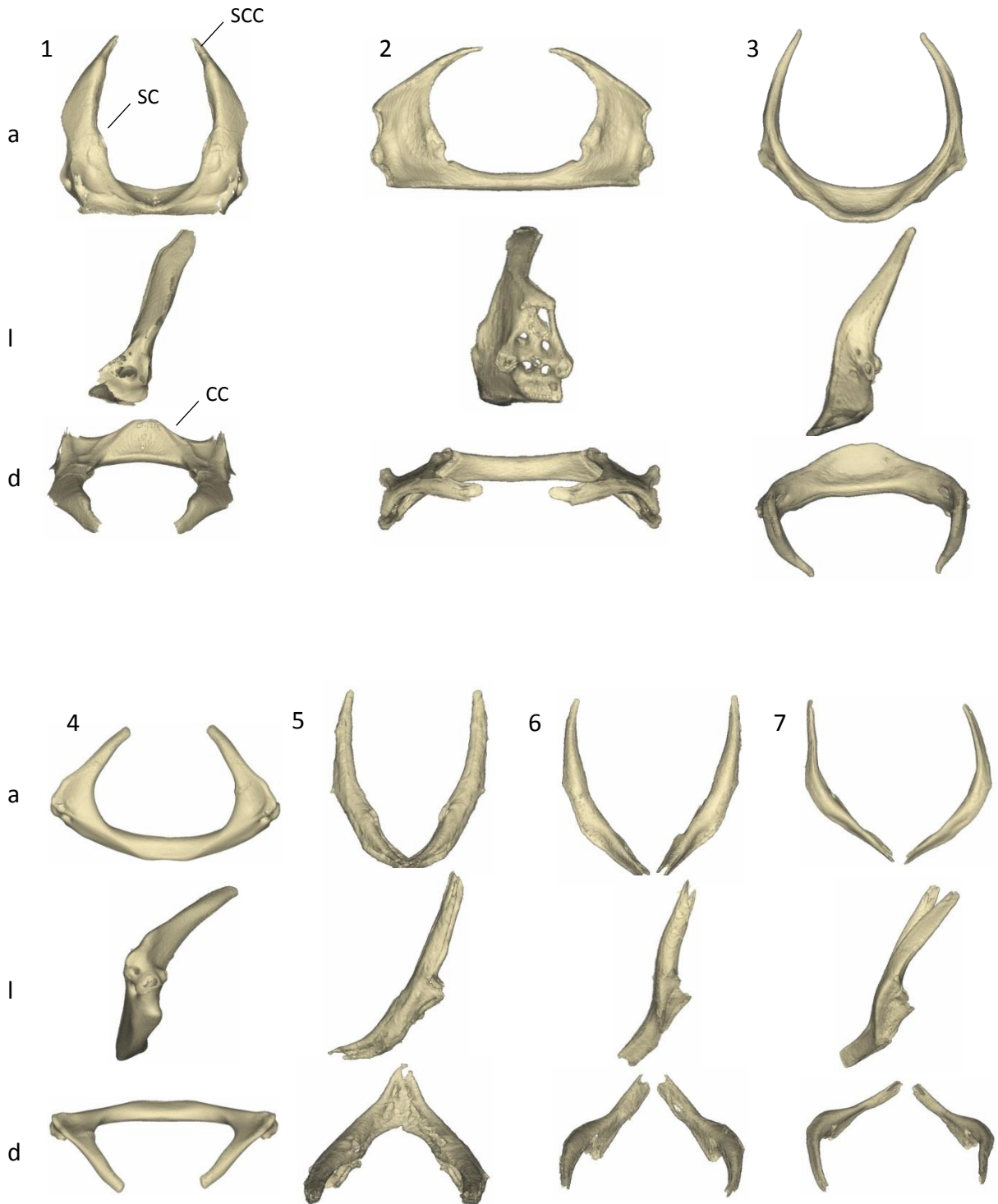


Figure 34. Chondrichthyan scapuolocoracoids showing morphological diversity in three views, Anterior (a), Lateral (l), and Dorsal (d). 1, Heterodontiformes (*Heterodontus francisci*); 2, Pristiformes (*Pristis clavata*); 3, Pristiophoriformes (*Pristiophorus nudipinnis*); 4, Squatiniformes (*Squatina nebulosa*); 5-7, Hexanchiformes (*Chlamydoselachus anguineus*, *Hexanchus nakamurai* and *Hepranchias perlo*) CC, coracoid; SC, scapular; SCC, suprascapula.

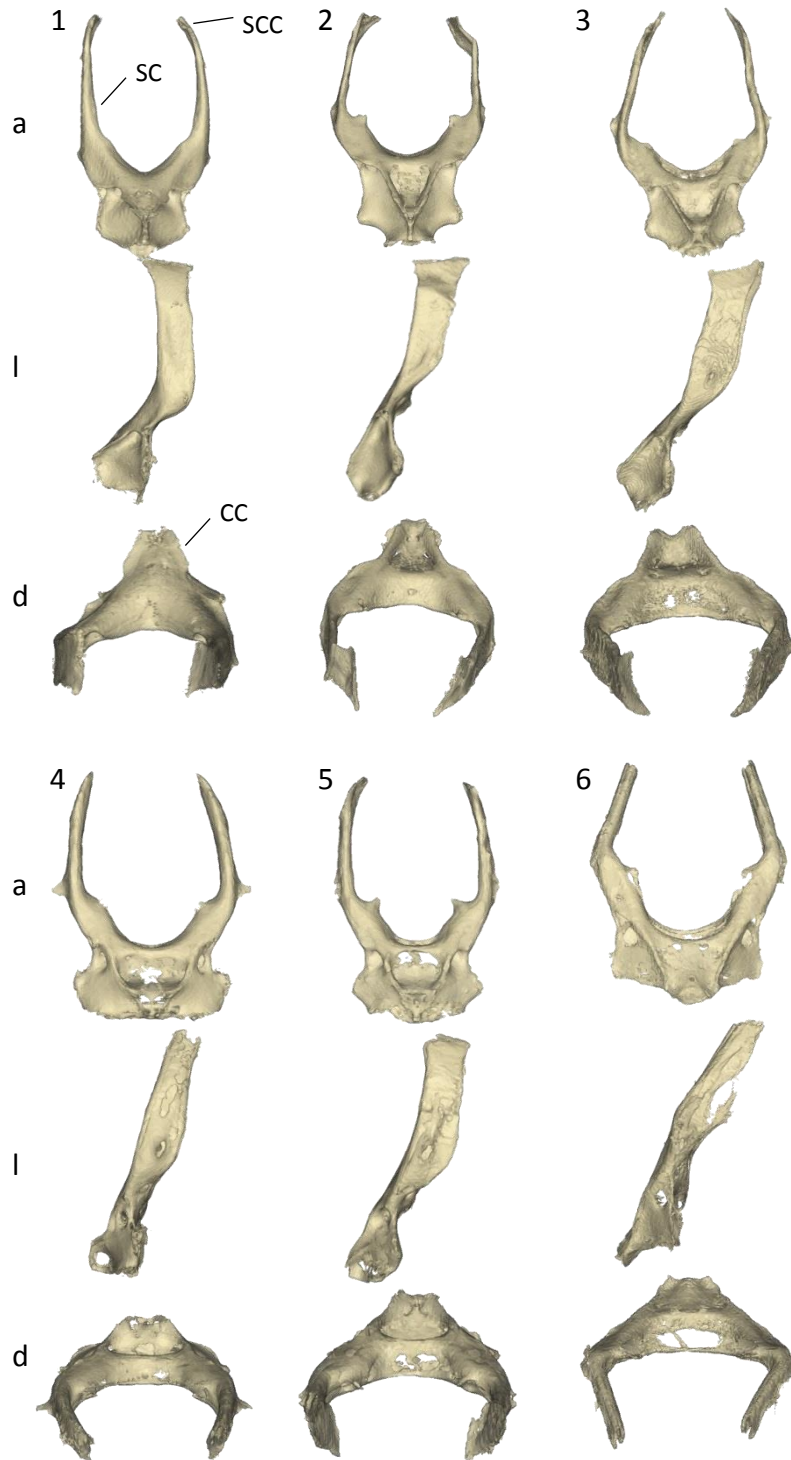


Figure 35. Chondrichthyan scapuolcoracoids showing morphological diversity across the order Chimaeriformes in three views, Anterior (a), Lateral (l), and Dorsal (d). 1, Callorhinchidae (*Callorhynchus milii*); 2-3, Chimaeridae (*Chimaera cubana* and *Hydrolagus novaezealandiae*); 4-6, Rhinochimaeridae (*Harriotta raleighana*, *Neoharriotta carri*, and *Rhinochimaera atlantica*). CC, coracoid; SC, scapular; SCC, suprascapula.

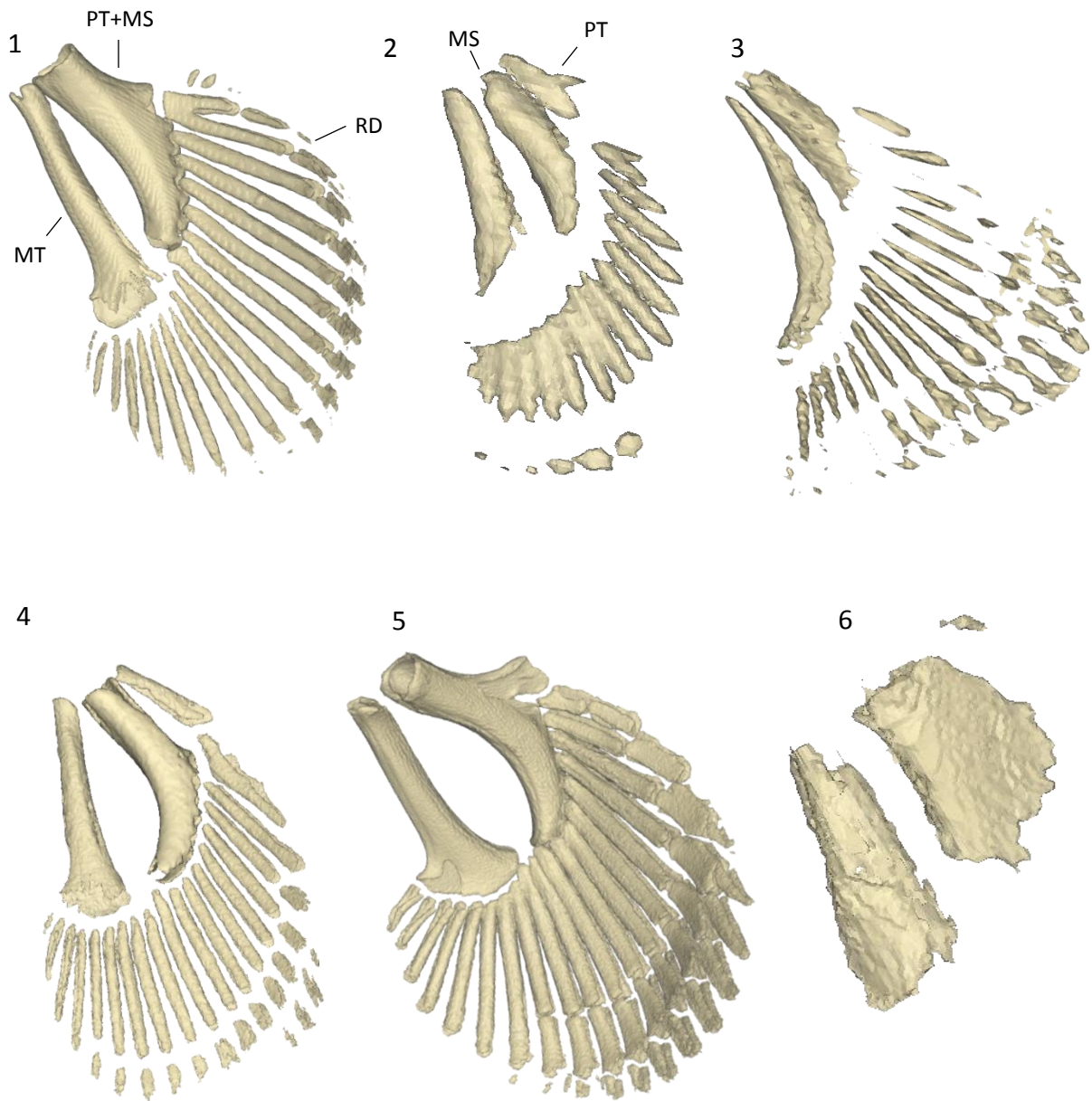


Figure 36. Pectoral fin variation in the Orectolobiforms; 1, *Parascyllium collare*; 2, *Brachaelurus waddi*; 3, *Orectolobus maculatus*; 4, *Chiloscyllium plagiosum*; 5, *Hemiscyllium ocellatum*; 6, *Stegostoma fasciatum*. MS, mesopterygium; MT, metapterygium; PT, propterygium; RD, radials.

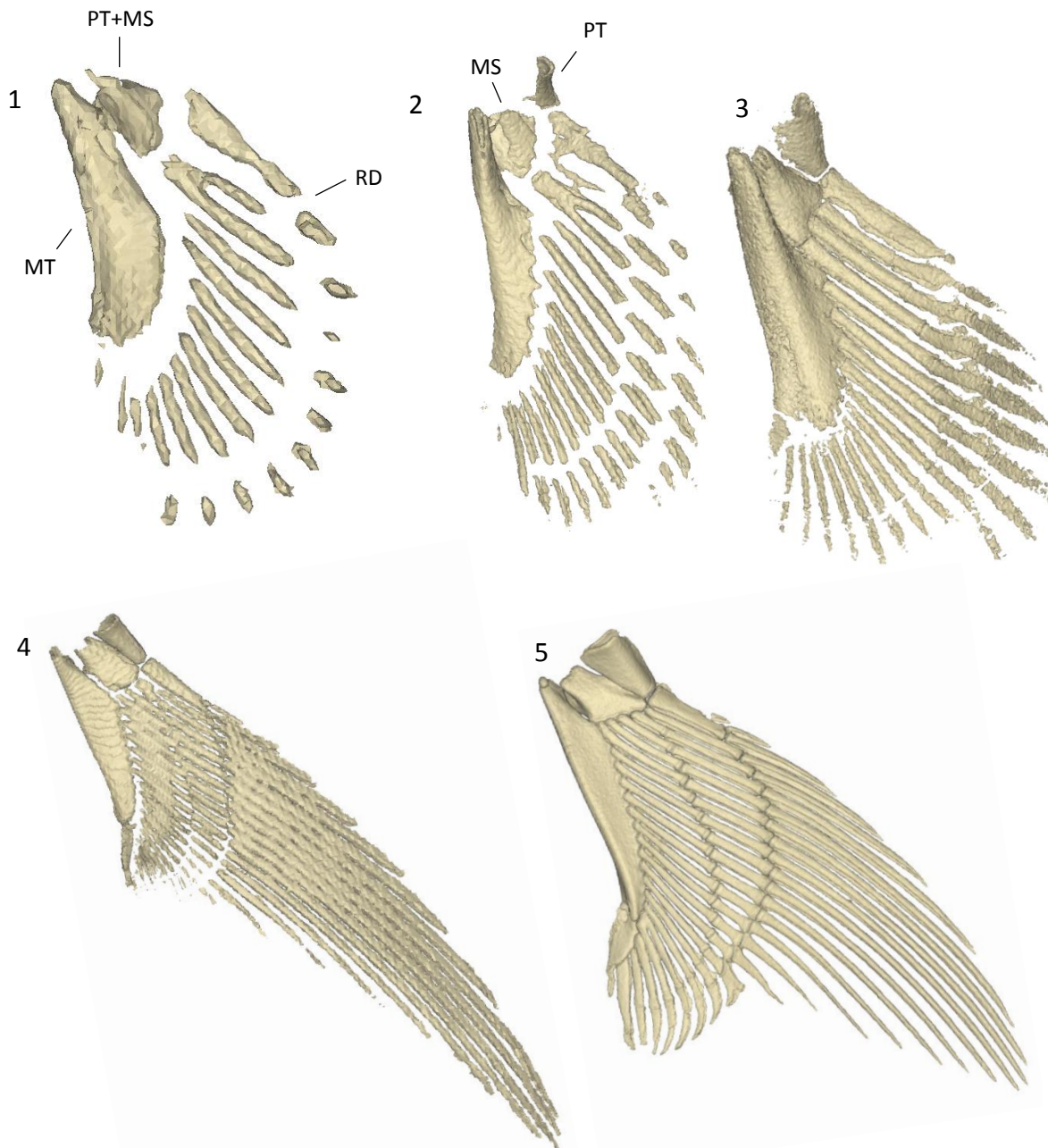


Figure 37. Pectoral fin variation in the Carcharhiniformes; 1, Scyliorhinidae (*Schlyiorhinus meadi*); 2, Proscyllidae (*Eridacnis radcliffei*); 3, Triakidae (*Mustelus manazo*); 4, Carcharhinidae (*Carcharhinus galapagensis*); 5, Sphrynidae (*Sphyrna tiburo*). MS, mesopterygium; MT, metapterygium; PT, propterygium; RD, radials.

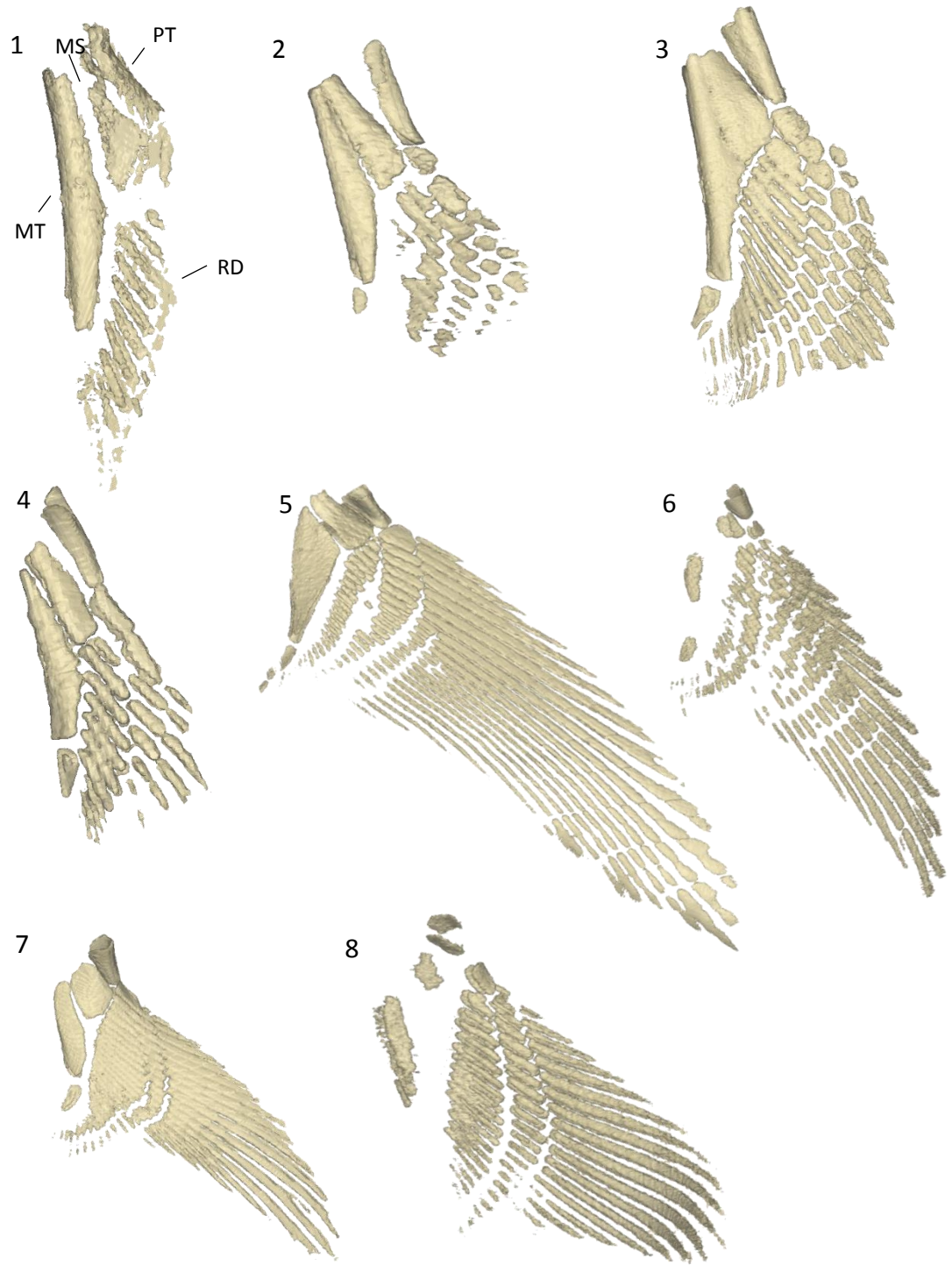


Figure 38. Pectoral fin variation in the Lamniformes; 1, *Mitsukurina owstoni*; 2, *Carcharias taurus*; 3, *Odontaspis ferox*; 4, *Pseudocarcharias kamoharai*; 5, *Alopias superciliosus*; 6, *Carcharodon carcharias*; 7, *Isurus oxyrinchus*; 8, *Lamna ditropis*. MS, mesopterygium; MT, metapterygium; PT, propterygium; RD, radials.

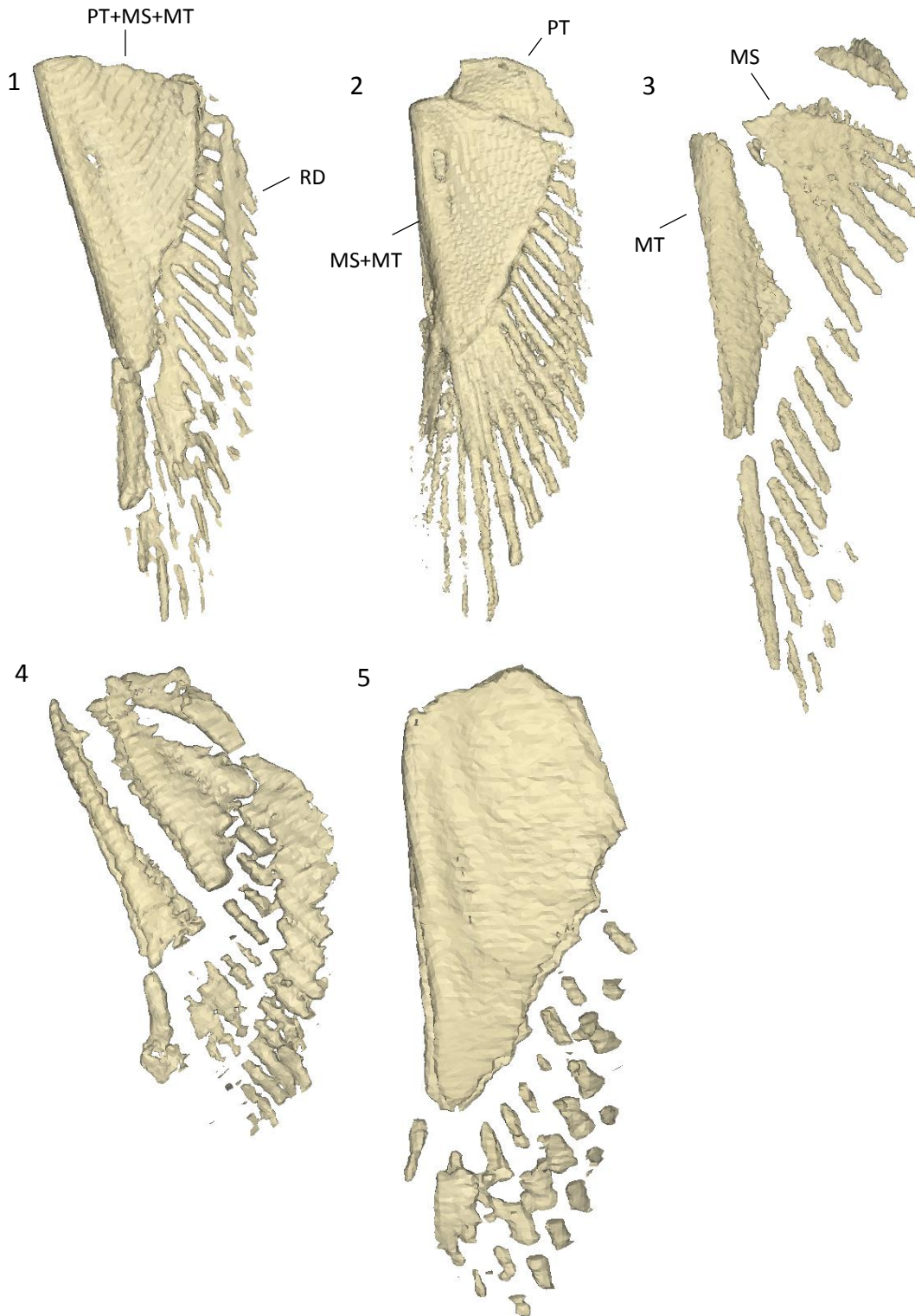


Figure 39. Pectoral fin variation in the Squaliformes; 1, *Centrophorus tessellatus*; 2, *Deania calcea*; 3, *Etmopterus sheikoi*; 4, *Centroscymnus owstoni*; 5, *Dalatias licha*. MS, mesopterygium; MT, metapterygium; PT, propterygium; RD, radials.

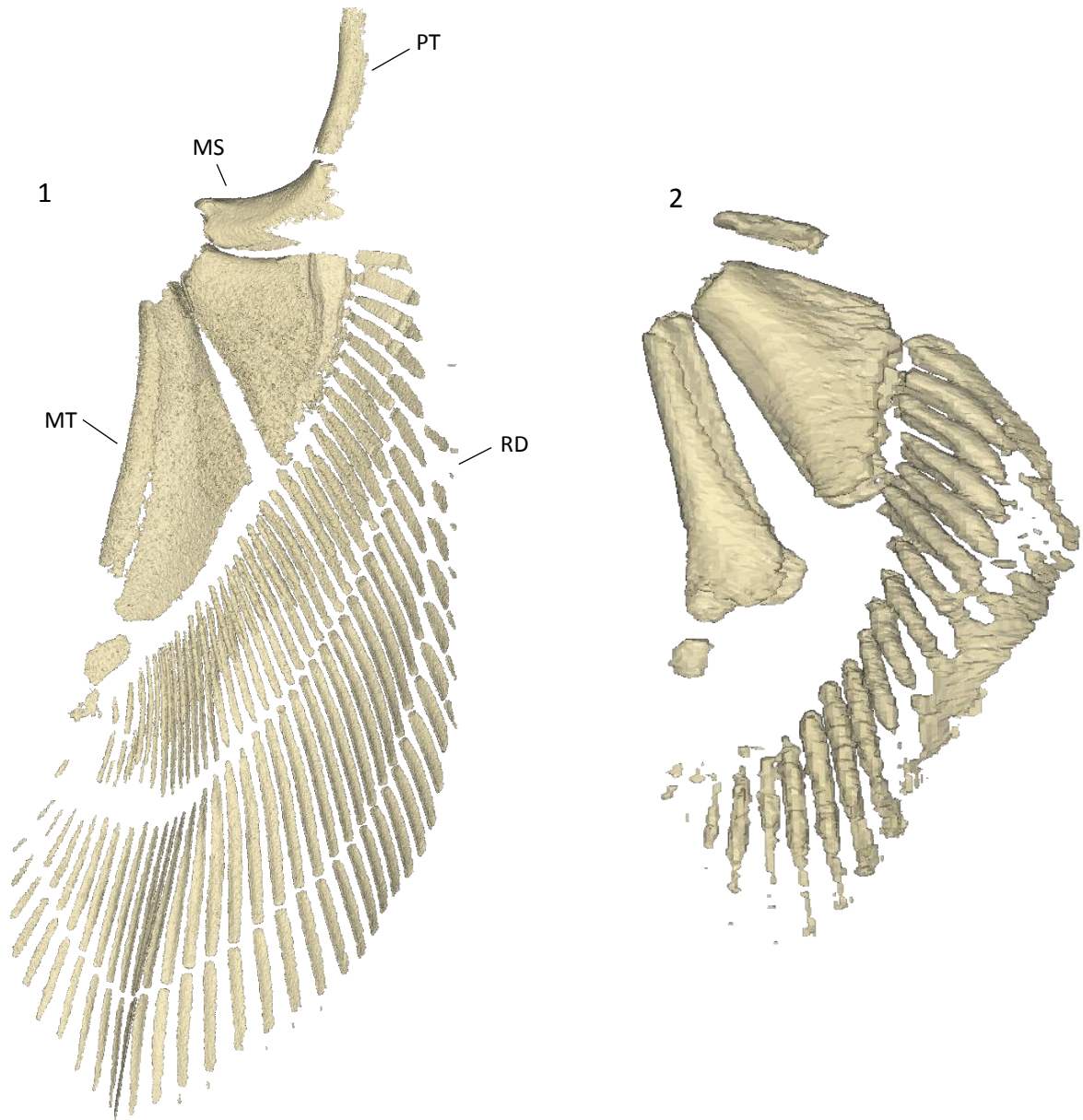
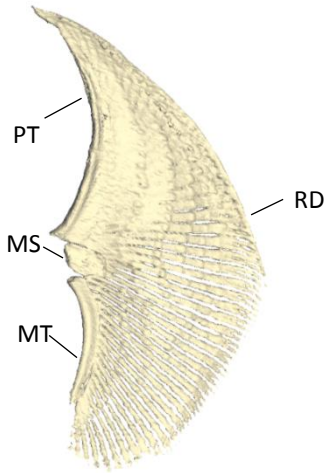


Figure 40. Right pectoral fins of 1, Squatinidae (*Squatina nebulosa*) and 2, Pristiophoridae (*Pristiophorus nudipinnis*). MS, mesopterygium; MT, metapterygium; PT, propterygium; RD, radials.

1



2



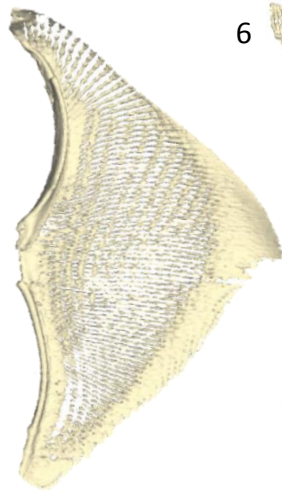
3



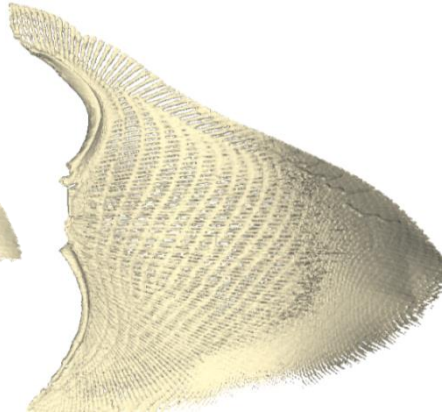
4



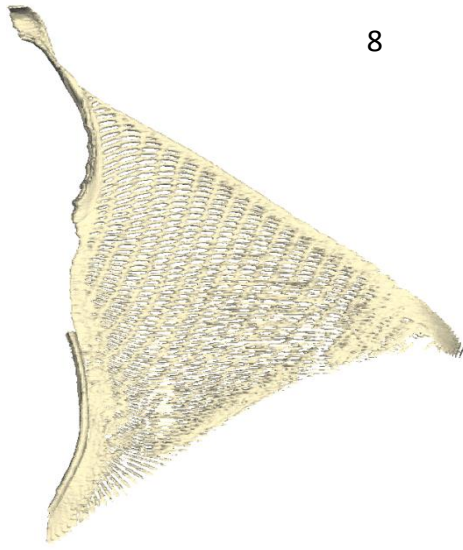
5



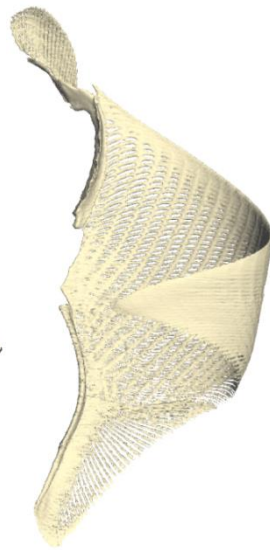
6



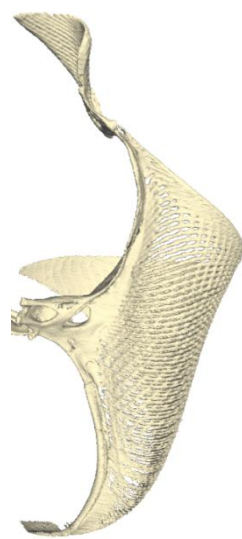
7



8



9



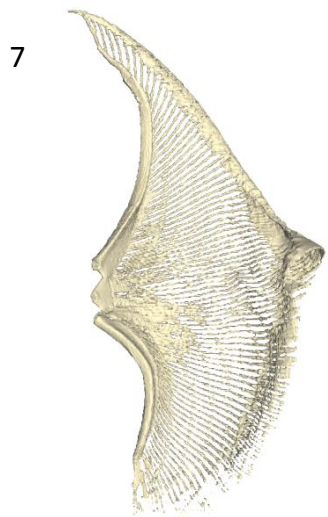
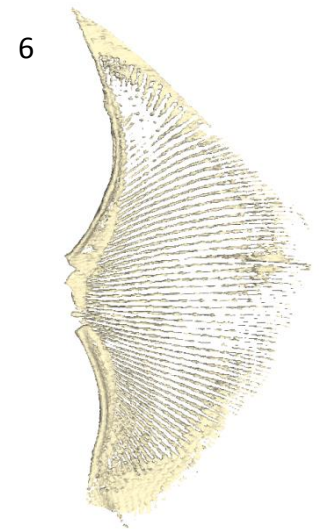
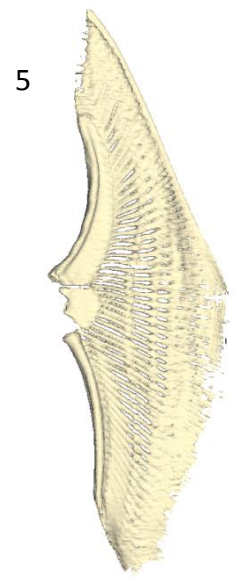
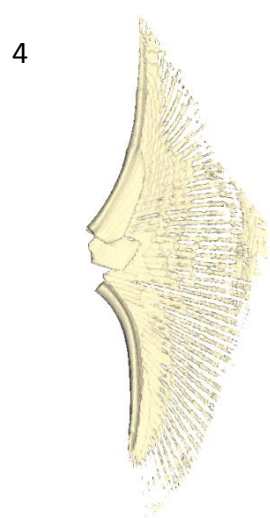
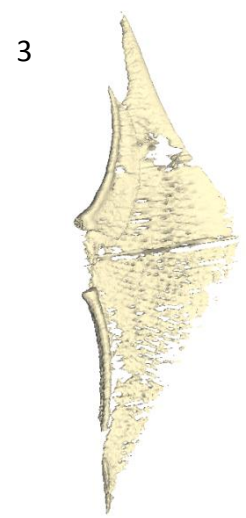
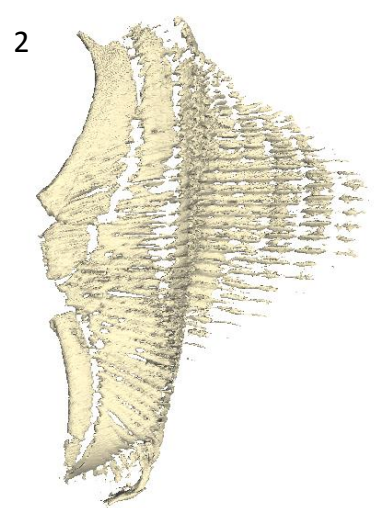
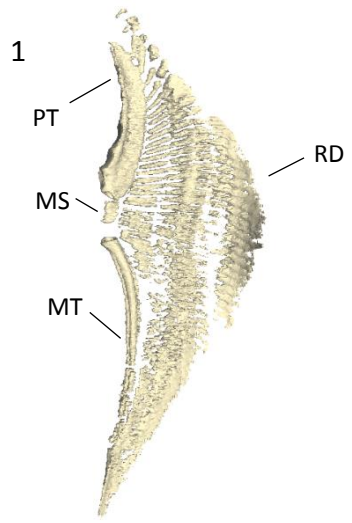


Figure 41. Right pectoral fins of Myliobatiformes; 1, *Platyrrhinoidis triseriata*; 2, *Zanobatus schoeleini*; 3, *Urolophus aurantiacus*; 4, *Urotrygon chilensis*; 5, *Neotrygon kuhlii*; 6, *Gymnura altavela*; 7, *Pteromylaeus bovinus*; 8, *Rhinoptera bonasus*; 9, *Mobula munkiana*. MS, mesopterygium; MT, metapterygium; PT, propterygium; RD, radials.

Figure 42. Right pectoral fins of Pristidae and the Rajiformes; 1, *Pristis clavata*; 2, *Rhina ancylostoma*; 3, *Rhynchobatus springeri*; 4, *Aptychotrema vincentiana*; 5, *Rhinobatos lentiginosus*; 6, *Irolita waitii*; 7, *Dactylobatus armatus*; 8, *Dentiraja lemprieri*; 9, *Anacanthobatis folirostris*. MS, mesopterygium; MT, metapterygium; PT, propterygium; RD, radials.

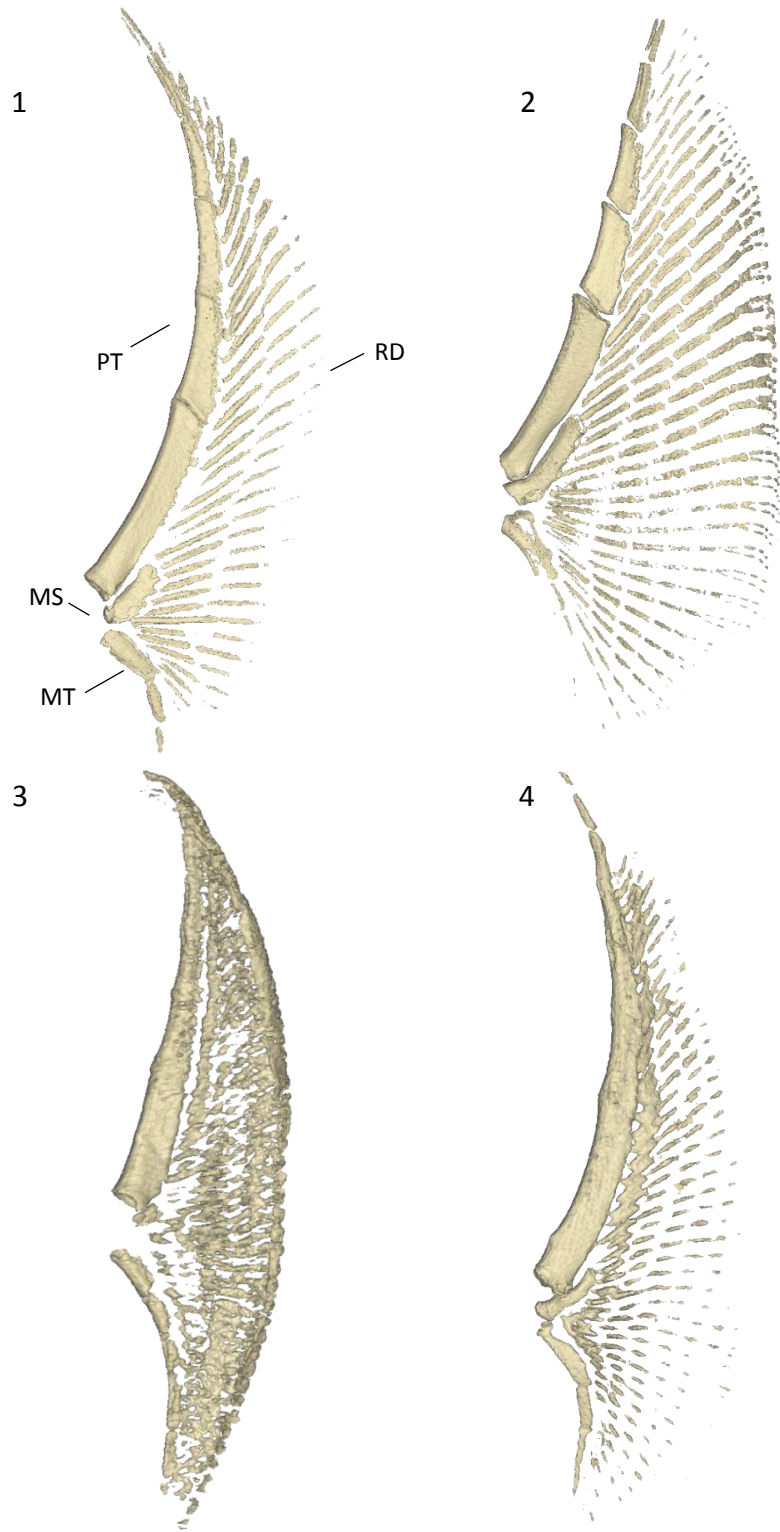


Figure 43. Right pectoral fins of the Torpediniformes; 1, *Narcine brasiliensis*; 2, *Narke japonica*; 3, *Hypnos monopterygius*; 4, *Torpedo fuscomaculata*. MS, mesopterygium; MT, metapterygium; PT, propterygium; RD, radials.

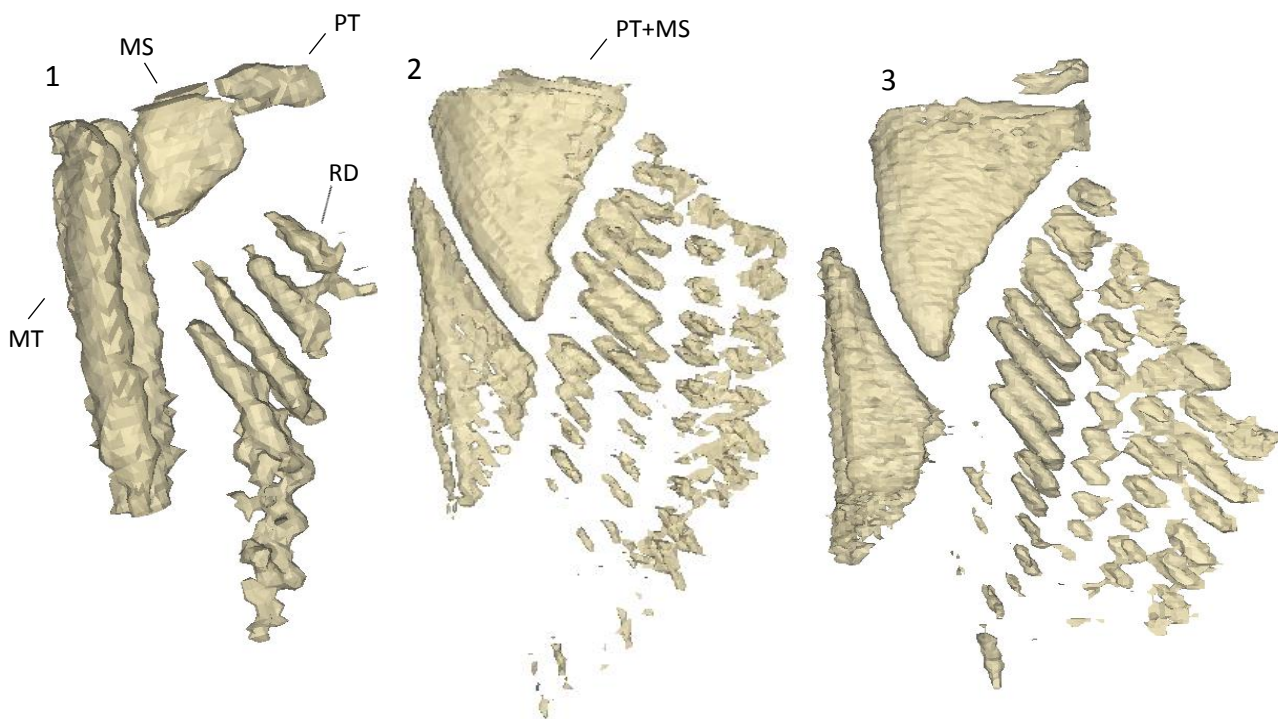


Figure 44. Right pectoral fins of the Hexanchiforms; 1, Chlamydoselachidae (*Chlamydoselachus anguineus*); 2-3, Hexanchidae (*Hepttranchias perlo* and *Hexanchus nakamurai*). MS, mesopterygium; MT, metapterygium; PT, propterygium; RD, radials.

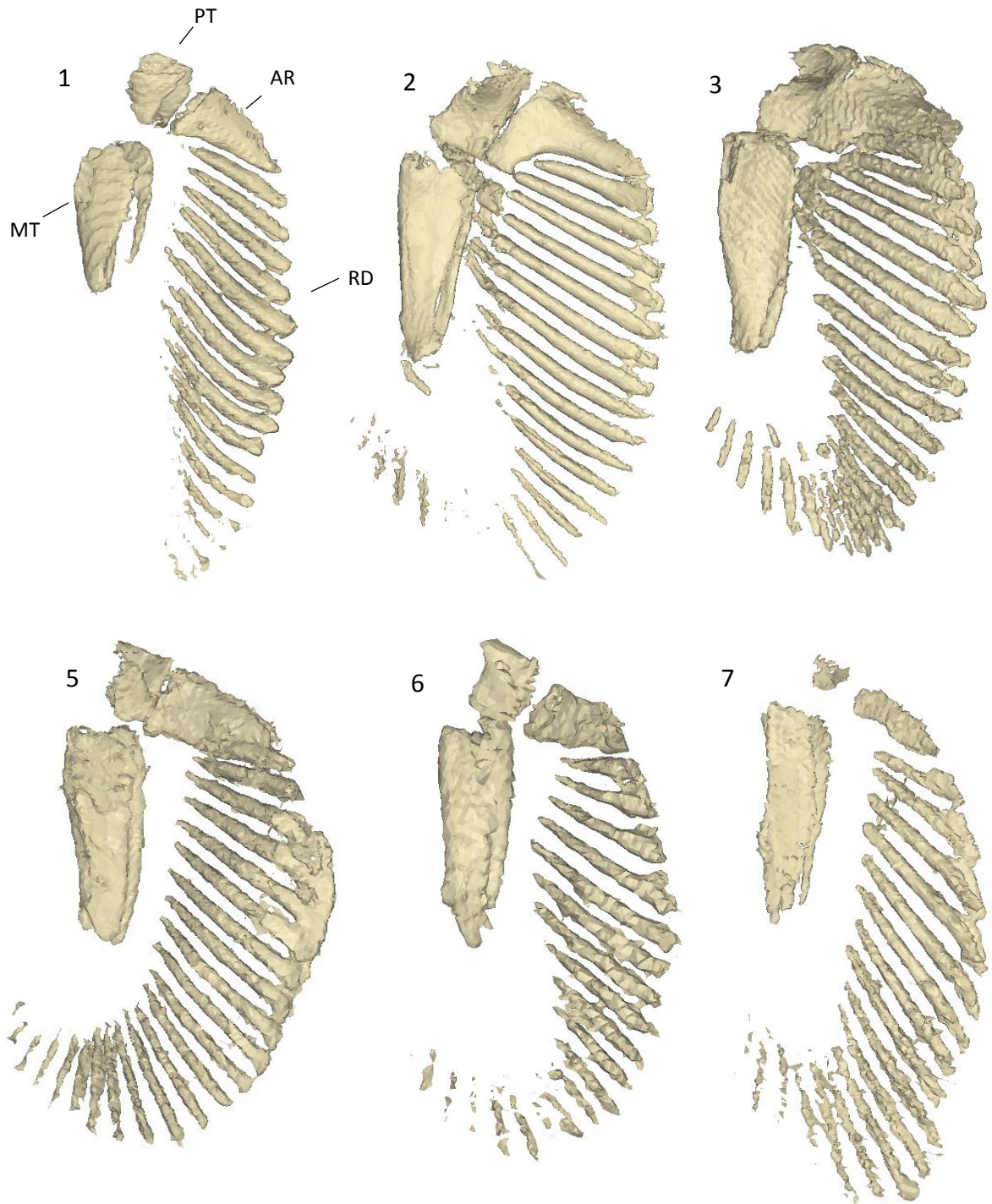


Figure 45. Right pectoral fins of the Chimaeriforms; 1, Callorhynchidae (*Callorhynchus milii*); 2-3, Chimaeridae (*Chimaera cubana* and *Hydrolagus novaezealandiae*); 4-6, Rhinochimaeridae (*Harriotta raleighana*, *Neoharriotta carri*, and *Rhinochimaera atlantica*). AR, anterior radial; MT, metapterygium; PT, propterygium; RD, radials.

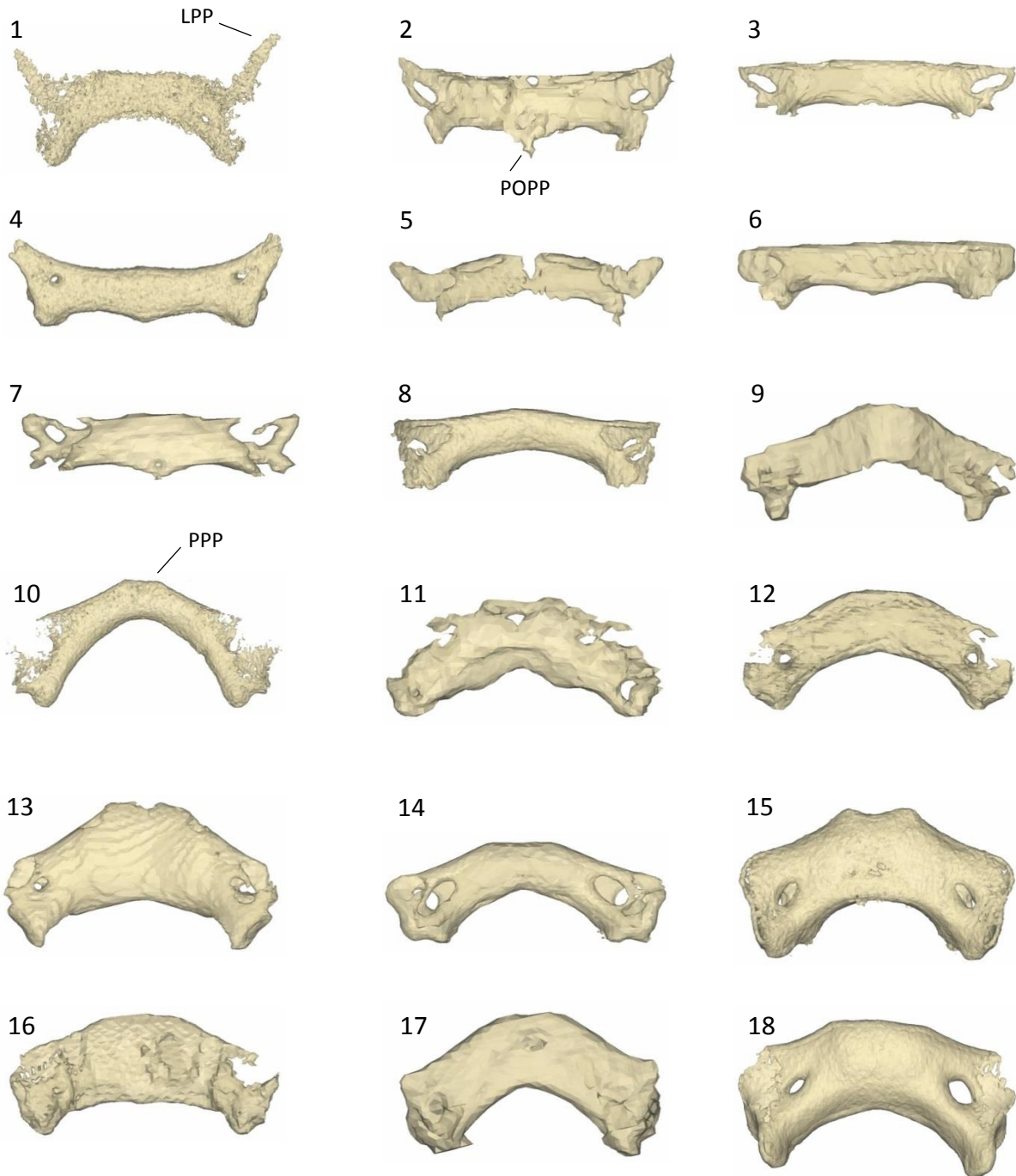


Figure 46. Puboischiadic bars from chondrichthyans showing morphological diversity across the order Carcharhiniformes. 1-7, Scyliorhinidae (*Apristurus macrostomus*, *Bythaelurus waddi*, *Cephaloscyllium isabellum*, *Galeus sauteri*, *Poroderma africanum*, *Schroederichthys chilensis*, and *Scyliorhinus meadi*); 8, Proscylliidae (*Eridacnis radcliffei*); 9, Leptochariidae (*Leptocharias smithii*); 10, Triakidae (*Mustelus manazo*); 11, Hemigaleidae (*Hemipristis elongatus*); 12-16, Carcharhinidae (*Carcharhinus galapagensis*, *Negaprion brevirostris*, *Rhizoprionodon terraenovae*, *Scoliodon macrorhynchus*, and *Triaenodon obesus*); 16-17, Sphyrnidae (*Eusphyrna blochii* and *Sphyrna tiburo*). LPP, lateral prepelvic process; POPP, postpelvic process; PPP, prepelvic process.

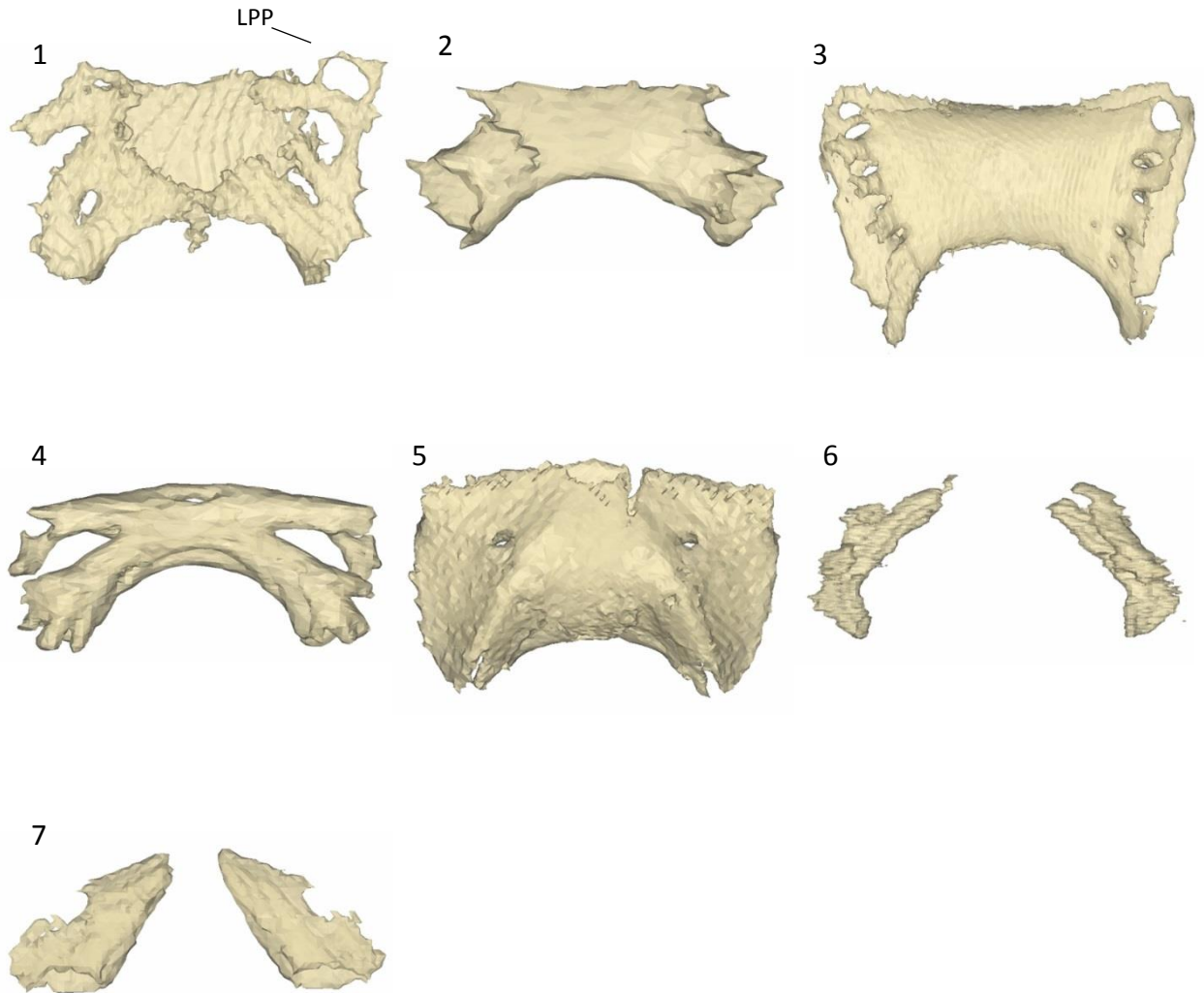


Figure 47. Puboischiadic bars from chondrichthyan showing morphological diversity across the order Lamniformes. 1, Mitsukurinidae (*Mitsukurina owstoni*); 2-3, Odontaspididae (*Carcharias taurus* and *Odontaspis ferox*); 4, Pseudochariidae (*Pseudocarcharias kamoharai*); 5, Alopiidae (*Alopias superciliosus*); 6-7, Lamnidae (*Carcharodon carcharias*, and *Isurus oxyrinchus*). LPP, lateral prepelvic process; POPP, postpelvic process; PPP, prepelvic process.

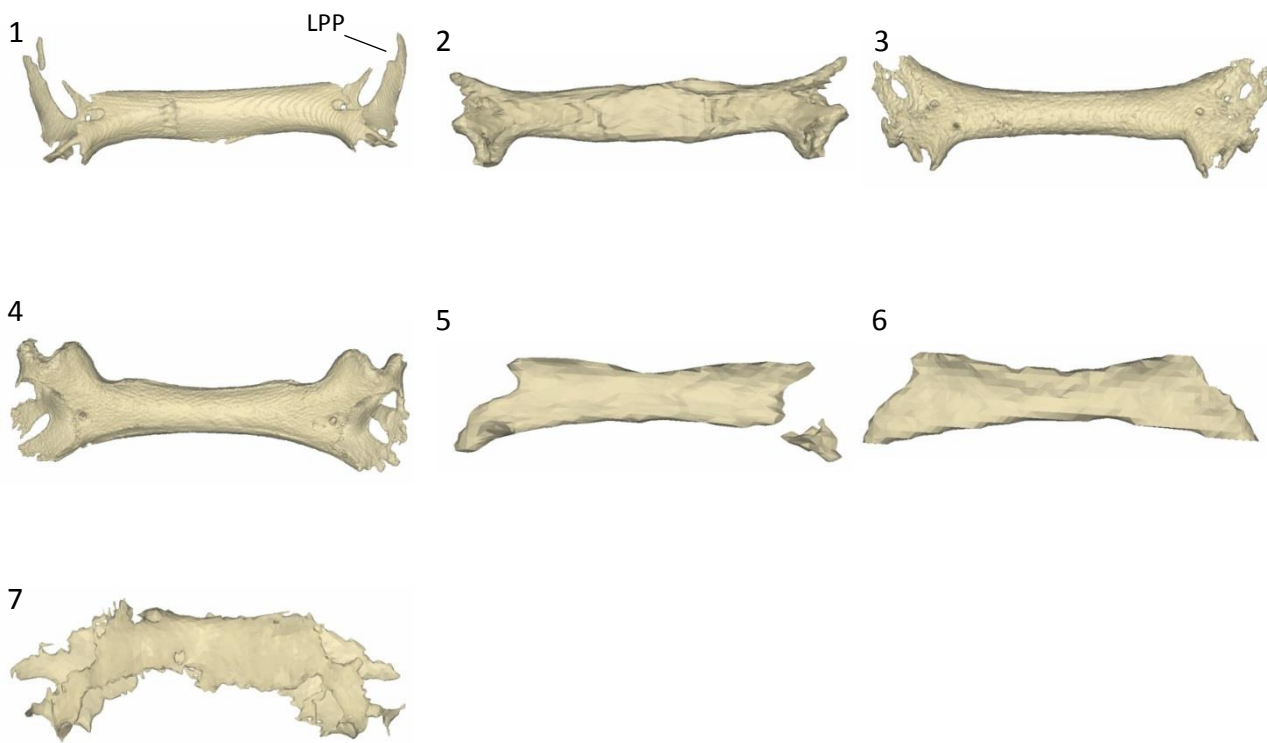


Figure 48. Puboischiadic bars from chondrichthyan showing morphological diversity across the order Orectolobiformes. 1, Parascylliidae (*Parascyllium collare*); 2, Orectolobidae (*Orectolobus maculatus*); 3-4, Hemiscylliidae (*Chiloscyllium plagiosum* and *Hemiscyllium ocellatum*); 5-6, Ginglymostomatidae (*Ginglymostoma cirratum* and *Nebrius ferrugineum*); 7, Stegostomatidae (*Stegostoma fasciatum*). LPP, lateral prepelvic process.

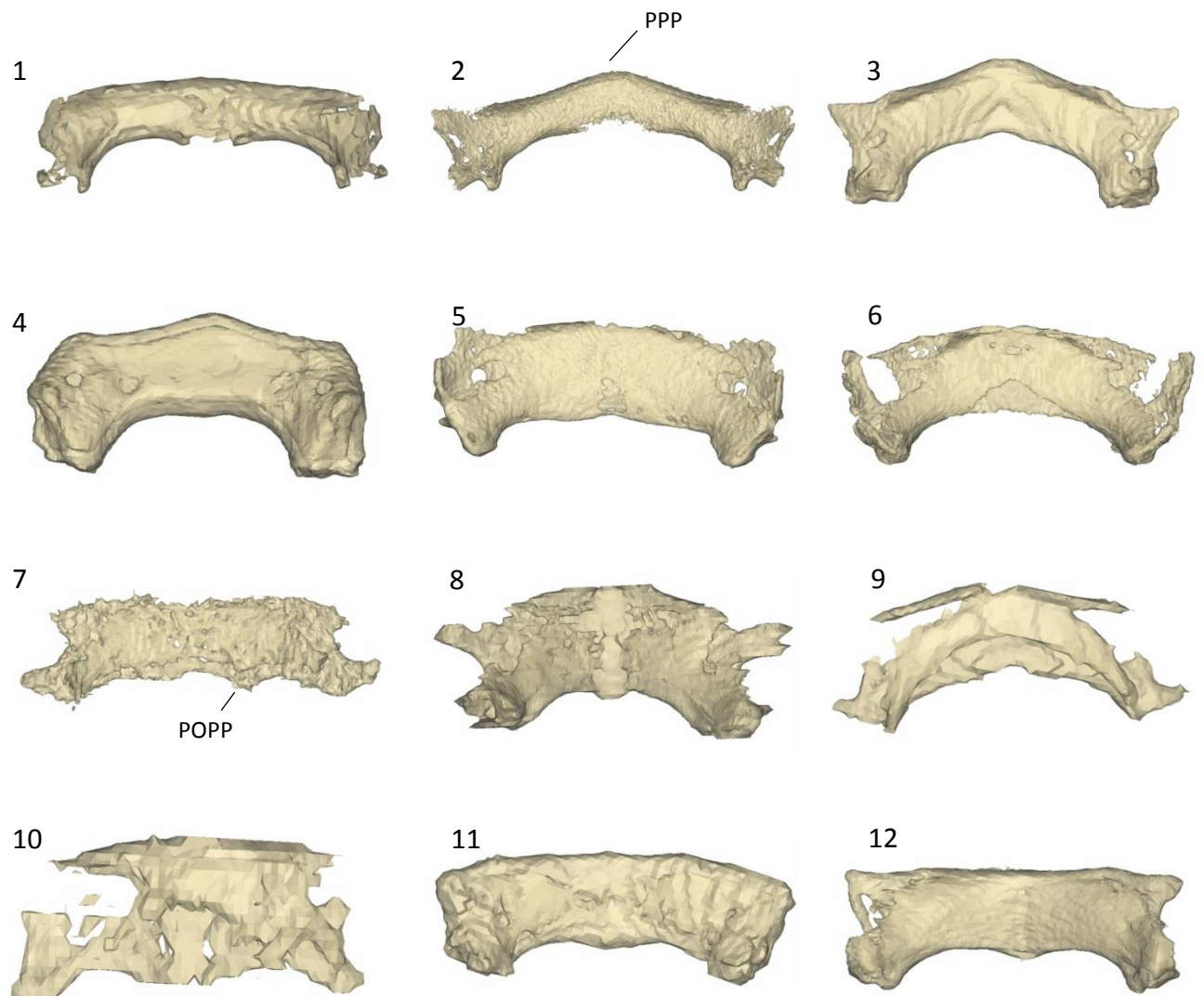


Figure 49. Puboischiadic bars from chondrichthyan showing morphological diversity across the order Squaliformes. 1, Echinorhinidae (*Echinorhinus brucus*); 2-3, Squalidae (*Squalus acanthias* and *Squalus brevirostris*); 4-5, Centrophoridae (*Centrophorus tessellatus* and *Deania calcea*); 6-7, Etmopteridae (*Etmopterus sheikoi* and *Trigonognathus kabeyai*); 8-10, Somniosidae (*Centroscymnus owstoni*, *Scymnodon rigens* and *Zameus squamulosus*); 11, Oxynotidae (*Oxynotus centrina*); 12, Dalatiidae (*Dalatias licha*). POPP, postpelvic process; PPP, prepelvic process.

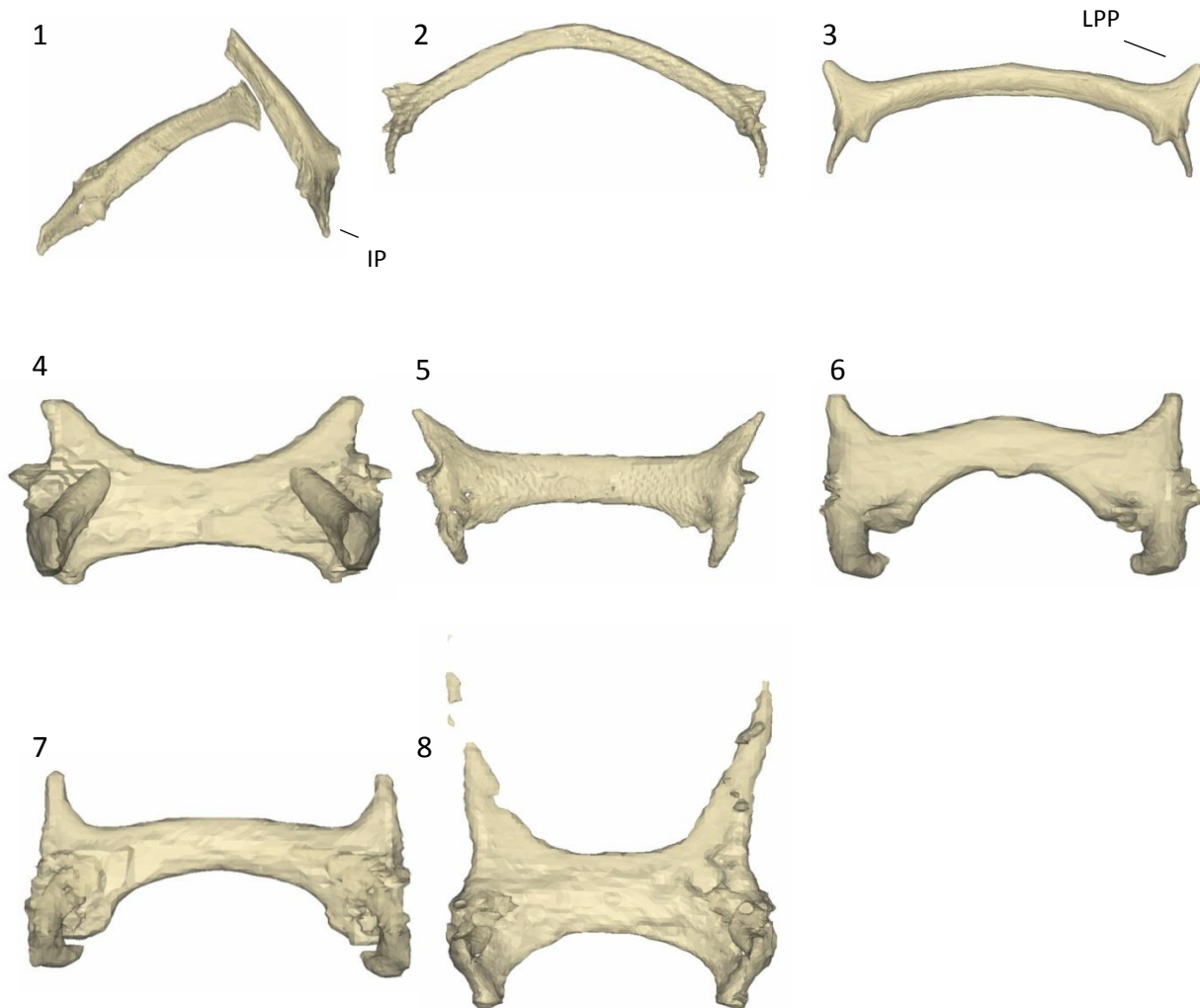


Figure 50. Puboischiadic bars from chondrichthyan showing morphological diversity across the order Rajiformes. 1, Rhinidae (*Rhina ancylostoma*); 2, Rhynchobatidae (*Rhynchobatus springeri*); 3-4, Rhinobatidae (*Aptychotrema vincentiana* and *Rhinobatos lentiginosus*); 5, Arhynchobatidae (*Irolita waitii*); 6-7, Rajidae (*Dactylobatus armatus* and *Raja eglantaria*); 8, Anacanthobatidae (*Anacanthobatis folirostris*). IP, iliac process; LPP, lateral prepelvic process.

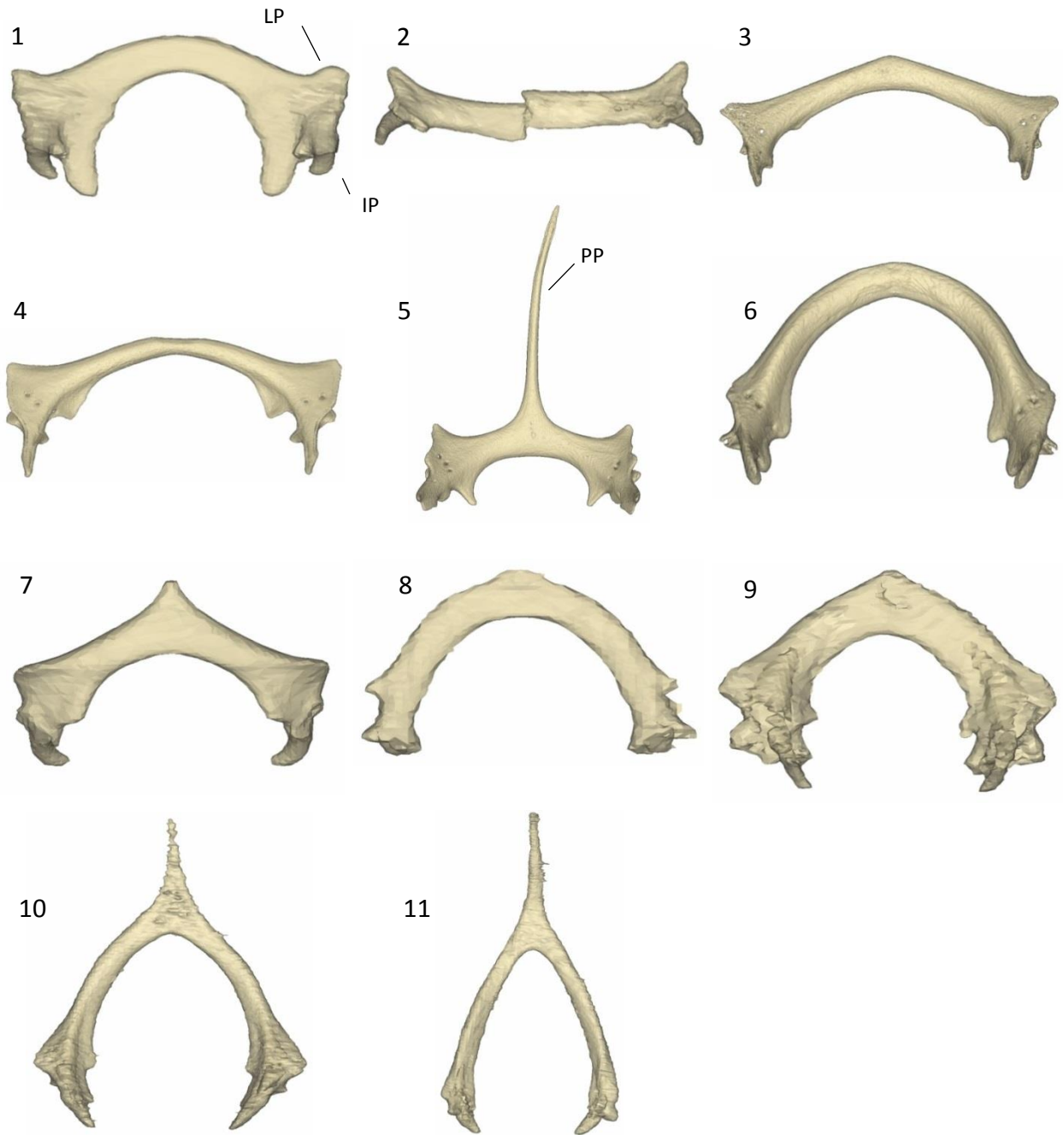


Figure 51. Puboischiadic bars from chondrichthyan showing morphological diversity across the order Myliobatiformes. 1, Zanobatidae (*Zanobatus schoeleini*); 2, Platyrrhinidae (*Platyrrhinoidis triseriata*); 3, Urolophidae (*Urolophus aurantiacus*); 4, Urotrygonidae (*Urotrygon chilensis*); 5, Potamotrygonidae (*Potamotrygon motoro*); 6-7, Dasyatidae (*Dasyatis zugei* and *Neotrygon kuhlii*); 8, Gymnuridae (*Gymnura altaveala*); 9, Myliobatidae (*Pteromylaeus bovinus*); 10, Rhinopteridae (*Rhinoptera bonasus*); 11, Mobulidae (*Mobula munkiana*). IP, iliac process; LPP, lateral prepelvic process; PPP, prepelvic process.

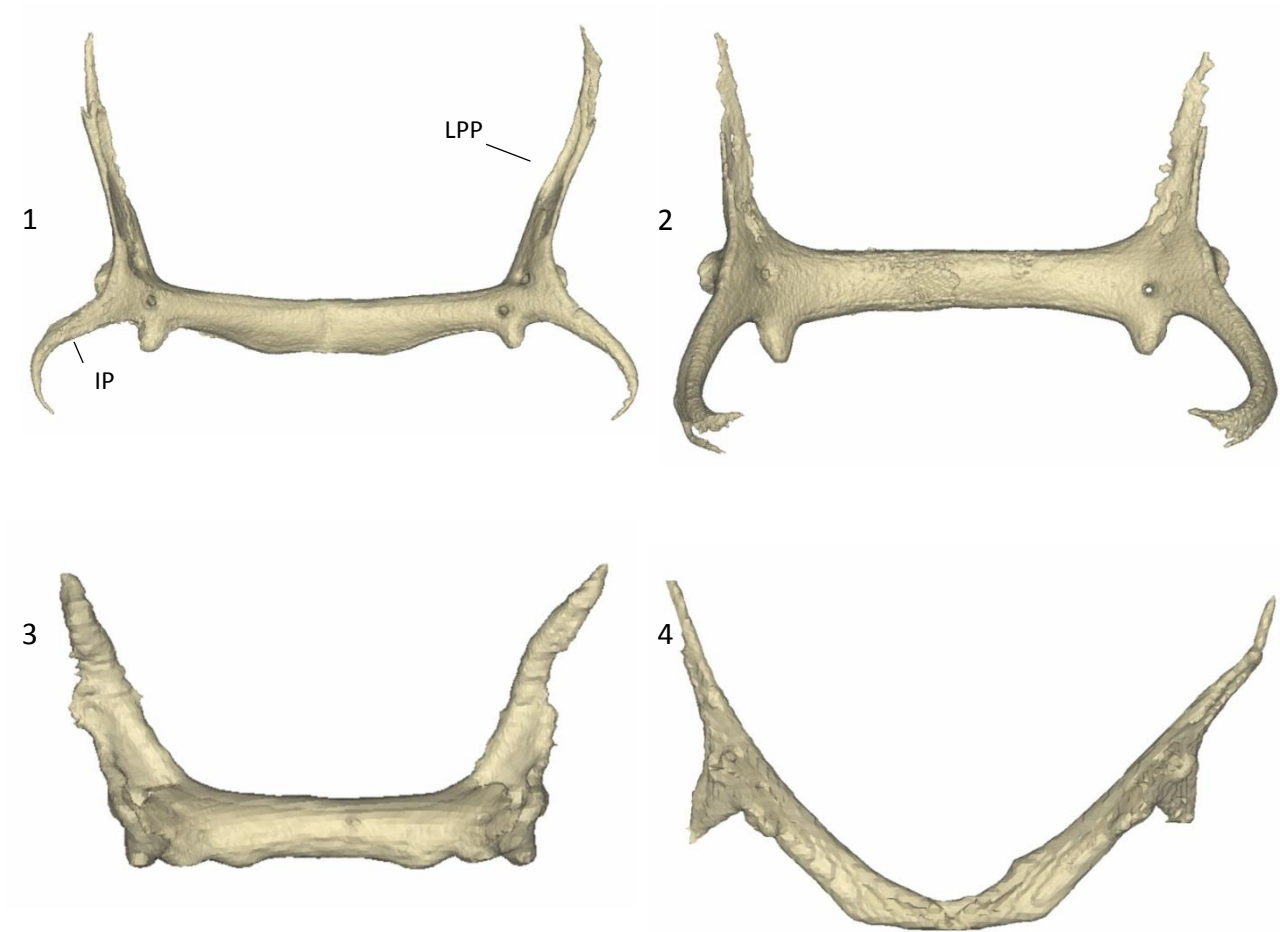


Figure 52. Pubischiadic bars from chondrichthyan showing morphological diversity across the order Torpediniformes. 1, Narcinidae (*Narcine brasiliensis*); 2, Narkidae (*Narke japonica*); 3, Hypnidae (*Hypnos monopterygius*); 4, Torpedinidae (*Torpedo fuscomaculata*). IP, iliac process; LPP, lateral prepelvic process.

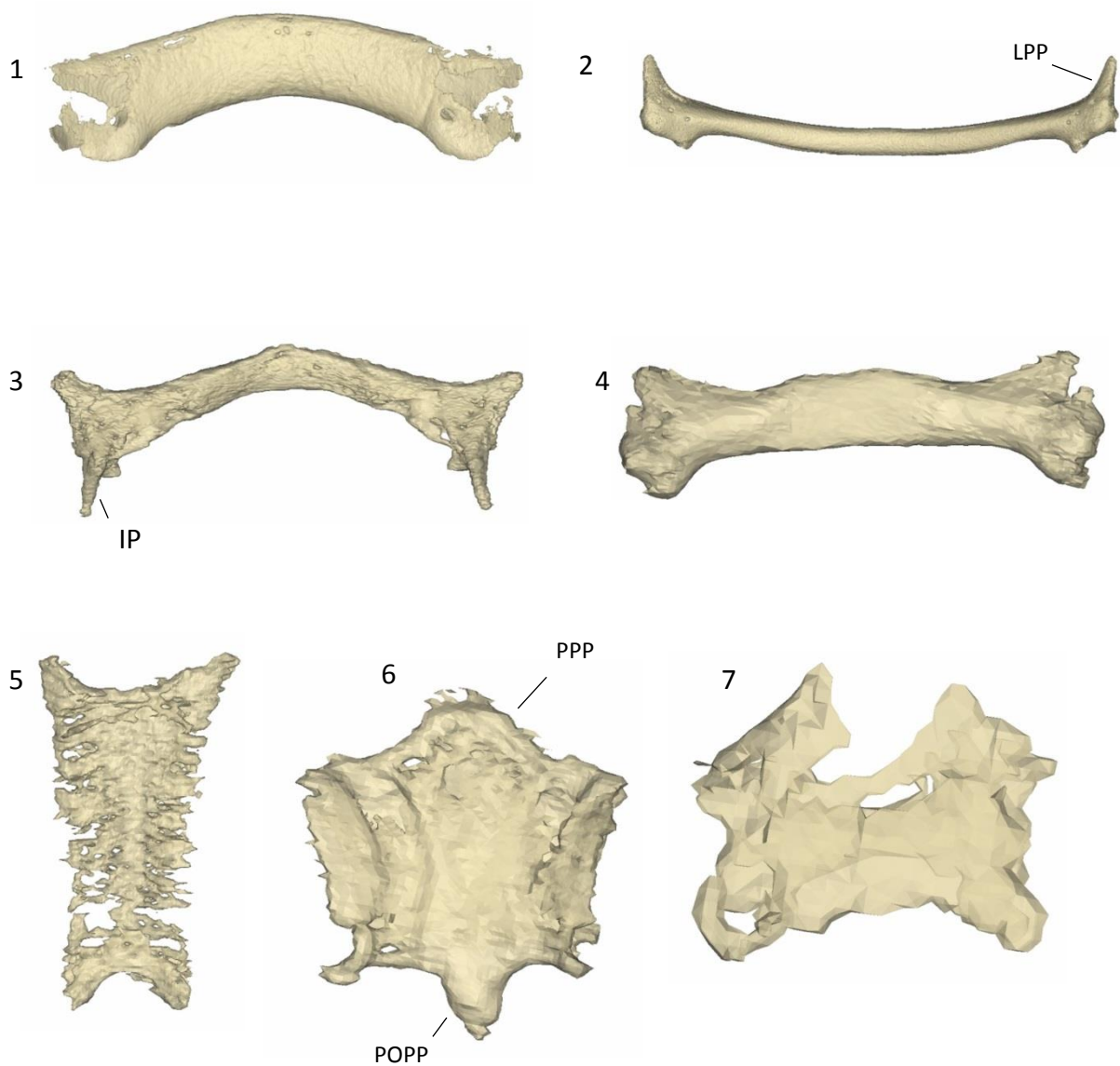


Figure 53. Puboischiadic bars from chondrichthyan orders showing morphological diversity across the orders: 1, Heterodontiformes (*Heterodontus francisci*); 2, Pristiformes (*Pristis clavata*); 3, Pristiophoriformes (*Pristiophorus nudipinnis*); 4, Squatiniformes (*Squatina nebulosa*); 5-7, Hexanchiformes (*Chlamydoselachus anguineus*, *Hexanchus nakamurai* and *Hepttranchias perlo*). IP, iliac process; LPP, lateral prepelvic process; POPP, postpelvic process; PPP, prepelvic process.

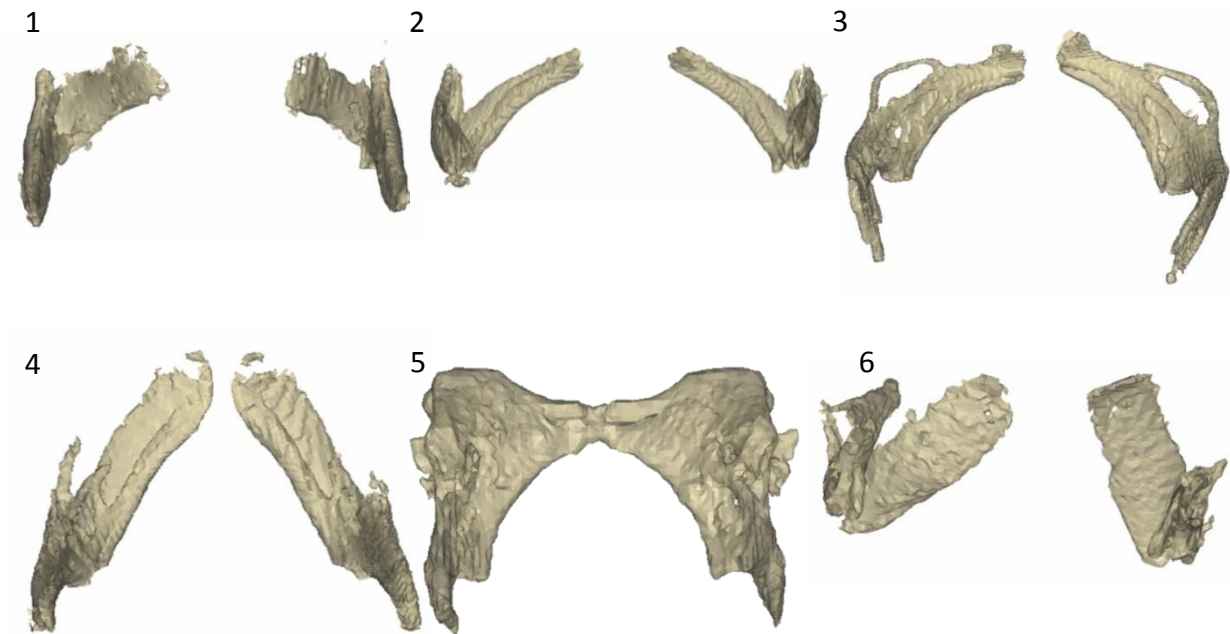


Figure 54. Puboischiadic bars from chondrichthyans showing morphological diversity across the order Chimaeriformes. 1, Callorhynchidae (*Callorhynchus milii*); 2-3, Chimaeridae (*Chimaera cubana* and *Hydrolagus novaezealandiae*); 4-6, Rhinochimaeridae (*Harriotta raleighana*, *Neoharriotta carri*, and *Rhinochimaera atlantica*).

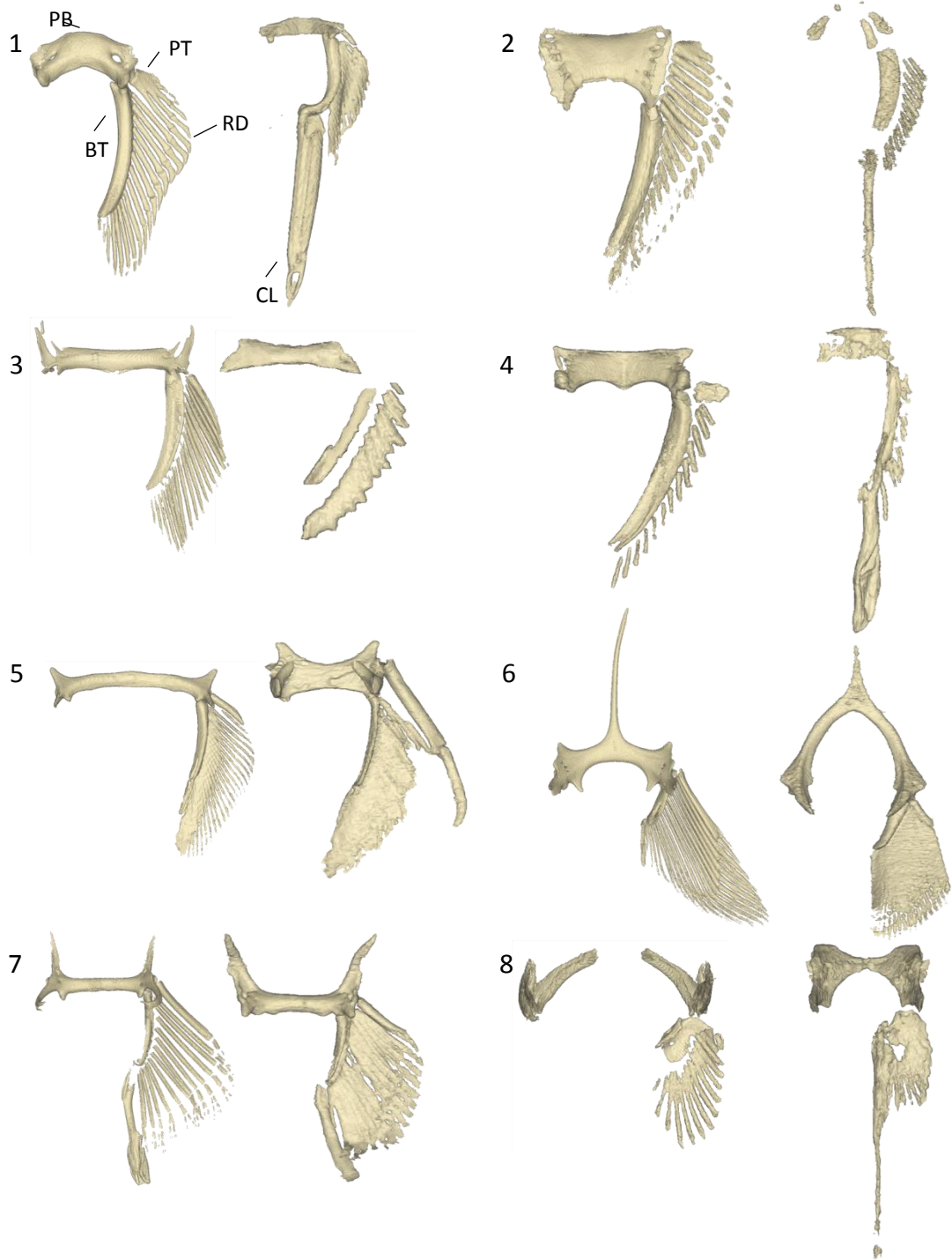
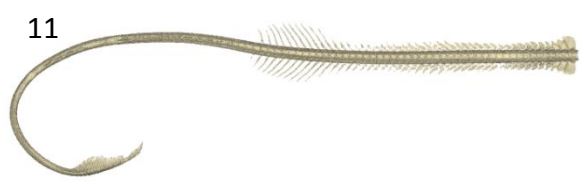
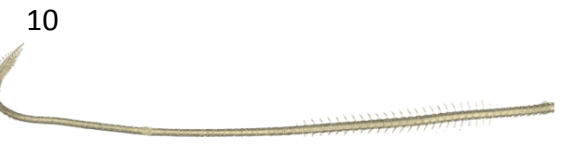
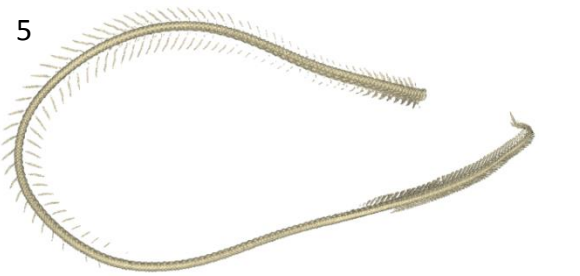


Figure 55. Variations observed in the clarity of pelvic fin structures of some orders of chondrichthyan; 1, Carcharhiniformes (*Sphyrna tiburo* and *Leptocharias smithii*); 2, Lamniformes (*Odontaspis ferox* and *Lamna ditropis*); 3, Orectolobiformes (*Parascyllium collare* and *Nebrius ferrugineum*); 4, Squaliformes (*Dalatias licha* and *Zameus squamulosus*); 5, Rajiformes (*Aptychotrema vincentiana* and *Irolita waitii*); 6, Myliobatiformes (*Potamotrygon motoro* and *Rhinoptera bonasus*); 7, Torpediniformes (*Narke japonica* and *Hypnos monoptyergius*); 8, Chimaeriformes (*Chimaera cubana* and *Neoharriotta raleighana*). BT, basypterygium; CL, claspers; PB, puboischiadic bar; PT, propterygium; RD, radials.



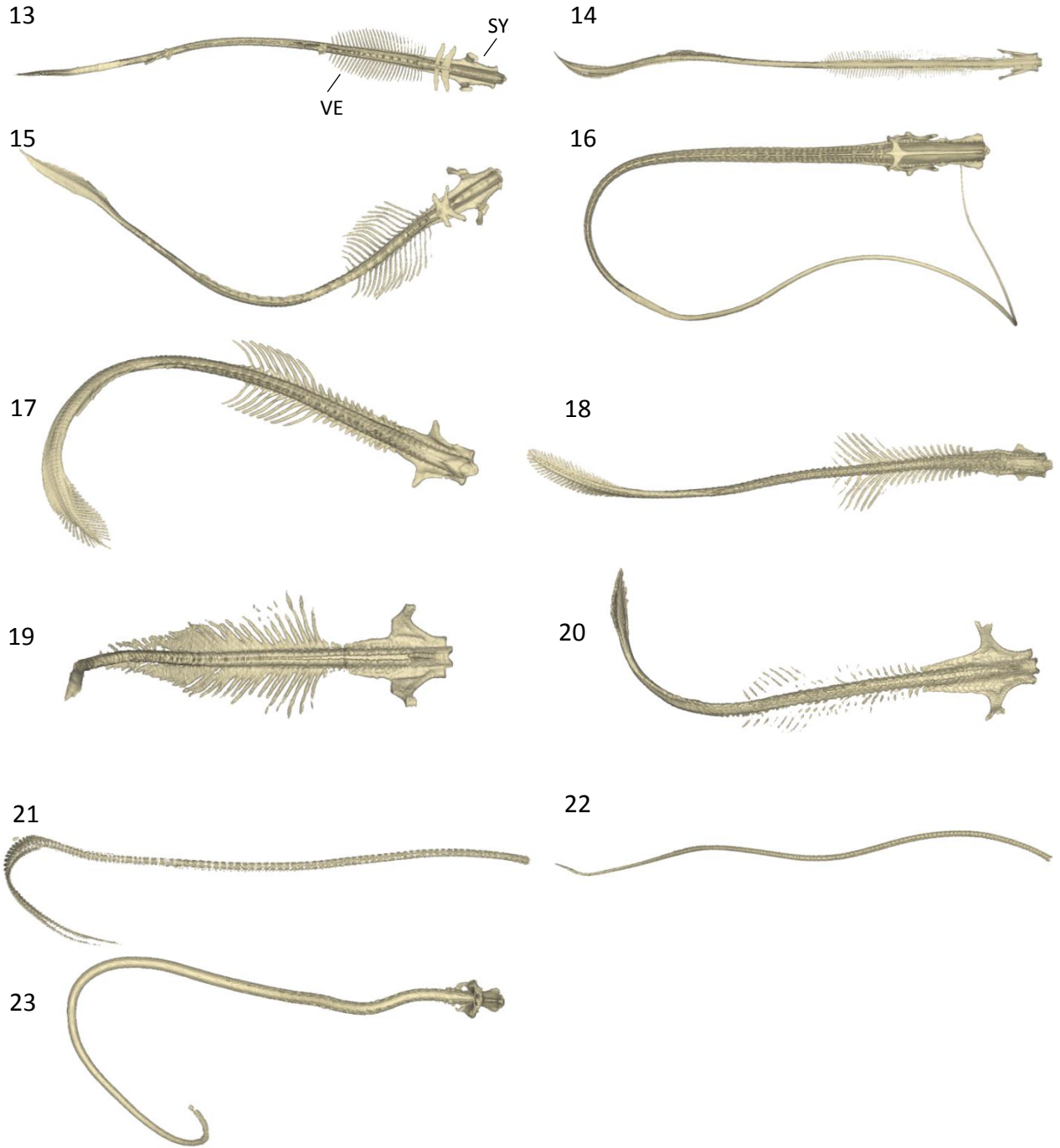


Figure 56. Examples of vertebral columns with and without vertebral ribs; 1, *Galeus sauteri*; 2, *Sphyrna tiburo*; 3, *Carcharias taurus*; 4, *Carcharodon carcharias*; 5, *Parascylium collare*; 6, *Stegostoma fasciatum*; 7, *Echinorhinus brucus*; 8, *Etmopterus splendidus*; 9, *Trigonognathus kabeyai*; 10, *Squalus brevirostris*; 11, *Squatina nebulosa*; 12, *Pristiophorus nudipinnis*; 13, *Rhynchobatus springeri*; 14, *Pristis clavata*; 15, *Platyrhinoidis triseriata*; 16, *Dasyatis zugei*; 17, *Narcine brasiliensis*; 18, *Narke japonica*; 19, *Hypnos monapterygus*; 20, *Torpedo fuscomaculata*; 21, *Hexanchus nakamurai*; 22, *Heptranchias perlo*; 23, *Hydrolagus novaezealandiae*. SY, synarcual; VR, vertebral ribs.

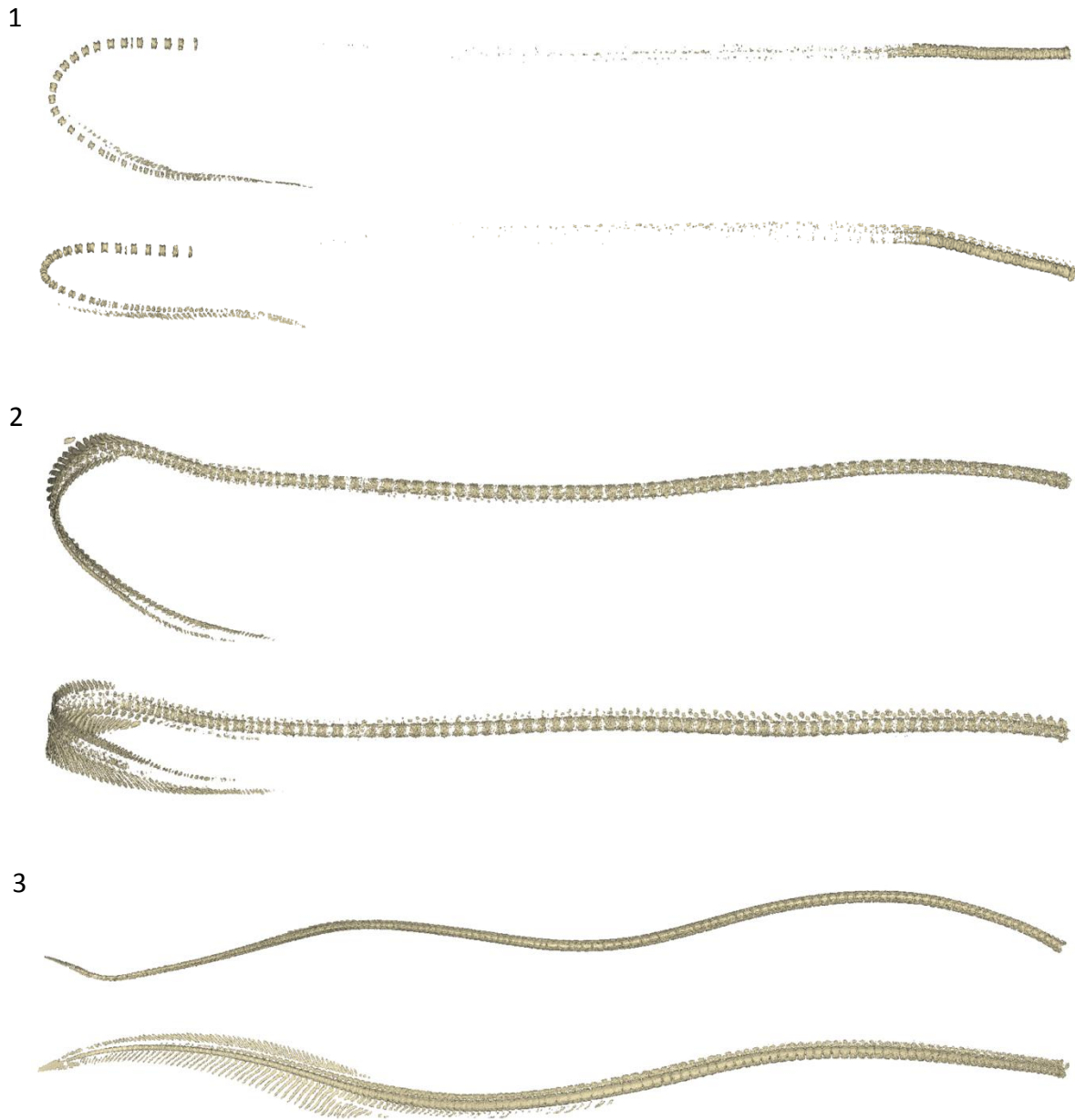


Figure 57. Dorsal (upper) and lateral (lower) views showing the variations in calcification of the vertebral column of the Hexanchiforms; 1, *Chlamydoselachus anguineus*; 2, *Hexanchus nakamurai*; 3, *Heptranchias perlo*.

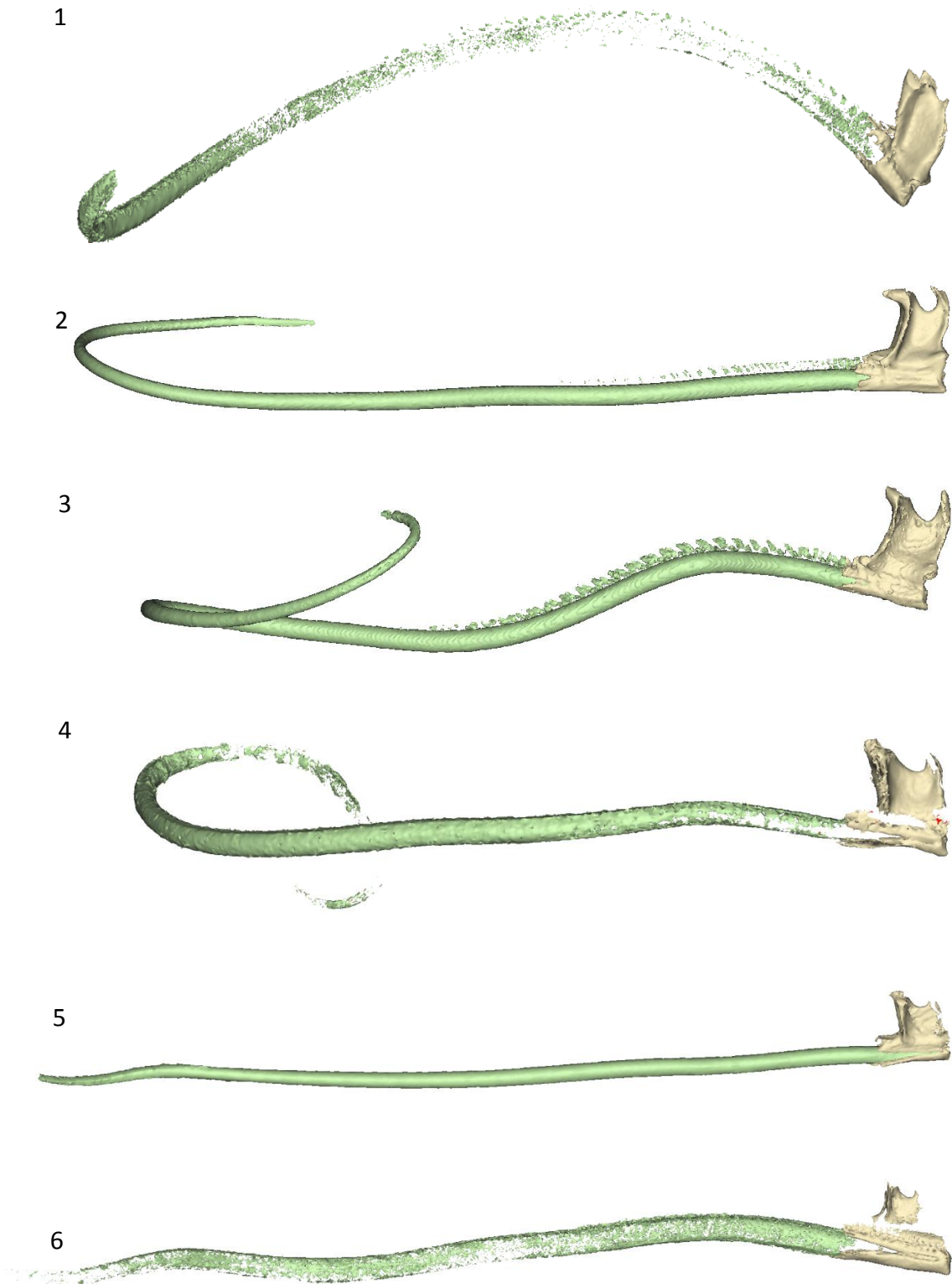


Figure 58. Variations in the vertebral tube (pale green) and synarcual (pale yellow) of the Chimaeriform fishes; 1, *Callorhynchus milli*; 2, *Chimaera cubana*; 3, *Hydrolagus novaezealandiae*; 4, *Harriotta raleighana*; 5, *Neoharriotta carri*; 6, *Rhinochimaera atlantica*.

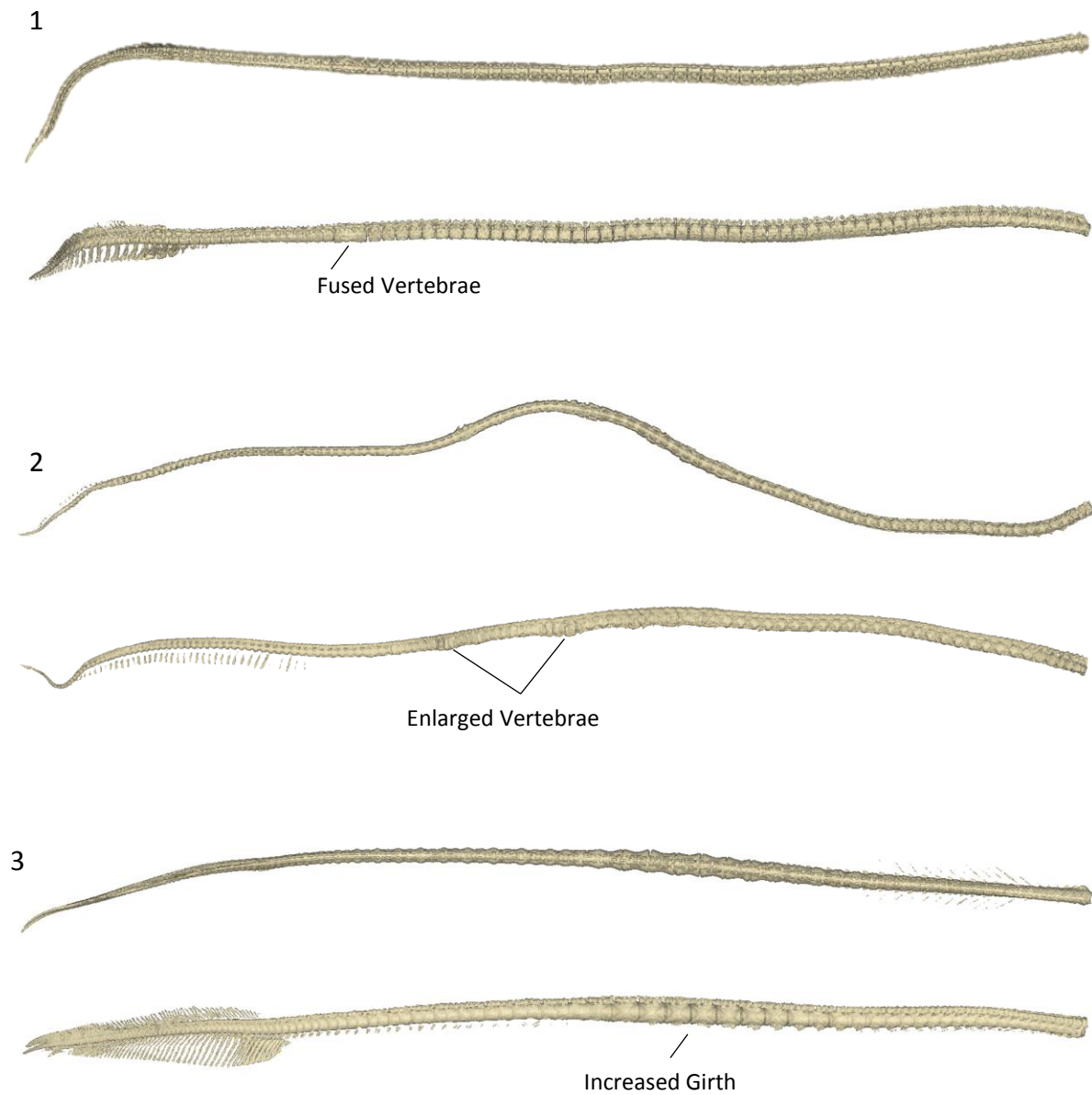
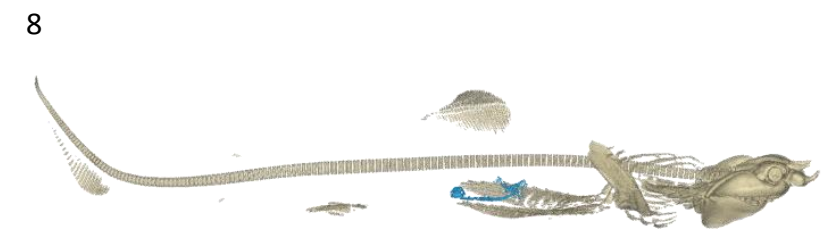
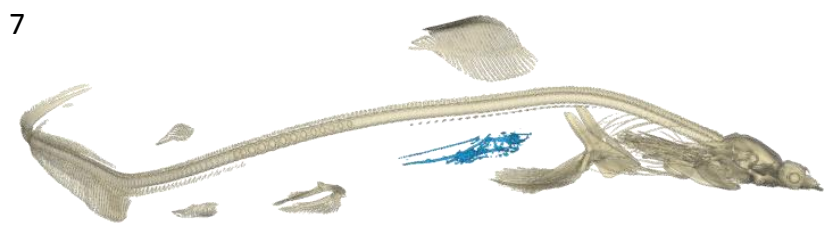
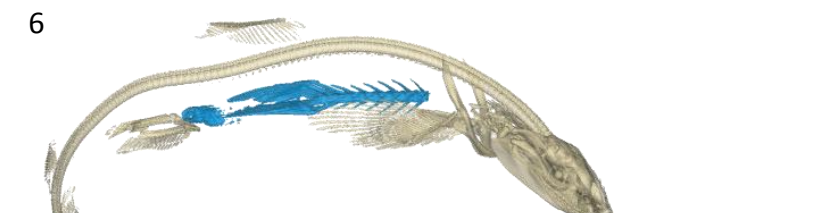
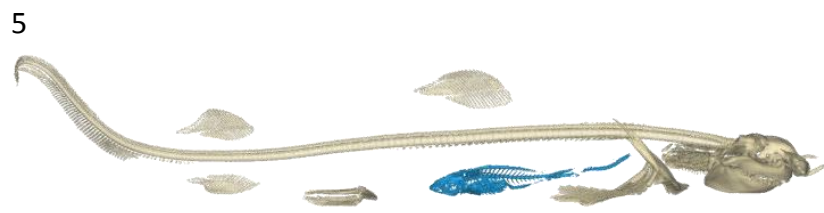
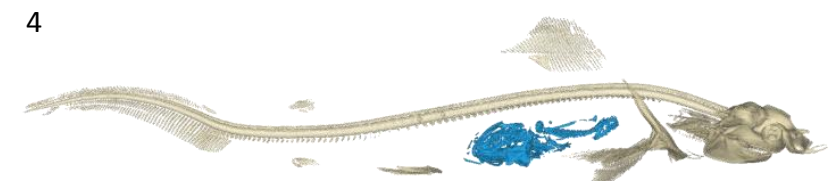
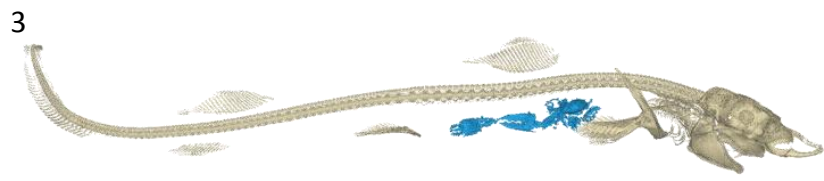
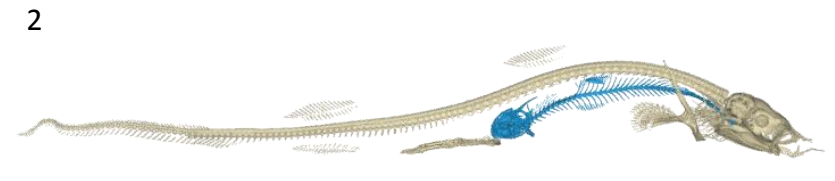
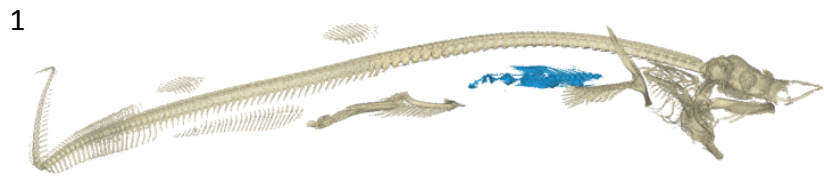


Figure 59. Dorsal and lateral views of examples of abnormal characteristics observed in the vertebral columns of 1, *Centroscyrnus owstoni*; 2, *Bythaelurus canescens*; 3, *Rhizoprionodon terraenova*.



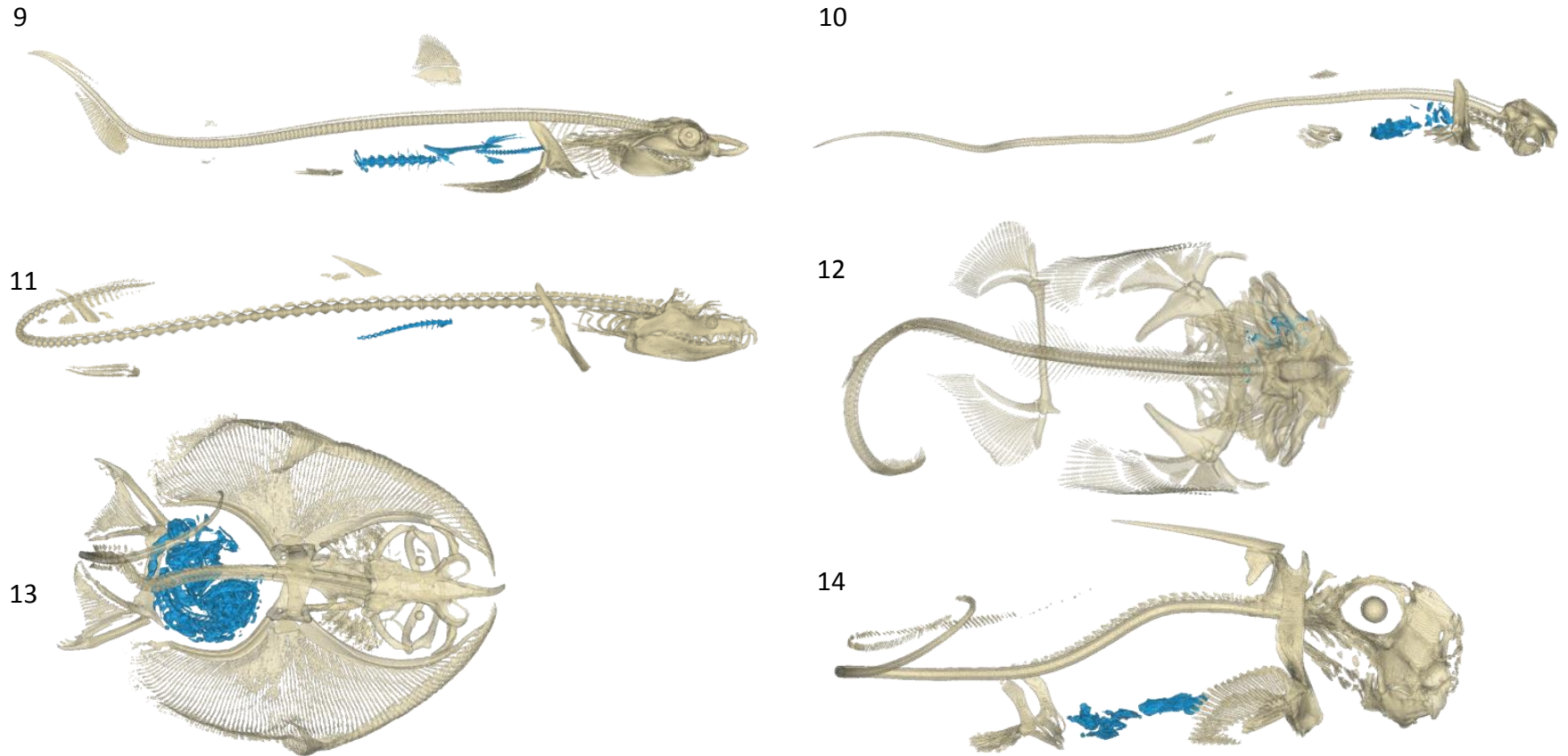


Figure 60. Examples of stomach contents in scanned chondrichthyans. 1, *Galeus sauteri*; 2, *Eridacnis radcliffei*; 3, *Mustelus manazo*; 4, *D. Carcharhinus plumbeus*; 5, *Negaprion brevirostris*; 6, *Triaenodon obesus*; 7, *Sphyrna lewini*; 8, *Carcharodon carcharias*; 9, *Isurus oxyrinchus*; 10, *Stegostoma fasciatum*; 11, *Trigonognathus kabeyi*; 12, *Squatina nebulosa*; 13, *Dactylobatus armatus*; 14, *Hydrolagus novaezealandiae*.

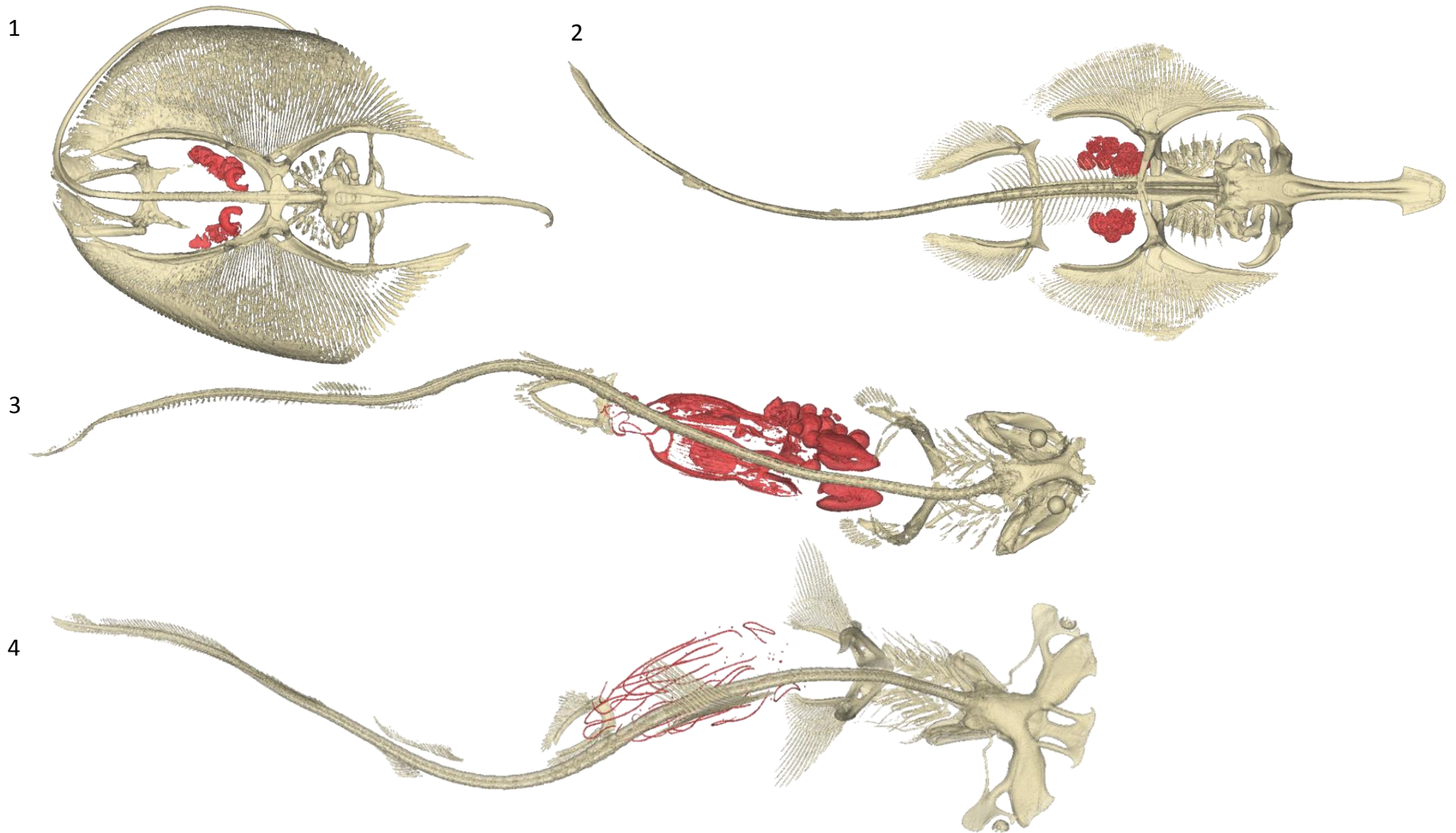


Figure 61. Four specimens with embryonic offspring visible in the CT scans. 1, *Anacanthobatis folirostris*; 2, *Aptychotrema vincentiana*; 3, *Bythaelurus canescens*; 4, *Sphyrna corona*.

Table 1. Characteristics of ideal scanning candidates

Whole body specimen
>1m TL or mature individual if small species <ul style="list-style-type: none">• Very small species are good candidates for high resolution scans
Good contrast in x-ray
Relatively straight specimen- not bent or curved
No obvious trauma (broken or crushed structures)
Available tissue sample

Table 2. Kernel and KV settings for the CT Scanners used in this study

Scanner (Location)	Kernel	KV
Somatom 64-Slice (MUSC)	B10S	80
Somatom Force (MUSC)	QR54*	90, 150 (dual)*
GE Phoenix Vtome x S (AMNH)	---	80-180
Somatom 64 Slice (Brompton)	B30f	100
Toshiba (Orange County)	FC04	120
Somatom 64-Slice (Children's)	B41f	120
Somatom Volume Zoom (WHOI)	H41s	120
Somatom 16-Slice (UC Irvine)	B31s	120

*The segmentation of *Rhina ancyclostoma* was completed using a QR32 Kernel with 90kv and 150kv.

Table 3. Skeletal structures observed in the segmented CT scans. An 'X' denotes presence of the structure in at least one specimen from the group.

Structure	Sharks	Batoids	Holocephalans
Anal Fin	X		X
Anterior Angular Cartilage		X	
Anterior Radial			X
Antorbitals		X	
Basibranchial	X	X	X
Basilhyal	X	X	X
Branchial Rays	X	X	
Branchial Stays		X	
Ceratobranchials	X	X	X
Ceratohyal	X		X
Chondrocranium	X	X	X
Claspers	X	X	X
Dermal Denticles	X	X	
Dorsal Fin(s)	X	X	X
Egg Cases Or Embryos	X	X	
Epibranchials	X	X	X
Eye Cup	X	X	
Hyomandibular	X	X	X
Hypobranchials	X	X	X
Labial Cartilage	X	X	X
Lateral Line			X
Lens	X	X	X
Meckel's Cartilage	X	X	X
Mesopterygium	X	X	
Metapterygium (pectoral)	X	X	X
Metapterygium (pelvic, also called basipterygium)	X	X	X
Palatoquadrate	X	X	
Palatal Cartilage		X	
Pectoral Radials	X	X	X
Pelvic Radials	X	X	X
Pharyngobranchials	X	X	X
Pharyngohyal			X
Posterior Angular Cartilage		X	
Propterygium (Pectoral)	X	X	X
Propterygium (Pelvic)	X	X	X

Pseudohyoid		X	
Puboischiadic Bar	X	X	X
Scapulocoracoid	X	X	X
Spine	X	X	X
Spiracular Cartilage	X	X	
Stomach Contents	X	X	X
Suprascapula		X	
Synarcual		X	X
Tooth Plate (Upper And Lower)	X	X	X
Ventral Pseudohyal		X	
Vertebral column.	X	X	X

Appendix I. Summary of scans and segmentations completed including Order, Family, Genus, and Species coverage. Also included are specimen identification numbers and the location the scanning took place along with the type of scanner used. Abbreviations are as follows:

Collections

AMNH, American Museum of Natural History (New York, NY); **BMNH**, British Museum of Natural History (London, UK); **BPBM**, Bernice Pauahi Bishop Museum (Honolulu, Hawai'i); **CSIRO**, *Commonwealth Scientific and Industrial Research Organisation* (Hobart, Tasmania, Australia); **FMNH**, *Field Museum of Natural History* (Chicago, IL); **GMBL**, *Grice Marine Biological Laboratory* (Charleston, SC); **HUMZ**, *Hokkaido University Museum* (Hokkaido, Japan); **LACM**, *Natural History Museum of Los Angeles County* (Los Angeles, CA); **MCZ**, *Museum of Comparative Zoology at Harvard University* (Cambridge, MA); **SIO**, *Scripps Institute of Oceanography*, San Diego, CA; **UF**, *University of Florida* (Gainesville, FL); **USNM**, *United States National Museum, Smithsonian Institution* (Washington, DC). The following abbreviations designate new specimens to be accessioned into the AMNH collections, **HO**, collected by Hans Ho; **MB**, collected by Ana Verissimo; and **Mauritius**, collected by Paul Clerkin.

Scanner Location

MUSC, Medical University of South Carolina; **AMNH**, American Museum of Natural History; **RBH**, Royal Brompton Hospital; **CMH**, Children's Memorial Hospital; **TTC**, Toshiba Training Center; **UC Irvine**, University of California at Irvine; and **Woods Hole**, Woods Hole Oceanographic Institute. Scans completed at the Royal Brompton Hospital were shared with us by Pepijn Kamminga, those from the Chicago Children's Memorial Hospital were shared by Dr. Kenshu Shimada, and scans completed at the Toshiba Training Center and UC Irvine were shared by Dr. Adam Summers and Dr. Mason Dean.

Scanner Type

S64, Somatom Sensation 64-slice (Siemens); **Force**, Somatom Force (Siemens); **HRCT**, High Resolution CT Scanner, GE Phoenix Vtome X240; **S16**, Somatom Sensation 16-slice (Siemens); **Volume Zoom**, Somatom Volume Zoom (Siemens); **Toshiba**, Toshiba Aquillion.

ORDER	FAMILY	SPECIES	SPECIMEN ID	SCANNER LOCATION	SCANNER TYPE
HEXANCHIFORMES	CHLAMYDOSELACHIDAE	<i>Chlamydoselachus anguineus</i>	UF 44302	MUSC	S64
	HEXANCHIDAE	<i>Heptranchias perlo</i>	GMBL 96-12	MUSC	Force
		<i>Hexanchus nakamurai</i>	UF 165855	MUSC	S64
SQUALIFORMES	ECHINORHINIDAE	<i>Echinorhinus brucus</i>	BMNH 19001167	RBH	S64

	SQUALIDAE	<i>Squalus acanthias</i>	GMBL 7313	MUSC	Force
		<i>Squalus brevirostris</i>	AMNH 258171	AMNH	HRCT
		<i>Squalus cf. mitsukurii</i>	SC #4	MUSC	S64
	CENTROPHORIDAE	<i>Centrophorus tessellatus</i>	USNM 400703	MUSC	Force
		<i>Deania calcea</i>	MB85-015114	MUSC	S64
	ETMOPTERIDAE	<i>Etmopterus sheikoi</i>	HO 411 or 410	AMNH	HRCT
		<i>Etmopterus splendidus</i>	AMNH 258170	AMNH	HRCT
		<i>Trigonognathus kabeyai</i>	BPBN 38354	AMNH	HRCT
	SOMNIOSIDAE	<i>Centroscymnus owstoni</i>	Mauritius 1944	MUSC	S64
		<i>Scymnodon ringens</i>	MB85-015115	MUSC	Force
		<i>Zameus squamulosus</i>	USNM 400734	MUSC	Force
	OXYNOTIDAE	<i>Oxynotus centrina</i>	USNM 206065	MUSC	Force
	DALATIIDAE	<i>Dalatias licha</i>	Mauritius 4582	MUSC	S64
PRISTIOPHORIFORMES	PRISTIOPHORIDAE	<i>Pristiophorus nudipinnis</i>	CSIRO unregistered	Woods Hole	Volume Zoom
SQUATINIFORMES	SQUATINIDAE	<i>Squatina nebulosa</i>	AMNH 258172	AMNH	HRCT
HETERODONTIFORMES	HETERODONTIDAE	<i>Heterodontus francisci</i>	AMNH 96795	AMNH	HRCT
ORECTOLOBIFORMES	PARASCYLLIIDAE	<i>Parascyllium collare</i>	CSIRO H 2692-12	AMNH	HRCT
	BRACHAELURIDAE	<i>Brachaelurus waddi</i>	USNM 39998	MUSC	S64
	ORECTOLOBIDAE	<i>Orectolobus maculatus</i>	USNM 50725	MUSC	S64
	HEMISCYLLIIDAE	<i>Chiloscyllium plagiosum</i>	AMNH 258165	AMNH	HRCT
		<i>Hemiscyllium ocellatum</i>	AMNH 44128	AMNH	HRCT
	GINGLYMOSTOMATIDAE	<i>Ginglymostoma cirratum</i>	USNM 127110	MUSC	S64
		<i>Nebrius ferrugineum</i>	USNM 206988	MUSC	S64
	STEGOSTOMATIDAE	<i>Stegostoma fasciatum</i>	LACM 38125-2	MUSC	S64
LAMNIFORMES	MITSIKURINIDAE	<i>Mitsukurina owstoni</i>	HUMZ 204610	MUSC	S64

		<i>Mitsukurina owstoni</i>	LACM 47362	TTC	Toshiba
	ODONTASPIDIDAE 1	<i>Carcharias taurus</i>	UF 103326	MUSC	S64
	ODONTASPIDIDAE 2	<i>Odontaspis ferox</i>	BPBM 9334	CMH	S64
	PSEUDOCARCHARIIDAE	<i>Pseudocarcharias kamoharai</i>	LACM 45857	TTC	Toshiba
	ALOPIIDAE	<i>Alopias superciliosus</i>	LACM 38117-38	CMH	S64
	LAMNIDAE	<i>Carcharodon carcharias</i>	MCZ 171013	Woods Hole	Volume Zoom
		<i>Isurus oxyrinchus</i>	GMBL 8446	MUSC	Force
		<i>Lamna ditropis</i>	FMNH 117475	CMH	S64
CARCHARHINIFORMES	SCYLORHINIDAE	<i>Apristurus macrostomus</i>	AMNH 258158	AMNH	HRCT
		<i>Asymbolus analis</i>	CSIRO H 3431-02	AMNH	HRCT
		<i>Bythaelurus canescens</i>	USNM 205009	MUSC	Force
		<i>Cephaloscyllium isabellum</i>	USNM 320594	MUSC	Force
		<i>Galeus sauteri</i>	AMNH 258160	AMNH	HRCT
		<i>Poroderma africanum</i>	USNM 221658	MUSC	Force
		<i>Scyliorhinus meadi</i>	GMBL 8312	MUSC	S64
	PROSCYLLIDAE	<i>Eridacnis radcliffei</i>	AMNH 258156	AMNH	HRCT
	LEPTOCHARIIDAE	<i>Leptocharias smithii</i>	USNM 202651	MUSC	Force
	TRIAKIDAE	<i>Mustelus manazo</i>	AMNH 258162	AMNH	HRCT
	HEMIGALEIDAE	<i>Hemipristis elongatus</i>	LACM 37712-1	MUSC	S64
	CARCHARHINIDAE	<i>Carcharhinus galapagensis</i>	GMBL Uncatalogued	MUSC	S64
		<i>Carcharhinus plumbeus</i>	GMBL 79-60	MUSC	Force
		<i>Loxodon macrorhinus</i>	USNM 201721	MUSC	Force
		<i>Negaprion brevirostris</i>	GMBL TL 990	MUSC	S64
		<i>Rhizoprionodon terraenovae</i>	GMBL Uncatalogued	MUSC	Force
		<i>Scoliodon macrorhynchus</i>	AMNH 258155	AMNH	HRCT

		<i>Triaenodon obesus</i>	USNM 216792	MUSC	Force
	SPHYRNIDAE	<i>Eusphyrna blochii</i>	USNM 205342	MUSC	Force
		<i>Sphyrna corona</i>	USNM 206987	MUSC	Force
		<i>Sphyrna lewini</i>	USNM 203101	MUSC	Force
		<i>Sphyrna media</i>	USNM 205377	MUSC	Force
		<i>Sphyrna tiburo</i>	AMNH Uncat	AMNH	HRCT
		<i>Sphyrna tudes</i>	USNM 159197	MUSC	Force
		<i>Sphyrna zygaena</i>	USNM 325631	MUSC	Force
PRISTIFORMES	PRISTIDAE	<i>Pristis clavata</i>	CSIRO H 2504	Woods Hole	Volume Zoom
RAJIFORMES	RHINIDAE	<i>Rhina ancylostoma</i>	LACM 38117-38	MUSC	S64
	RHYNCHOBATIDAE	<i>Rhynchobatus springeri</i>	AMNH 258310	MUSC	S64
	RHINOBATIDAE	<i>Aptychotrema vincentiana</i>	CSIRO MUW 101	MUSC	S64
		<i>Rhinobatos lentiginosus</i>	GMBL 74-37	MUSC	S64
TORPEDINIFORMES	NARCINIDAE	<i>Benthobatis yangi</i>	AMNH 258311	AMNH	HRCT
		<i>Narcine brasiliensis</i>	AMNH 77069	AMNH	HRCT
	NARKIDAE	<i>Narke japonica</i>	AMNH 258312	AMNH	HRCT
	HYPNIDAE	<i>Hypnos monopterygius</i>	USNM 84374	MUSC	S64
	TORPEDINIDAE	<i>Torpedo fuscomaculata</i>	USNM 320677	MUSC	Force
RAJIFORMES	ARHYNCHOBATIDAE	<i>Brochiraja leviveneta</i>	CSIRO H 3132-05	AMNH	HRCT
		<i>Irolita waitii</i>	CSIRO H 133-1	MUSC	S64
		<i>Pavoraja nitida</i>	CSIRO CA 2817	AMNH	HRCT
	RAJIDAE	<i>Dactylobatus armatus</i>	UF 41302	MUSC	S64
		<i>Dentiraja lemprieri</i>	CSIRO H 85-01	MUSC	S64
		<i>Okamejei acutispina</i>	AMNH 258307	AMNH	HRCT
		<i>Raja eglantaria</i>	GMBL 02-155	MUSC	S64

	ANACANTHOBATIDAE	<i>Anacanthobatis folirostris</i>	UF 40141	MUSC	S64
MYLIOBATIFORMES	PLATYRHINIDAE	<i>Platyrrhinoidis triseriata</i>	USNM 26275	MUSC	S64
	ZANOBATIDAE	<i>Zanobatus schoenleinii</i>	UF 176858	MUSC	S64
	UROLOPHIDAE	<i>Urolophus aurantiacus</i>	AMNH 258305	AMNH	HRCT
	UROTRYGONIDAE	<i>Urotrygon chilensis</i>	AMNH 233905	AMNH	HRCT
	POTAMOTRYGONIDAE	<i>Potamotrygon motoro</i>	AMNH 97428	AMNH	HRCT
	DASYATIDAE	<i>Dasyatis americana</i>	GMBL 72-158	MUSC	S64
		<i>Dasyatis zugei</i>	AMNH 258174	AMNH	HRCT
		<i>Neotrygon kuhlii</i>	HO 56	MUSC	S64
	GYMNURIDAE	<i>Gymnura altavela</i>	GMBL 81-86	MUSC	S64
	MYLIOBATIDAE	<i>Pteromylaeus bovinus</i>	USNM 202763	MUSC	S64
	RHINOPTERIDAE	<i>Rhinoptera bonasus</i>	GMBL 73-7	MUSC	S64
	MOBULIDAE	<i>Mobula munkiana</i>	SIO 85-34	UC Irvine	S16
CHIMAERIFORMES	CALLORHINCHIDAE	<i>Callorhinchus milii</i>	USNM 320578	MUSC	Force
	CHIMAERIDAE	<i>Chimaera cubana</i>	USNM 400700	MUSC	S64
		<i>Hydrolagus novaezealandiae</i>	USNM 320628	MUSC	Force
	RHINOCHIMAERIDAE	<i>Harriotta raleighana</i>	USNM 320579	MUSC	Force
		<i>Neoharriotta carri</i>	USNM 400695	MUSC	Force
		<i>Rhinochimaera atlantica</i>	USNM 400698	MUSC	S64

Appendix II

Post Processing Reconstructions

Once scan data were collected from the scanners, different reconstruction settings were used in order to ready the data for segmentation. Only scans which were completed at the Medical University of South Carolina (MUSC) and the American Museum of Natural History (AMNH) could be manipulated in post processing for this project. All scans which were shared with us for this project had already been through the post processing reconstruction settings necessary for the original researchers work. The post processing reconstruction algorithms and adjusted scan settings are available in Table 2.

Stitching Scan Data

Scan data from the high-resolution CT scanning facility at the AMNH were completed in multiple scans and digitally stitched together by the post-doctoral fellows working in the Vertebrate Paleontology department at AMNH. Scan stitching at AMNH was completed using both the GE software connected to the scanner and Volume Graphics Studio Max 2.1 (Heidelberg, Germany). Scan data collected on the Siemens Somatom Sensation (64 slice) CT scanner at MUSC was usually completed in one scan per specimen, however some large specimens were scanned in two sections and the data were then either stitched together using 3D Stitching in ImageJ (US National Institutes of Health, Maryland, USA) or segmented in two portions with structures later moved in 3-Matic Research Version 9.0 (Materialise, Leuven, Belgium) to the correct location in the skeleton. Data from the MUSC Siemens Somatom Force (DSCT) scanner were collected in one scan for each specimen and required no post scan stitching.

Uploading CT Scan Data

Different options for uploading scans to the Mimics Software were used in this project depending on the scan source. All Medical scans were uploaded into Mimics Software without further formatting after the necessary stitching of the multi-part scans was completed. High-resolution scans from AMNH often had to undergo further formatting within the Mimics upload wizard to reduce the file size of the project in Mimics. These formatting changes included reducing the data from 16-bit to 8-bit for exceptionally large datasets or reducing the area of the scan slices loaded into mimics within the New Project Wizard in Mimics. In some high-resolution scans a subset of the scan data located at the margins between the scan sections had to be uploaded separately in order to fill some areas which were lost during the manual stitching of the sections.

Merging Structures

In cases where one structure required two or more thresholds to complete an accurate segmentation, the different STL files had to be merged together in the 3Matic software. The structures which most commonly required multiple thresholds were the vertebral column and the radials (both pectoral and pelvic). 3Matic was also used to move structures when scan data was completed in two parts but could not be stitched together before segmenting the scan. Moving structures usually only required the translation of structures or structure parts along the XY and Z planes, however when the animal was moved between scan sections, the structures would also need to be rotated in order to line up with the rest of the skeletal elements.

Literature Cited

- Achenbach, S., Boehmer, K., Pflederer, T., Ropers, D., Seltmann, M., Lell, M., Anders, K., Kuettner, A., Uder, M., Daniel, W.G., and Marwan, M. 2010. Influence of slice thickness and reconstruction kernel on the computed tomographic attenuation of coronary atherosclerotic plaque. *Journal of cardiovascular computed tomography*, 4(2), 110-115.
- Aschliman, N. C., Claeson, K. M., and McEachran, J. D. 2012. Phylogeny of Batoidea. *Biology of sharks and their relatives*. Edited by JC Carrier, JA Musick, and MR Heithaus. Indiana University Press, Bloomington, Ind, 57-94.
- Benini, A., and Bonar, S. K. 1996. Andreas Vesalius: 1514-1564. *Spine*, 21(11), 1388-1393.
- Bromham, L., Woolfit, M., Lee, M. S., and Rambaut, A. 2002. Testing the relationship between morphological and molecular rates of change along phylogenies. *Evolution*, 56(10), 1921-1930.
- Buckwalter, J. A. 2000. Advancing the Science and Art of Orthopaedics Lessons from History*. *The Journal of Bone and Joint Surgery*, 82(12), 1782-1782.
- Cignoni, P., Ranzuglia, G., Callieri, M., Corsini, M., Ganovelli, F., Pietroni, N., and Tarini, M. 2011. MeshLab.
- Compagno, L. J. 1990. Alternative life-history styles of cartilaginous fishes in time and space. In *Alternative life-history styles of fishes* (pp. 33-75). Springer Netherlands.
- Compagno L. J. V. 1973. Interrelationship of living elasmobranchs. Pp. 15-61. In: P.H. Greenwood *et al. Interrelationships of fishes*. Academic Press, New York.
- Compagno LJV, M. Dando, and S.L. Fowler. 2005. *Sharks of the World*. Princeton, NJ: Princeton University Press.
- Compagno, L.J.V. 1977. Phyletic relationships of living sharks and rays. *American Zoologist*, 17 (2): 303-322.
- Compagno, L.V.J. 1984. FAO species catalogue, Vol 4, Sharks of the world. An annotated and illustrated catalogue of shark species known to date. Part 2, *Carcharhiniformes*. *FAO Fish.Synop.* 125, Vol 4, Pt. 2. 655 pp.
- Corrigan, S. and L.B. Beheregaray. 2009. A recent shark radiation: molecular phylogeny, biogeography and speciation of wobbegong sharks (family: Orectolobidae). *Mol. Phylogenet. Evol.* 52, 205–216.
- Daniel, J. F. 1922. *The elasmobranch fishes*. University of California Press.
- Davis, J. S. 2014. *Functional Morphology of Mastication in Musteloid Carnivorans* (Doctoral dissertation, Ohio University).

- Dean, M. N., Bizzarro, J. J., & Summers, A. P. 2007. The evolution of cranial design, diet, and feeding mechanisms in batoid fishes. *Integrative and Comparative Biology*, 47(1), 70-81.
- de Carvalho, M.R. 1996. Higher-level elasmobranch phylogeny, basal squalians, and paraphyly. In: Stassny, M.L.J., Parenti, L.R., Johnson, G.D. (Eds.), *Interrelationships of Fishes*. Academic Press, San Diego, pp. 35–62.
- Descamps, E., Sochacka, A., De Kegel, B., Van Loo, D., Van Hoorebeke, L., & Adriaens, D. 2014. Soft tissue discrimination with contrast agents using micro-CT scanning. *BELGIAN JOURNAL OF ZOOLOGY*, 144(1), 20-40.
- Didier, D. A. 1995. Phylogenetic systematics of extant chimeroid fishes (Holocephali, Chimaeroidei). *Am. Mus. Novitates* 3119, 1– 86.
- Douady, C.J., M. Dosay, M.S. Shivji, and M.J. Stanhope. 2003. Molecular phylogenetic evidence refuting the hypothesis of Batoidea (rays and skates) as derived sharks. *Mol. Phylogenet. Evol.* 26, 215–221.
- Dunn, K. A. and J.F. Morrissey. 1995. Molecular phylogeny of elasmobranchs. *Copeia*: 526-531.
- Ebert, D. A., & Winton, M. V. 2010. Chondrichthyans of high latitude seas. *The biology of sharks and their relatives*, 2, 115-158.
- Ellis, J. R., & Shackley, S. E. 1995. Ontogenic changes and sexual dimorphism in the head, mouth and teeth of the lesser spotted dogfish. *Journal of fish biology*, 47(1), 155-164.
- Feduccia, A., & Slaughter, B. H. 1974. Sexual dimorphism in skates (Rajidae) and its possible role in differential niche utilization. *Evolution*, 164-168.
- Garman, S. W. 1913. The Plagiostomia (sharks, skates, and rays). - *Memoirs of the Museum of Comparative Zoology*, Harvard, 36: 1-515, 75 pls.
- Gignac, P. M., & Kley, N. J. 2014. Iodine-enhanced micro-CT imaging: Methodological refinements for the study of the soft-tissue anatomy of post-embryonic vertebrates. *Journal of Experimental Zoology Part B: Molecular and Developmental Evolution*, 322(3), 166-176.
- Goto, T. 2001. Comparative anatomy, phylogeny and cladistic classification of the order Orectolobiformes (Chondrichthyes, Elasmobranchii). *Mem. Grad. Sch. Fish. Sci.* 48(1):1-100.
- Harbison, S. T., McCoy, L. J., and Mackay, T. F. 2013. Genome-wide association study of sleep in *Drosophila melanogaster*. *BMC genomics*, 14(1), 281.
- Hasse, C. 1879. 'Das Natürliche System Der Elasmobranchier.' Jena.
- Haswell, W.A. Studies on the elasmobranch skeleton. *Proceedings of the Linnean Society of New South Wales*. Vol. 9. No. 1. 1884.

- Hedges, S.B., and L. L. Poling. 1999. A molecular phylogeny of reptiles. *Science* 283.5404: 998-1001.
- Iglésias, S.P., G. Lecointre, and D.Y. Sellos. 2005. Extensive paraphyly within sharks of the order Carcharhiniformes inferred from nuclear and mitochondrial genes. *Mol. Phylogenet. Evol.* 34, 569–583
- Kitamura, T., A. Takemura, S. Watabe, T. Taniuchi, and M. Shimizu. 1996. Molecular phylogeny of the sharks and rays of superorder squalia based on mitochondrial Cytochrome b gene. *Fisheries Science* 62(3): 340-343.
- Last, P., 2007. The state of chondrichthyan taxonomy and systematics. *Mar Freshw Res* 58, 7–9.
- Last, P. R. and J.D. Stevens. 2009. Sharks and rays of Australia. Melbourne, Australia: CSIRO.
- Libralato, S., V. Christensen, and D. Pauly. 2005. A method for identifying keystone species in food web models. *Ecol. Model.* 195, 153–171.
- Lucifora, L. O., and Vassallo, A. I. 2002. Walking in skates (Chondrichthyes, Rajidae): anatomy, behaviour and analogies to tetrapod locomotion. *Biological Journal of the Linnean Society*, 77(1), 35-41.
- Maia, A.M.R., C.A.D. Wilga, and G.V. Lauder. 2012. *Biomechanics of Locomotion in Sharks, Rays, and Chimeras. Biology of sharks and their relatives. Edited by JC Carrier, JA Musick, and MR Heithaus. Indiana University Press, Bloomington, Ind, 57-94.*
- Maisey, J., 1984. Higher elasmobranch phylogeny and biostratigraphy. *Zool. J. Linn. Soc.* 82, 33–54.
- Maisey, J. G. 2012. What is an ‘elasmobranch’? The impact of palaeontology in understanding elasmobranch phylogeny and evolution. *Journal of fish biology*, 80(5), 918-951.
- Maisey J, Chesek C, Miller D. 1996. Discovering fossil fishes. New York, NY: Henry Holt and Company: 223.
- Maisey, J.G., G.J.P. Naylor, and D.J. Ward. 2004. Mesozoic elasmobranchs, neoselachian phylogeny and the rise of modern elasmobranch diversity. Mesozoic Fishes 3 - Systematics, *Paleoenvironments and Biodiversity*: 17-56, 16 figs., 2 tabs., 1 app.
- Martin, R. A. 2005. Conservation of freshwater and euryhaline elasmobranchs: a review. *Journal of the Marine Biological Association of the United Kingdom*, 85(05), 1049-1073.
- Medewar P. 1996. *Is the scientific paper a fraud?* In: The Strange Case of the Spotted Mice and Other Essays. Cambridge: Oxford U. Press.
- Metscher, B. D. 2009. MicroCT for developmental biology: A versatile tool for high-contrast 3D imaging at histological resolutions. *Developmental Dynamics*, 238(3), 632-640.

- Müller, J. and Henle, F. G. J. 1841. Systematische beschreibung der Plagiostomen. Berlin. Plagiostomeni-xxii.
- Myers, R.A., J.K. Baum, T.D. Shepherd, S.P. Powers, and C.H. Peterson. 2007. Cascading effects of the loss of apex predatory sharks from a coastal ocean. *Science*.315:1846–1850
- Naylor, G., 1992. The phylogenetic relationships among requiem and hammerhead sharks: inferring phylogeny when thousands of equally parsimonious trees result. *Cladistics* 8, 295–318.
- Naylor, G.J.P., Ryburn, J.A., Fedrigo, O., López, J.A., 2005. Phylogenetic relationships among the major lineages of modern elasmobranchs. In: Hamlett, W.C., Jamieson, B.G.M. (Eds.), *Reproductive Biology and Phylogeny*, vol. 3. Science Publishers, Inc., Enfield, NH, pp. 1–25.
- Naylor, G.J.P., J.N. Caira, K.J.Jensen, K.A.M. Rosana, N.S. Straube and C. Lakner. 2012. "Elasmobranch phylogeny: A mitochondrial estimate based on 595 species." *The biology of sharks and their relatives*: 31-56.
- Nishida, K. 1990. Phylogeny of the suborder Myliobatidoidei. *Memoirs of the Faculty of Fisheries-Hokkaido University, Japan*.
- Nuzhdin, S. V., Pasyukova, E. G., Dilda, C. L., Zeng, Z. B., and Mackay, T. F. 1997. Sex-specific quantitative trait loci affecting longevity in *Drosophila melanogaster*. *Proceedings of the national academy of Sciences*, 94(18), 9734-9739.
- Pérez-Jiménez, J. C., O. Sosa-Nishizaki, and E. Furlong-Estrada. 2005. Artisanal shark fishery at “Tres Marias” Islands and Isabel Island in the Central Mexican Pacific. *Northwest Atlantic Fisheries Science*. 35, article 43.
- Popper, K. R. 1959. *The Logic of Scientific Discovery*. New York: Basic Books.
- Raup, D. and J. Sepkoski. 1982. Mass extinctions in the marine fossil record. *Science*, 215.
- Reiff, R.; Harwood, W. S.; Phillipson, T. “A Scientific Method Based Upon Research Scientists’ Conceptions of Scientific Inquiry, Session”, F3. *Proceedings of the 2002 Annual International Conference of the Association for the Education of Teachers in Science*, 2002, pp 546–556.
- Robinson, W. R. 2004. The Inquiry Wheel, an Alternative to the Scientific Method. A View of the Science Education Research Literature. *Journal of Chemical Education* 81, no. 6: 791.
- Rosa, R. S., Charvet-Almeida, P., & Quijada, C. C. D. 2010. Biology of the South American potamotrygonid stingrays. *Sharks and their relatives II: biodiversity, adaptive physiology, and conservation*. CRC Press, Boca Raton, 241-281.

- Rothchild, I. 2006. Induction, deduction, and the scientific method. *An eclectic overview of the practice of science, Society for the Study of Reproduction, Madison (WI), USA.*
- Sabaj Perez, M.H. (editor). 2014. Standard symbolic codes for institutional resource collections in herpetology and ichthyology: an Online Reference. Version 5.0 (22 September 2014). Electronically accessible at <http://www.asih.org/>, American Society of Ichthyologists and Herpetologists, Washington, DC.
- Schindler, D.E., T.E. Essington, J.F. Kitchell, C. Boggs, and R. Hilborn. 2008. Sharks and tunas: fisheries impacts on predators with contrasting life histories. *Ecol. Appl.* 12, 735–748.
- Shirai, S., 1992. Squalean phylogeny. Hokkaido University Press.
- Shirai, S., 1996. Phylogenetic interrelationships of neoselachians (Chondrichthyes: Euselachii). In: Stassny, M.L.J., Parenti, L.R., Johnson, G.D. (Eds.), *Interrelationships of Fishes*. Academic Press, San Diego, pp. 9–34.
- Sorenson, L., Santini, F., and Alfaro, M. E. 2014. The effect of habitat on modern shark diversification. *Journal of Evolutionary Biology*.
- Summers, A. P., Ketcham, R. A., & Rowe, T. 2004. Structure and function of the horn shark (*Heterodontus francisci*) cranium through ontogeny: development of a hard prey specialist. *Journal of Morphology*, 260(1), 1-12.
- Thies, D. and W.E. Reif. 1985. Phylogeny and evolutionary ecology of Mesozoic, Neoselachii. *News Jahrbuch für Geologie und Palaontologie Monatshefte, Abh.* 169: 331-361
- Underwood, C. J. 2006 Diversification of the Neoselachii (Chondrichthyes) during the Jurassic and Cretaceous. *Paleobiology*, 32 (2). pp. 215-235.
- van der Wall, E. E., Jukema, J. W., Schuijf, J. D., and Bax, J. J. 2011. 100 kV versus 120 kV: effective reduction in radiation dose?. *The international journal of cardiovascular imaging*, 27(4), 587-591.
- Vélez-Zuazo, X., and Agnarsson, I. 2011. Shark tales: a molecular species-level phylogeny of sharks (Selachimorpha, Chondrichthyes). *Molecular phylogenetics and evolution*, 58(2), 207-217.
- White, E.G., 1936. A classification and phylogeny of the elasmobranch fishes. American Museum novitates; no. 837
- White, W. T., and P. R. Last. 2012. A review of the taxonomy of chondrichthyan fishes: a modern perspective. *Journal of fish biology* 80.5: 901-917.
- Wilga, C. D., Motta, P. J., and Sanford, C. P. 2007. Evolution and ecology of feeding in elasmobranchs. *Integrative and Comparative Biology*, 47(1), 55-69.